EFFECT OF GINSENOSIDE RE ON SKCa CURRENTS IN HUMAN CORONARY ARTERY ENDOTHELIAL CELLS.

SUPORN SUKRITTANON

A THESIS SUBMITTED IN PARTIAL FULFILMENT
OF THE REQUIREMENTS FOR
THE DEGREE OF MASTER OF SCIENCE (PHYSIOLOGY)
FACULTY OF GRADUATE STUDIES
MAHIDOL UNIVERSITY
2011

Thesis
entitled

EFFECT OF GINSENOSIDE RE ON SKCa CURRENTS IN HUMAN CORONARY ARTERY ENDOTHELIAL CELLS.

……
Ms. Suporn Sukrittanon
Candidate

……
Asst. Prof. Wattana B Watanapa,
M.D., Ph.D.
Major adivisor

……
Mr. Luecha Boontaveekul,
M.D., M.Sc.
Co-advisor

……
Mr. Panapat Uawithya,
M.D., Ph.D.
Co-advisor

……
Mr. Sompol Tapechum,
M.D., Ph.D.
Co-advisor

……
Prof. Banchong Mahaisavariya,
M.D., Dip. Thai Board of Orthopedics
Dean
Faculty of Graduate Studies
Mahidol University

……
Assoc. Prof. Suwattanee Kooptiwut,
M.D., Ph.D.
Program Director
Master of Science Program in Physiology
Faculty of Medicine Siriraj Hospital
Mahidol University

Thesis
entitled

EFFECT OF GINSENOSIDE RE ON SKCa CURRENTS IN HUMAN CORONARY ARTERY ENDOTHELIAL CELLS.

was submitted to the Faculty of Graduate Studies, Mahidol University
for the degree of Master of Science (Physiology)
on
June 27, 2011

……
Ms. Suporn Sukrittanon
Candidate

……
Mr. Sorachai Srisuma,
M.D., Ph.D.
Chair

……
Asst. Prof. Wattana B Watanapa,
M.D., Ph.D.
Member

……
Mr. Sompol Tapechum,
M.D., Ph.D.
Member

……
Asst. Prof. Krongkarn Chootip
Ph.D.
Member

……
Prof. Banchong Mahaisavariya,
M.D., Dip. Thai Board of Orthopedics
Dean
Faculty of Graduate Studies
Mahidol University

……
Clin. Prof. Teerawat Kulthanan,
M.D., FIMS, FRCST, FICS
Dean
Faculty of Medicine Siriraj Hospital
Mahidol University

ACKNOWLEDGMENTS

I wish to express my sincere gratitude to Asst. Prof. Wattana B Watanapa, my major advisor, for her great scientific expertise, tremendously helpful suggestions, excellent instructions and endless kindness which have supported me throughout my study.

I would also like to express my thankfulness to all my co-advisor, Dr. Panapat Uawithya, Dr. Sompol Tapechum and Dr. Luecha Boontaveekul, for their valuable comments and suggestions.

My deepest appreciation is also to Ms. Katesirin Ruamyod for her considerable help and suggestions. In addition, I wish to express my grateful thanks to all members of the Department of Physiology for their encouragement and friendship.

I wish to thank the Siriraj Graduate Thesis Scholarship (Faculty of Medicine Siriraj Hospital, MU), the 60th Year Supreme Reign of His Majesty King Bhumibol Adulyadej (Faculty of Graduate Studies, MU) and Cerebos Awards for financial support.

Most of all I would like to thank my family for their unconditional love and moral support that has made everything possible.

Suporn Sukrittanon

EFFECT OF GINSENOSIDE RE ON SKCa CURRENTS IN HUMAN CORONARY ARTERY ENDOTHELIAL CELLS.

SUPORN SUKRITTANON 5036476 SIPS/M

M.Sc (PHYSIOLOGY)

THESIS ADVISORY COMMITTEE: WATTANA B. WATANAPA, M.D., Ph.D., LUECHA BOONTAVEEKUL, M.D., M.Sc., SOMPOL TAPECHUM, M.D., Ph.D., PANAPAT UAWITHYA, Ph.D., M.D.

ABSTRACT

Endothelial cells are important in regulating coronary circulation, by secreting vasodilators and/or vasoconstrictors. Ginsenoside Re (Re), an active component in ginseng, was reported to increase NO secretion from human umbilical vein endothelial cells. In other cell types, this compound was found to increase K^+ current or Ca^{2+}-sensitive K^+ (K_{Ca}) currents, leading to nitric oxide synthase (NOS) stimulation, increased NO secretion and vasodilation. Re, therefore, may increase K_{Ca} activity in human coronary artery endothelial cells (HCAECs). Cultured HCAECs exposed to different concentrations of Re were studied using the whole-cell patch clamp technique. Specific blockers of small- and intermediate-conductance K_{Ca} (SK_{Ca} and IK_{Ca}), non-selective cation (NSC) and inward-rectifier potassium (K_{ir}) channels were employed to study or inhibit individual currents. All currents were reported as mean ± SEM. Re dose-dependently increased outward currents (EC50 = 408.90 $\pm$ 1.59) nM; $P < 0.05$). 1 µM Re could significantly increase outward currents by 28.93 ± 7.54 % when the NSC channel was blocked by La^{3+}, but failed when the SK_{Ca} channel was inhibited by apamin. When NSC, inward rectifier, intermediate- and high-conductance K_{Ca} channels were simultaneously blocked (with La^{3+}, Ba^{2+}, clotrimazole and TEA), Re could still increase outward currents significantly (35.49 ± 4.22 %); this effect was again abolished by apamin. These results indicate that Re increased HCAEC outward currents by opening SK_{Ca} channels. Therefore, ginsenoside Re may also cause coronary vasodilation in humans, adding to the benefits of ginseng, with a promising future in the protection and/or treatment against coronary artery disease and other cardiovascular conditions.

KEY WORDS: GINSENOSIDE RE/ SKCa CURRENTS / HUMAN CORONARY ARTERY ENDOTHELIAL CELLS

135 pages

ผลของ GINSENOSIDE RE ต่อกระแส SKCa ในเซลล์บุโพรงหลอดเลือดแดงหัวใจมนุษย์
EFFECT OF GINSENOSIDE RE ON SKCa CURRENTS IN HUMAN CORONARY ARTERY ENDOTHELIAL CELLS.

ศุภร สุกฤตานนท์ 5036476 SIPS/M

วท.ม. (สรีรวิทยา)

คณะกรรมการที่ปรึกษาวิทยานิพนธ์: วัฒนา วัฒนาภา, พ.บ., Ph.D., ลือชา บุญทวีกุล, พ.บ., M.Sc., สมพล เทพชุม, พ.บ., Ph.D., ปณภัฏ เอื้อวิทยา, ปร.ด, พ.บ.

บทคัดย่อ

เซลล์บุโพรงหลอดเลือดมีความสำคัญต่อการควบคุมระบบไหลเวียนเลือดของหัวใจ โดยหลั่งสารที่ขยายหรือตีบหลอดเลือด มีรายงานพบว่า ginsenoside Re (Re) ซึ่งเป็นสารออกฤทธิ์ของโสม เพิ่มการหลั่งไนตริกออกไซด์ (NO) จากเซลล์บุโพรงหลอดเลือดดำสายสะดือมนุษย์ ในเซลล์ชนิดอื่นสารนี้ยังสามารถเพิ่มกระแสโพแทสเซียมหรือกระแสโพแทสเซียมที่กระตุ้นโดยแคลเซียม (K_{Ca}) นำไปสู่การกระตุ้น nitric oxide synthase (NOS), เพิ่มการหลั่ง NO และขยายหลอดเลือด ดังนั้น Re จึงอาจเพิ่มการทำงานของ K_{Ca} ในเซลล์บุโพรงหลอดเลือดแดงหัวใจมนุษย์ (HCAEC) ได้ ศึกษาเซลล์เพาะเลี้ยง HCAEC ที่ได้รับ Re ความเข้มข้นต่างๆ กันด้วยวิธี whole-cell patch clamp ใช้สารยับยั้งที่จำเพาะต่อช่อง K_{Ca} ชนิดนำไฟฟ้าต่ำ (SK_{Ca}) และปานกลาง (IK_{Ca}), ช่องไอออนบวกชนิดไม่เลือก (NSC) และช่องโพแทสเซียมชนิดปรับตรงด้านไหลเข้า (K_{ir}) เพื่อศึกษากระแสแต่ละชนิด รายงานกระแสทั้งหมดเป็นค่าเฉลี่ยบวกลบความคลาดเคลื่อนมาตรฐานของค่าเฉลี่ย (mean $\pm$ SEM) Re สามารถเพิ่มกระแสออกตามการเพิ่มความเข้มข้น (EC50 = 408.90 $\pm$ 1.59 nM, $P < 0.05$) เมื่อยับยั้ง NSC โดย La^{3+} พบว่า Re 1 mM สามารถเพิ่มกระแสออกได้ 28.93 $\pm$ 7.54 % อย่างมีนัยสำคัญทางสถิติ แต่ไม่สามารถเพิ่มกระแสออกหากยับยั้ง SK_{Ca} โดยใช้ apamin และเมื่อยับยั้ง NSC, K_{ir}, IK_{Ca} และ K_{Ca} ที่นำไฟฟ้าสูง โดยให้ La^{3+}, Ba^{2+}, clotrimazole และ TEA ไปพร้อมกัน พบว่า Re 1 mM ยังคงสามารถเพิ่มกระแสออกอย่างมีนัยสำคัญทางสถิติได้ 35.49 $\pm$ 4.22 % และผลนี้หายไปเมื่อให้ apamin ผลการทดลองเหล่านี้บ่งชี้ว่า Re เพิ่มกระแสออกของ HCAEC ได้โดยเปิด SK_{Ca} ดังนั้น ginsenoside Re อาจขยายหลอดเลือดแดงหัวใจมนุษย์ได้ นับเป็นประโยชน์อีกประการของโสม โดยในอนาคตอาจพัฒนามาใช้ในการป้องกันและ/หรือรักษาโรคหลอดเลือดหัวใจ และภาวะทางระบบหัวใจและหลอดเลือดอื่นๆ

135 หน้า

CONTENTS

CONTENTS (cont.)

LIST OF TABLES

LIST OF FIGURES

LIST OF FIGURES (cont.)

LIST OF FIGURES (cont.)

LIST OF FIGURES (cont.)

LIST OF FIGURES (cont.)

LIST OF ABBREVIATIONS

$[Ca^{2+}]_i$	Intracellular calcium concentration
$[Ca^{2+}]_o$	Extracellular calcium concentration
Ag/AgCl	Silver/silver chloride
ATP	Adenosine triphosphate
Ba^{2+}	Barium ion
BK_{Ca}	Large-conductance calcium-activated potassium channel
Ca^{2+}	Calcium ion
CaM	Calmodulin
cGMP	cyclic guanidine monophosphate
Cl_{Ca}	Ca^{2+}-activated Cl^- channel
Cl_{vol}	Volume-activated Cl^- channel
C_{max}	Maximum plasma concentration
DMSO	Dimethyl sulfoxide
EC50	Half effective concentration
EDHF	Endothelium-derived hyperpolarizing factor
EGTA	Ethylenediaminetetraacetic acid
eNOS	Endothelial nitric oxide synthase
ER	Endoplasmic reticulum
GR	Glucocorticoid receptor
GTP	Guanidine triphosphate
HCAEC	Human coronary artery endothelial cell
HEPES	4-(2-hydroxyethyl)-1-piperazineethanesulfonic acid
HUVEC	Human umbilical vein endothelial cell
$I_{Ca,L}$	L-type Ca^{2+} current

LIST OF ABBREVIATIONS

IK_{Ca}	Intermediate -conductance calcium-activated potassium channel
I_{Ks}	Delayed rectifier K^+ current
IP_3	Inositol triphosphate
K^+	Potassium ion
K_{ATP}	ATP-sensitive potassium channel
K_{Ca}	Calcium-activated potassium channel
K_{ir}	Inwardly rectifying potassium channel
La^{3+}	Lanthanum ion
LDL	Low-density lipoprotein
NO	Nitric oxide
NOS	Nitric oxide synthase
NSC	Nonselective cationic channel
PPDs	Protopanaxadiols
PPTs	Protopanaxatriols
SGLT1	Sodium-dependent glucose co-transporter 1
SK_{Ca}	Small-conductance calcium-activated potassium channel
SR	Sarcoplasmic reticulum
TBA	Tetrabutylammonium
TEA	Tetraethylammonium
TLC	Thin layer chromatography
T_{max}	Maximum drug concentration time
TNS	Trypsin-neutralizing solution
TRP	Transient receptor potential
UPLC/MS	Ultra performance liquid chromatography mass spectrometric

CHAPTER I
INTRODUCTION

Ginsengs are indigenous East Asian herbs known worldwide; they have been used as a medicine for longer than 2,000 years (1-3). They are cultivated in China, Korea (*Panax ginseng* C.A. Meyer), Vietnam (*Panax vietnamensis*), Japan (*Panax japonicus*), North America (*Panax quinquefolium*), and in the Himalayas (*Panax pseudo-ginseng*). Active components of ginsengs are composed of 30 different triterpene saponin ginsenosides, found mostly in the root and to a lesser extent in both the leaf and the berry (4).

Asian and North American ginsengs have similar components of ginsenosides, which can be divided by chemical structures to two types (4-8).

1. Protopanaxadiols, with sugar moieties at positions C-3 and C-20: Rb1, Rb2, Rb3, Rc, Rd, and Ra;

2. Protopanaxatriols, with sugar moieties at positions C-6 and C-20: Re, Rg1, Rg2, and Re.

Ginsenosides have a variety of actions on cardiovascular system, including antihypertensive effect, preventing ischemia/reperfusion injury, reducing heart rate, reducing contractility, vasorelaxation and antiarrhythmic effect (1, 5, 9-11). The ginsenoside components reported to cause vasorelaxation are Re (5, 10-12), Rb_1 (2), and Rg_1 (9). The mechanisms leading to vasorelaxation by ginsenosides are still unclear.

Endothelial cells control vascular tone by secreting vasorelaxants, e.g., nitric oxide (NO), prostacyclin and endothelium-derived hyperpolarizing factor (EDHF), as well as vasoconstrictors, e.g. endothelin (13-15). Interestingly, vascular endothelial cells also contain several ion channels, namely, Ca^{2+}-

activated K^+ channels (K_{Ca}), including large- (BK_{Ca}), intermediate- (IK_{Ca}), and small-conductance (SK_{Ca}) Ca^{2+}-activated K^+ channels; ATP-sensitive potassium channels (K_{ATP}); inwardly rectifying potassium channels (K_{ir}); and nonselective cationic channels (NSC) (1, 16-18). The release of nitric oxide is controlled by changes in the membrane that cause an initial increase in cytosolic Ca^{2+} concentration (19). This, in turn, leads to opening of Ca^{2+}-dependent K^+ channels, causing K^+ efflux and hyperpolarization. Endothelial cells do not have voltage-sensitive Ca^{2+} channel, so the hyperpolarization further enhances the driving force for Ca^{2+} influx via NSC channels. High intracellular Ca^{2+} stimulates nitric oxide synthase (NOS) to convert L-arginine to L-citrulline and NO (13, 14). The types of Ca^{2+}-activated K^+ channels involved in nitric oxide release are likely to be IK_{Ca} and SK_{Ca} channels, while the involvement of BK_{Ca} channels is still unclear (5-7, 9).

Studies have found that ginsenoside Re stimulates endothelial NO production and release in human umbilical vein endothelial cells (11), guinea pig ventricular myocytes (5, 10) and rat thoracic aortic smooth muscle cells (12). Moreover, in human aortic endothelial cells (2) and human umbilical vein endothelial cells (9), ginsenosides Rb_1 and Rg_1 induced nitric oxide production which could be inhibited by a endothelial nitric oxide synthase inhibitor, L-NAME. This supports the postulate that ginsenosides stimulate nitric oxide production via endothelial nitric oxide synthase (eNOS), a known vasoprotective molecule.

Li et al. (1, 13) found that ginsenoside extracts increase NOS activity and NO in porcine aortic endothelial cells. These effects were reversed by TEA inhibition of Ca^{2+}-activated K^+ channels. It was thus suggested that ginsenoside extracts may increase the opening of Ca^{2+}-activated K^+ channels resulting in membrane hyperpolarization, leading to more Ca^{2+} influx into endothelial cells and thus activation of NOS activity, with subsequent increase in NO secretion.

In this project, ginsenoside Re was focused, as opposed to using extracts or other ginsenoside components, because ginsenoside Re is readily available in pure form and it is one of the most studied of the ginsennosides (5, 10-12). As mentioned above, ginsenoside Re is known to possess a vasorelaxing effect, acting via endothelial cell and NO (11). Moreover, ginsenoside Re activated eNOS activities and increases NO release via K_{Ca} in rat thoracic aortic smooth muscle cell, causing vasodilation (12).

Studies in ventricular myocytes found that ginsenoside Re could increase NO secretion in these cells by enhancing eNOS activities, with a consequent decrease in action potential duration (5, 10), suggesting an associated increase in potassium permeability. Therefore, ginsenoside Re may increase Ca^{2+}-activated K^+ channel activity, or that of other K^+ channels, in human coronary artery endothelial cells (HCAECs), leading subsequently to increased intracellular Ca^{2+}, eNOS activation and vasorelaxation. It is also possible that other channels in the endothelial cells may be involved in ginsenoside Re effects.

Research questions

1. What are the ginsenoside Re effects on whole-cell currents of HCAECs?
2. Is SK_{Ca} channel affected by ginsenoside Re?

Hypothesis

1. Ginsenoside Re enhances whole-cell currents of HCAECs.
2. Ginsenoside Re may do so by increasing the currents through SK_{Ca} channel.

Objectives

1. To investigate the effects of ginsenoside Re on HCAEC whole-cell currents.

2. To construct a dose-response curve and determine the EC50 of ginsenoside Re effect on whole-cell current in HCAECs.

3. To test whether ginsenoside Re affects the currents through SK_{Ca} channel.

CHAPTER II
LITERATURE REVIEW

2.1 Ginseng (Origin, Botanical Descriptions)

Ginseng is in Ginseng family or *Araliaceae,* and genus *Panax*, called *Panax ginseng* (20). The genus Panax came from Greek, 'Pan' means 'all' and 'axos' means 'cure' (20). Thus, the literal meaning of 'Panax' can be translated as 'cure-all' (20). The term 'ginseng' represents two Chinese ideograms: 'gin' (pronounced ren) refers to 'man' because the shape of the ginseng root resembles a man and 'seng' (pronounced shen) refers to 'essence' because it is believed to embody man's three mythical essences – body, mind and spirit (20). Ginseng is also referred to as the lord or king of herbs (20).

Ginseng grows in cool weather and is found distributed in two areas. One is the range from 85° to 140° E longitude to 22° to 48° N latitude, i.e., China, Korea and Japan (6). The other is the range from 70°–90° W longitude and 34° to 47° N latitude, which coincides with the southern part of the Canada and the United States of America (6).

The name of ginseng species varies by the area that they are cultivated: China and Korea (*Panax ginseng* C.A. Meyer), Vietnam (*Panax vietnamensis*), Japan (*Panax japonicus*), North America (*Panax quinquefolium*), and in the Himalayas (*Panax pseudo-ginseng*) (4).

The two most commonly used species are Asian ginseng (*Panax ginseng* C. A. Meyer), which is almost extinct in its natural habitat but is still cultivated (4, 21). The other is American ginseng (*P. quinquefolius* L.), which is both harvested from the wild and cultivated (4, 21).

The root of P. ginseng is thick, plump, spindle-shaped and yellowish in color. The shape of ginseng root depends on the composition of the surrounding soils (6). Light and sandy soils cause long, straight, and carrot-like tap roots (6). Heavy and stony soils cause short and thicken roots (6). The rootstock of P. ginseng is un-

branched, thick and plump (6). In wild ginseng, rootstock is elongated but short, thick, compact and upright in cultivated ginseng (6). The leaves are arranged in a circle around the stem and leafstalk (6). The leafstalk is 8-15 cm long, smooth and rounded (6). Each leaf consists of 3-7 leaflets which are serrated and wedge-shaped at the base, narrowing to a sharp point at the apex (6). The flower is umbel-shaped which consists of 4-40 flowers (6). The ginseng fruit is pea-sized that is initially green and becomes red when matures (6). (Figure 2.1)

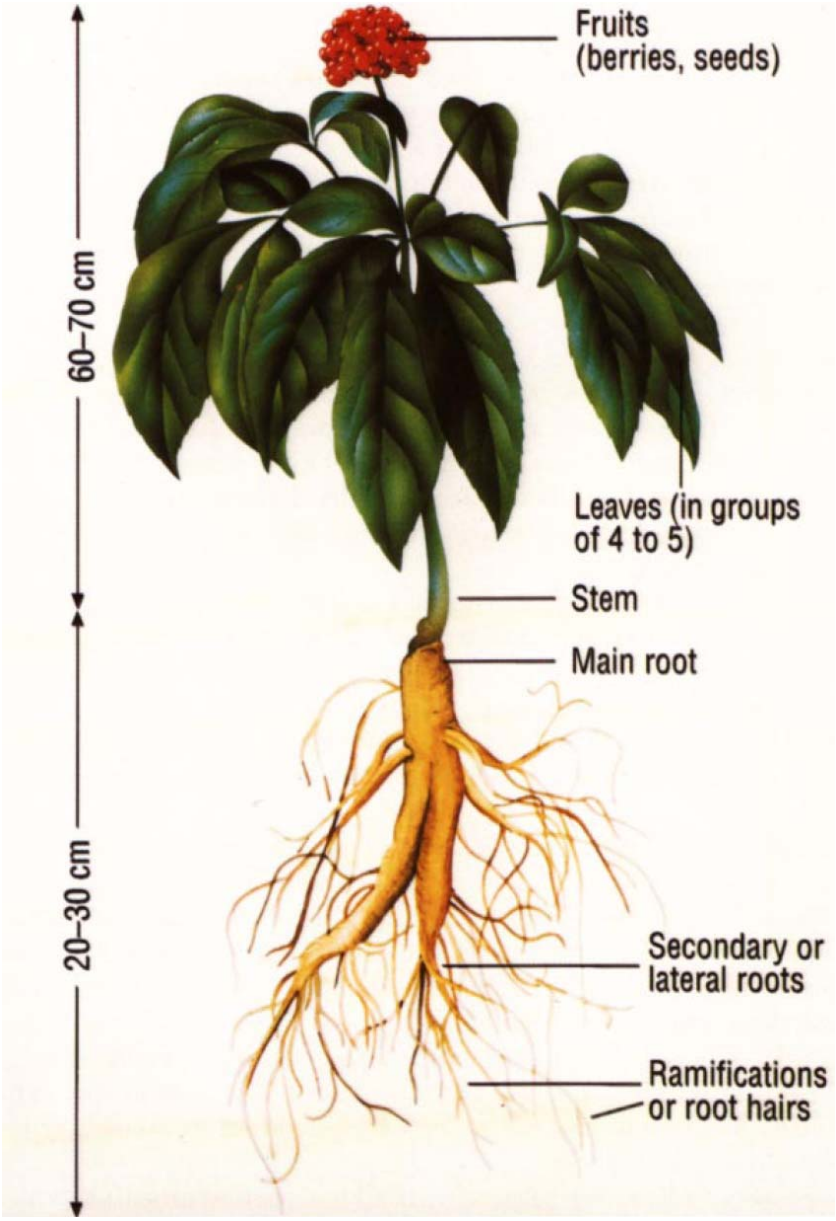

Figure 2.1 Panax ginseng (6).

Ginseng is difficult to cultivate because it needs very specific environmental conditions and is very slow growing (6). The plant cannot endure a strong sunlight and needs a shade to grow (6), which is why it is often found in a deep forest (6). Moreover, the optimum temperature for growing ginseng is only between 0-25°C (6). Analysis of saponin in ginseng root by high performance liquid chromatography (HPLC) revealed that the saponin in the root increased in the 3rd year, decreased in the 4th year and increased again in the 5th and 6th years (22). The 5th or 6th year ginseng is mature enough for commercial purposes (22).

After harvested, the roots are air-dried for a few days; they are called "white ginseng" (3, 6). The white ginseng can maintain its quality for 12-15 months if kept carefully (3, 6). Another method to keep the roots after harvesting is to steam them at 120-130°C for 2-4 hours; ginseng roots processed this way are called "red ginseng" (3, 6). The red ginseng has higher total saponin content and can be kept for 2-3 years if stored properly (22).

2.2 Ginsenosides

Extraction of ginseng by thin layer chromatography (TLC) and methanol extraction experiments demonstrated that the plant has approximately 200 components, such as polyacetylenes, alkaloids, polysaccharides, oligosaccharides, oligopeptides, phytosterols, flavonoids, lipids, minerals, amino acids, fatty acids, phenols, vitamin B1, vitamin B2 and ginsenosides (7, 20, 21). Currently, almost all of the pharmacological effects of ginseng are linked to the active components called ginsenosides which are known as dammarane triterpene saponins (7, 20, 21, 23, 24). Ginsenoside contents were found to vary between 0.5-20 percent, depending on the species, age of ginseng, part of plants, conservation and extraction methods (6, 8, 20). Ginsenosides have a steroid-like structure that consists of four rings (20, 23). (Figure 2.2) Different biological activities of ginsenosides are due to the sugar moieties and aglycone at C-3 (R_1), C-6 (R_2), or C-20 (R_3) (20, 25).

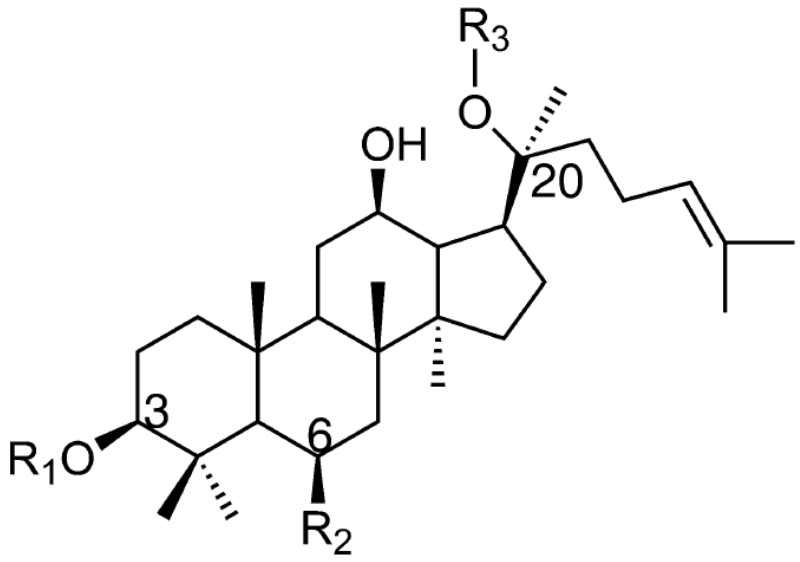

Figure 2.2 Ginsenoside structure (20).

Currently, more than 30 ginsenosides from Panax ginseng have been detected and grouped into two major types by chemical structures.[5-8] (Table 2.1)

1. protopanaxadiols (PPDs), with sugar moieties at positions C-3 (R_1) and C-20 (R_3) such as Rb_1, Rb_2, Rb_3, Rc, Rd, and Ra

2. protopanaxatriols (PPTs), with sugar moieties at positions C-6 (R_2) and C-20 (R_3) such as Rg_1, Rg_2, Rf and Re.

Table 2.1. Two major types of ginsenosides (20).

Ginsenoside	R_1	R_2	R_3
Protopanaxatriol			
Rg_1	H	-O-*glc*	*glc*
Rg_2	H	-O-*glc*(2-1)*rha*	H
Re	H	-O-*glc*(2-1)*rha*	*glc*
Rf	H	-O-*glc*(2-1)*glc*	H
Rh_1	H	-O-*glc*	H
F1	H	-OH	*glc*
Protopanaxadiol			
Rb_1	*glc*(2-1)*glc*	H	*glc*(6-1)*glc*
Rb_2	*glc*(2-1)*glc*	H	*glc*(6-1)*ara*(p)
Rg_3	*glc*(2-1)*glc*	H	H
Rh_2	*glc*	H	H
Rc	*glc*(2-1)*glc*	H	*glc*(6-1)*ara*(f)
Rd	*glc*(2-1)*glc*	H	*glc*
Ra	*glc*(2-1)*glc*	H	*glc*(6-1)*glc*
F2	*glc*	H	*glc*
Compound Y	H	H	*glc*(6-1)*ara*(p)
Compound K	H	H	*glc*
Compound O	*glc*	H	*glc*(6-1)*ara*(p)
Compound Me	*glc*	H	*glc*(6-1)*ara*(f)

It can be seen from ginsenoside's chemical structures that these substances are amphiphilic with a polar or hydrophilic head at carbohydrate side chains and a nonpolar or hydrophilic domain at the steroid-like skeletons (22). The hydrophilic parts can interact with membrane phospholipids and the hydrophobic parts can interact with the hydrophobic section of fatty acids and cholesterol (20). The amphiphilic properties of ginsenosides lead to the interactions between ginsenosides and various membrane proteins, such as receptors, transporters and ion channels that are involved in a wide range of physiology activities (20).

2.3 Ginsenoside Re

2.3.1 Structure and chemical properties

Ginsenoside Re is one of the components of protopanaxatriols, which has been found about 0.1% (w/w) in the root and 0.7% (w/w) in the berry (11). The structure of ginsenoside Re consists of two carbohydrate moieties; Glc or glucopyranoside moieties at C-6 position and Rha or rhamnopyranoside moieties at C-20 position, MW: 947.17 (10).

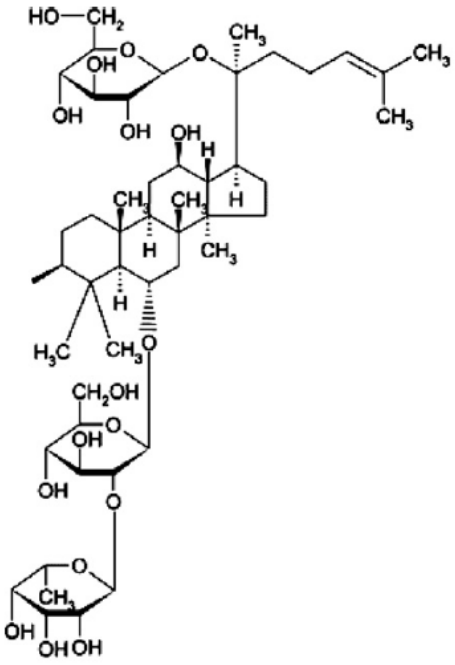

Figure 2.3 The chemical structure of ginsenoside Re (11).

2.3.2 Metabolism, absorption and distribution

Pharmacokinetic studies of ginsenoside Re by ultra performance liquid chromatography mass spectrometric (UPLC/MS) method in mice found that oral absorption of 10 mg/kg ginsenoside Re was only 0.28% with 29.0 ± 25.4 ng/ml maximum plasma concentration (C_{max}) and 0.4 ± 0.2 h maximum drug concentration time (T_{max}) (26). Moreover, injection of 1 mg/kg of ginsenoside Re into mice showed very fast systemic clearance with a half-life of 0.2 ± 0.03 h in male and 0.5 ± 0.08 h in female (26). In addition, intravenous injection in Sprague–Dawley rats with 5 ml/kg of "SHENMAI", which contained ginasnoside Re and was used for treatment of coronary atherosclerotic cardiopathy in China, found that ginsenoside Re had a half-life of about 0.5 h (27). In human, after intravenous injection of "SHENMAI", the concentration-time curve of Re could be fitted with a two-compartment model, T1/2alpha was 0.10 h and T1/2beta was 1.2 h (28). The absorption of ginsenosides in general, not just ginsenoside Re, after oral administration, is very low because of their massive molecular structures (29). The sodium-dependent glucose co-transporter 1 (SGLT1) is a possible protein that is involved in transportation of ginsenosides from gastrointestinal tract into the blood (29). Ways to increase the bioavailability of ginsenosides include co-administration with adrenaline, emulsification of ginsenosides into lipid based formulation, and suppression of p-glycoprotein efflux system (29).

The major pathway of ginsenosides metabolism after oral and intravenous administration is deglycosylation pathway (30). Major metabolites of protopanaxadiols are compound K and protopanaxadiol, while ginsenoside Rh_1, F1 and protopanaxatriol are major metabolites of protopanaxatriols (29, 31, 32). The metabolites of ginsenoside Re are ginsenosides Rg_1, Rg_2, Rh_1, F1 and protopanaxatriol after oral and intravenous administration (29-33).

After ingestion of ginsenoside Re, the C-20 is acid-hydrolyzed in the stomach by deglycosylation of β-D-glucopyranosyl and then converted to ginsenoside Rg_2 (29, 32) or hydrolyzed in the intestine by *Bifidobacterium sp., Leuconostoc paramesenteroides* and *Aspergillus uasmii* (33). In the intestine, ginsenoside Rg_2 is transformed into ginsenoside Rh_1 by *Bifidobacterium sp* elimination of α-L-rhamnopyranosyl (33). Moreover, ginsenoside Re that was not hydrolyzed in the stomach could be changed to ginsenoside Rg_1 by *Bacteroides* JY-6 or *Aspergillus*

niger in the intestine by cutting of the α-L-rhamnopyranosyl (29, 31-33). Then, ginsenoside Rg_1 is deglycosylated to ginsenoside Rh1 and F1 by *Bacteroides* JY-6 via hydrolysis of β-D-glucopyranosyl at C-20 and C-6, respectively (29, 31, 32). Finally, both of ginsenoside Rh_1 and F_1 were hydrolyzed to protopanaxatriol by *Bacteroides* JY-6 through cleaving of the β-D-glucopyranosyl at C-6 and C-20, respectively (29, 31). (Figure 2.4)

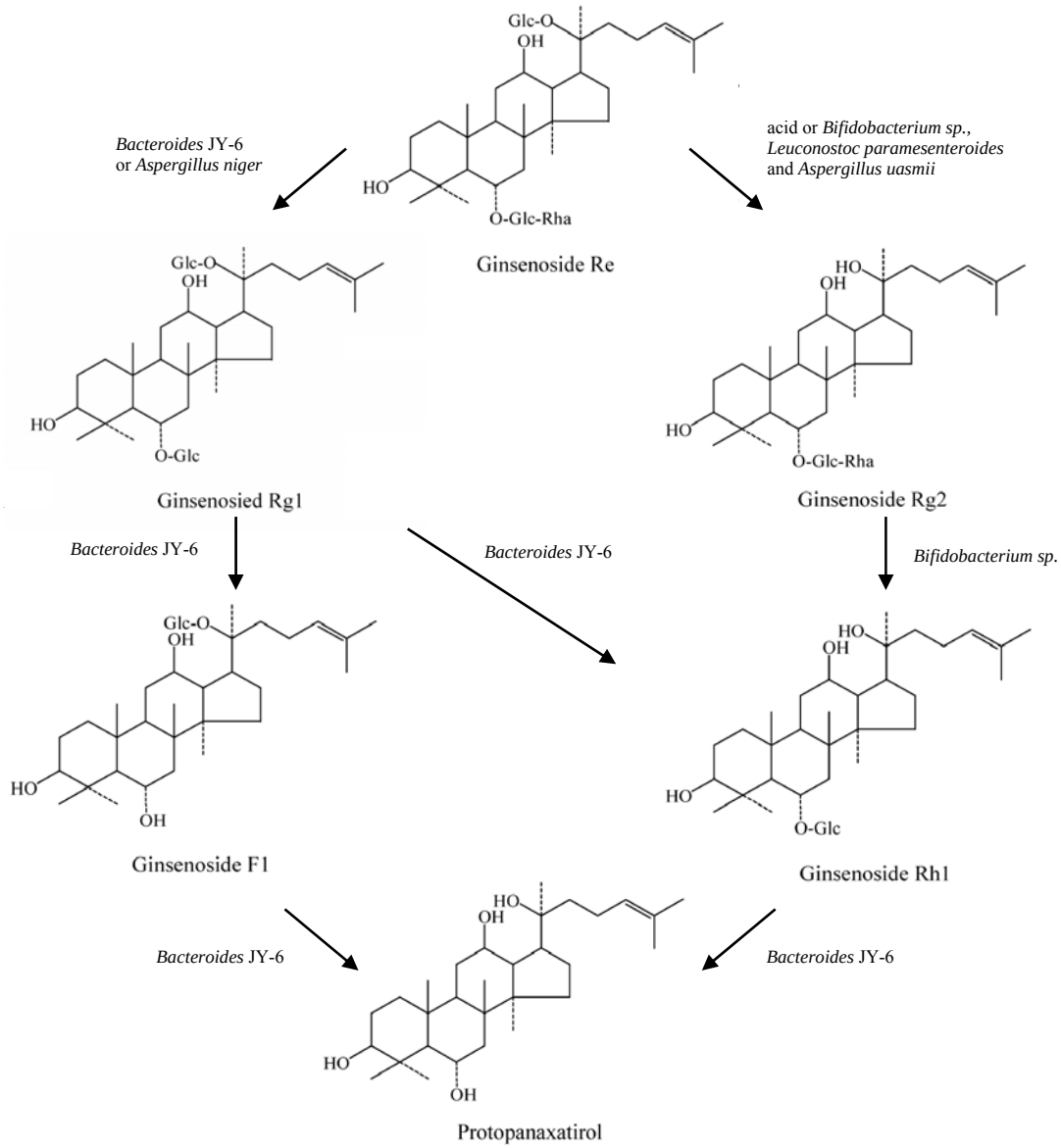

Figure 2.4 Metabolic pathway of ginsenoside Re (31).

2.4 Effect of ginsenoside Re

2.4.1 Nervous system

Pretreatment with ginsenoside Re significantly increased cell viability in 3-(4,5-dimethylthioazol-2-yl) 2,5-diphenyltetrazolium bromide (MTT) assay and significantly decreased lactate dehydrogenase (LDH) release (a marker for cell death) in amyloid β peptide-induced rat pheochromocytoma cell toxicity and hydrogen peroxide-induced newborn rat astrocyte toxicity (34, 35). Moreover, in a study employing newborn rat astrocyte toxicity and another study with middle cerebral artery occlusion rats, pretreatment with ginsenoside Re significantly increased superoxide dismutase (SOD), glutathione peroxidase (GPx) and glutathione reductase (GR) activities (35, 36). These studies showed the effect of ginsenoside Re in preventing cell damage.

2.4.2 Cardiovascular system

In single guinea pig ventricular myocytes, ginsenoside Re decreased both action potential duration at 20% repolarization (APD_{20}) and 90% repolarization (APD_{90}) (10). It was demonstrated that peak inward currents were decreased and late outward currents were increased by ginsenoside Re, indicating that ginsenoside Re could inhibit L-type Ca^{2+} currents ($I_{Ca,L}$) and activate delayed rectifier K^+ currents (I_{Ks}), respectively (10). Using whole-cell patch-clamp technique, it was found that ginsenoside Re enhanced I_{Ks} and suppressed $I_{Ca,L}$ (10). The increment of I_{Ks} and decrement of $I_{Ca,L}$ by ginsenoside Re were inhibited by both nitric oxide synthase (NOS) inhibitor (*S*-Methylisothiourea, SMT) and nitric oxide scavenger (*N*-acetyl-*L*-cystein, LNAC), all of which indicated that the mechanisms involved nitric oxide actions (37). Moreover, thiol-alkylating reagent (N-ethylmaleimide, NEM) and guanylate cyclase inhibitor (1H-[1,2,4]oxadiazolo[4,3-a]quinoxalin-1-one, ODQ) inhibited I_{Ks} enhancement and $I_{Ca,L}$ suppression, respectively (37). These results have shown that ginsenoside Re increased I_{Ks} via direct *S*-nitrosylation of the channel protein and decreased $I_{Ca,L}$ via cGMP-dependent pathway (37). In addition, ginsenoside Re-induced I_{Ks} enhancement of guinea pig ventricular myocytes was inhibited by endothelial NOS (eNOS) inhibitor (L-N5-(l-iminoethyl)ornithine, L-

NIO), Akt inhibitor (SH-6), c-Src inhibitor (PP2) and the PI3-kinase inhibitor (wortmannin). These experiments indicated that ginsenoside Re activated eNOS via a c-Src/PI3-kinase/Akt-dependent pathway and then increased nitric oxide production (5). Increment of I_{Ks} was inhibited by androgen receptor (AR) blocker (nilutamide), estrogen receptor-α (ERα) blocker (ICI-182,780), and progesterone receptor (PR) blocker (mifepristone) (5). Furthermore, ginsenoside Re did not stimulate proliferation of androgen-sensitive human prostate adenocarcinoma (LNCaP) cells and estrogen-sensitive human breast adenocarcinoma (MCF-7) cells (5). Besides, ginsenoside Re did not alter fluorescence resonance energy transfer signals for agonist-induced recruitment of co-activator to the ligand binding domain (LBD) of AR, ERα and PR (5). These results implied that ginsenoside Re activated eNOS via a c-Src/PI3-kinase/Akt-dependent mechanism of non-genomic pathway of sex steroid receptors. It did not activate genomic pathway of sex steroid receptors because it could not recruit co-activators to AR, ERα and PR (5).

Ginsenoside Re suppressed electromechanical alternans (EMA) in cat ventricular myocytes, cat atrial myocytes, Langendorff-perfused cat hearts and human left atrial myocytes (38). In cat ventricular myocytes, ginsenoside Re increased intracellular Ca^{2+} concentration ($[Ca^{2+}]_i$) transient during alternans and decreased sarcoplasmic reticulum (SR) Ca^{2+} content (38). The decrement of SR Ca^{2+} content was due to increasing SR Ca^{2+} release (38). Single-channel recording of SR Ca^{2+} release channels, also known as ryanodine receptors (RyRs), found that ginsenoside Re increased the open probability of these channels (38). It was concluded that ginsenoside Re suppressed EMA in cardiomyocytes by inducing the open probability of RyRs and SR Ca^{2+} released, respectively (38). In chick cardiomyocyte model of acute oxidant injury induced by both exogenous and endogenous oxidants, it was shown that ginsenoside Re decreased 2′,7′-dichlorofluorescein (DCF) fluorescence (measuring reactive oxygen species), and reduced the percentage of propidium iodide (PI) uptake (labelling necrotic cells) (39). In rat ventricular myocytes, ginsenoside Re reduced ventricular myocyte shortening, reduced $[Ca^{2+}]_i$ transient and induced NOS activity (40). The decrement of ventricular myocyte shortening was eliminated by NOS inhibitor (N^{ω}-nitro-L-arginine methyl ester, L-NAME) (40).

Activating Ca^{2+}-activated K^+ (K_{Ca}) channels by ginsenoside Re in rat thoracic aortic smooth muscle cells was dose-dependent with half effective concentration (EC50) of 4.1±0.3 μM (12). The open probability of K_{Ca} channels were inhibited when eNOS inhibitor was present (12). Moreover, Akt inhibitor, PI3-kinase inhibitor and ERα receptor inhibitor blocked the activation of K_{Ca} channels by ginsenoside Re, which indicated that ginsenoside Re activated K_{Ca} channels through c-Src/PI3- kinase/Akt-dependent mechanism of ERα receptor via non-genomic pathway (12).

$[Ca^{2+}]_i$ of human umbilical vein endothelial cell (HUVEC) was dose-dependently increased by ginsenoside Re, with an EC50 of 316 nM and peaked at 30 seconds after application (11). The increment of $[Ca^{2+}]_i$ was eliminated by nonselective cation channel blockers (2-APB) and the absence of extracellular Ca^{2+} (11). Moreover, ginsenoside Re induced NO production with an EC50 of 615 nM and peaked at 100 seconds after application, which was abolished by nonselective cation channel blockers, a lack of extracellular Ca^{2+} and eNOS inhibitor (11). Besides, enhancement of phosphorylated eNOS by ginsenoside Re was prevented by nonselective cation channel inhibitor and loss of extracellular Ca^{2+} (11). Moreover, increment of $[Ca^{2+}]_i$, NO production and phosphorylated eNOS were abrogated by glucocorticoid receptor (GR) antagonist (RU486) and GR siRNA (11). This study indicated that ginsenoside Re bound to GR and increased Ca^{2+} influx via nonselective cation channel enhancing $[Ca^{2+}]_i$, eNOS phosphorylation and NO production (11).

2.4.3 Gastrointestinal system

Cisplatin is a chemotherapy drug for cancers with gastrointestinal adverse effects, such as nausea and vomiting. The symptoms are partially associated with oxidant injury in gastrointestinal tract (41). Pretreatment with ginsenoside Re or American ginseng berry extract (AGBE) significantly attenuated kaolin intake in cisplatin-induced pica in rat (41). Moreover, AGBE reduced the electron spin resonance (ESR) signal which detected superoxide anion and hydroxyl radical (41). Ginsenoside Re is a major component of AGBE, thus ginsenoside Re might have the same antioxidant effect as AGBE (41).

2.4.3 Endocrine and Immunological system

In diabetic rats, treatment with ginsenoside Re for two weeks significantly reduced fasting serum glucose, serum total cholesterol and serum triglyceride levels by about 23%, 32% and 44%, respectively (42). Further, ginsenoside Re significantly increased glutathione levels and decreased malondialdehyde levels in kidneys and eyes of normal rats as well as non-diabetic rats (42). This study showed that the ginsenoside Re could drop blood glucose and lipid levels, moreover, ginsenoside Re had an antioxidant effect in diabetic rats (42). Treatment with ginsenoside Re decreased interferon-gamma (IFN-γ), interferon-related GTPase family M member 1 (IRGM); which induced autophagy, the conversion from LC3(microtubule-associated protein light chain 3)-I to LC3-II; which was a marker of autophagy, and cell death in activated $CD4^+$ T cells that isolated form human peripheral blood mononuclear cells (43). Moreover, ginsenoside Re increased proliferation and cell division and decreased cell death of activated $CD4^+$ T cells (43). This study found that ginsenoside Re enhanced $CD4^+$ T cells survival by decreasing cell death and suppressing autophagy activity (43).

2.5 Vascular endothelial cells

2.5.1 Structural and Functional properties

Vascular endothelium, located in the internal surface of blood vessels, is the biggest organ in the whole body (44). It consists of a single layer of vascular endothelial cells which acts as a selectively permeable barrier (45). Because they are in contact with the circulating blood, endothelial cells have the strategic function of controlling the metabolic and regulatory pathways. Their normal functions include permeation of specific molecules, e.g., proteins, lipid-transporting particles (LDL), metabolites and hormones; non-thrombogenic surface preservation; platelet and leukocyte interaction; vascular smooth muscle cell proliferation and especially vasomotor tone regulation (45, 46). All of these mechanisms were elicited by humoral and hemodynamic stimuli (46). Vascular endothelial cells produce vasodilators, e.g., endothelium-derived relaxing factor (EDRF) or nitric oxide (NO), prostacyclin and

endothelium-derived hyperpolarizing factor (EDHF), as well as vasoconstrictors, e.g. endothelin-1, thromboxane A2, prostaglandin H_2 (13, 14, 45, 46). Normal vascular tone was controlled by a balanced secretion of vasodilators and vasoconstrictors from vascular endothelial cells. When the balance was changed or disturbed, endothelial dysfunction ensues (47).

2.5.2 Mechanism of vasodilator and vasoconstrictor release

2.5.2.1 Endothelium-derived relaxing factor (EDRF)/nitric oxide (NO)

NO is an essential signaling molecule produced by endothelial cells, with important roles in body functions, such as vasodilation, inflammation, gene expression and neurotransmission (48). At rest, NO maintains normal vascular tone by being secreted constitutively from vascular endothelial cells (45). Increased NO production is stimulated by acetylcholine, histamine, and substance P (14), leading to increased inositol triphosphate (IP_3) and Ca^{2+} release from endoplasmic reticulum (ER), respectively (14, 46). Increment of $[Ca^{2+}]_i$ activates opening of K_{Ca} channels and K^+ efflux which cause hyperpolarization of endothelial cells, increasing the discrepancy between Ca^{2+} equilibrium potential and the membrane potential, that is, the Ca^{2+} driving force, leading to enhanced Ca^{2+} influx via nonselective cation channels (13, 14). The Ca^{2+} influx from extracellular fluid is important to NO production. It is the interaction between Ca^{2+} and calmodulin, with tetrahydrobiopterin (BH4), nicotinamide adenine dinucleotide phosphate (NADPH) and flavin adenine mono- and dinucleotides (FMN/FAD) as coactivators, that results in subsequent endothelial nitric oxide synthase (eNOS) activation. The enzyme converts guanidine-nitrogen terminal of L-arginine to L-citrulline and NO (13, 14, 19, 45, 46, 49, 50). In addition, shear stress is a physical stimulus that causes a local enhancement of NO synthesis by activating NOS itself (45, 46). From the endothelial cells, NO diffuses to vascular smooth muscle cells and then interacts with an iron atom of the heme prosthetic group of soluble guanylate cyclase, causing an elevation of cyclic guanidine monophosphate (cGMP) levels (14, 45, 46, 50). The increment of cGMP inhibited the contractile apparatus by decreasing $[Ca^{2+}]_i$ leaded to vasorelaxation (45, 46).

Moreover, a cGMP-dependent mechanism also inhibited platelet aggregation, leukocyte adhesion, migration, and proliferation of vascular smooth muscle cells (45).

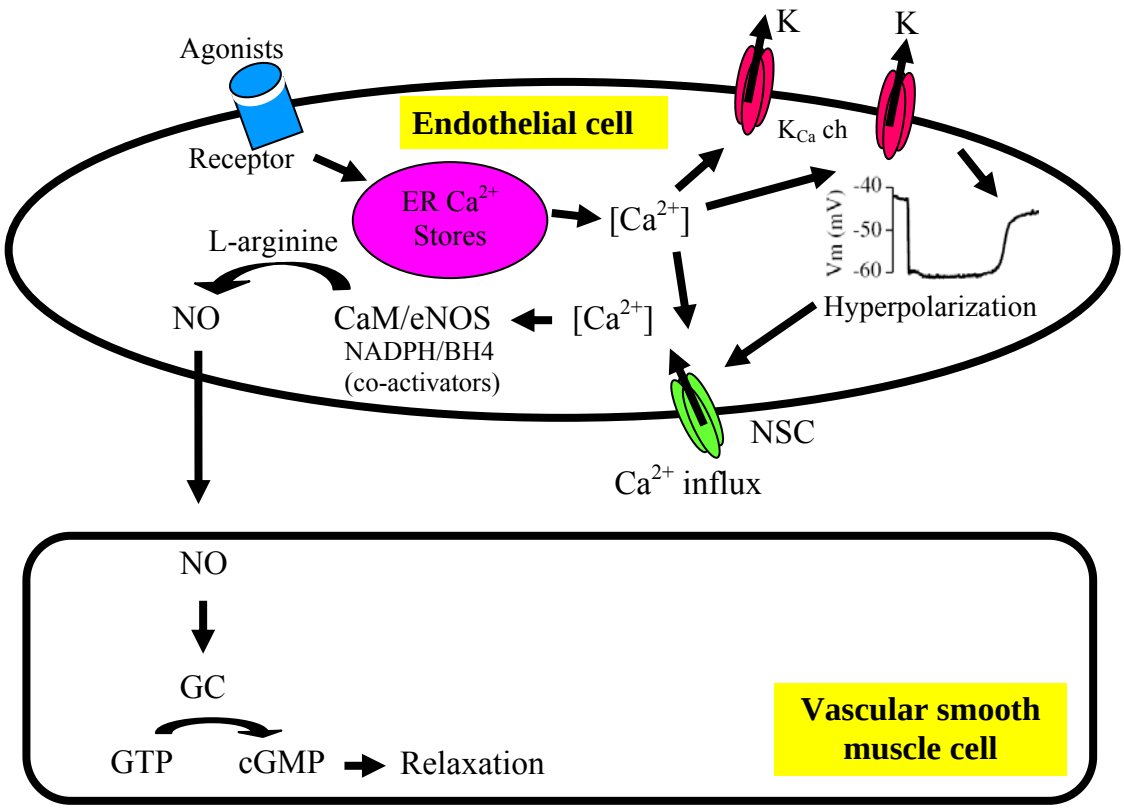

Figure 2.5 Nitric oxide (NO) production (46, 50, 51).

The secretion of NO is initiated by agonist-activated receptor ($5HT_{1B}$-serotonergic, α_2-adrenergic and endothelin-ET_B receptors) causing Ca^{2+} released from endoplasmic reticulum. Increment of internal Ca^{2+} stimulates the opening of K_{Ca} channels followed by membrane hyperpolarization and the subsequent increase in Ca^{2+} driving force. Ca^{2+} influxes into endothelial cells via NSC channels, resulting in eNOS stimulation, catalyzing the change from L-arginine to L-citrulline and NO production. NO reaches vascular smooth muscle cells and activates guanylate cyclase, which in turn converts GTP to cGMP, leading ultimately to vasorelaxation.

2.5.2.2 Prostacyclin

Unlike NO, prostacyclin is non-constitutively secreted from vascular endothelial cells (45). Synthesis of prostacyclin is initiated also by increased cytoplasmic calcium ions leading to activation of arachidonic acid by cyclo-oxygenase and prostacyclin synthase (46). It is produced in response to humoral and hemodynamic stimuli like shear stress, hypoxia, bradykinin and adenosine diphosphate (45). Prostacyclin effects are synergistic with NO; its actions include vasodilatation and inhibition of platelet adhesion and aggregation (45, 50). Stimulation of adenyl cyclase by prostacyclin causes an increase of cyclic adenosine monophosphate (cAMP), which leads to the action of vascular smooth muscle cells and platelets (45, 46, 50).

2.5.2.3 Endothelium-derived hyperpolarizing factor (EDHF)

EDHF is another endothelial vasodilator; it is activated by acetylcholine and inhibited by ouabain, a sodium/potassium ATPase inhibitor (45). Increased intracellular calcium concentration is required to elicit EDHF secretion (46). The relaxation is initiated by increasing potassium ions via increasing conductance of potassium channels, which causes hyperpolarization of vascular smooth muscle cells (45, 46, 50). Calcium-activated potassium channels (K_{Ca}) is responsible for vascular relaxation more than ATP-dependent potassium channels (K_{ATP}) (46, 50). EDHF may be a back-up mechanism. (46). If NO could not be synthesized or activated, EDHF could preserve relaxation of vascular smooth muscle cells in both normal and resistance vessels (46).

2.5.3 Mechanism of vasoconstrictors release

2.5.3.1 Endothelin-1

Endothelin-1 which is secreted from vascular endothelial cells had two different functions. In vascular smooth muscle cells, endothelin-1 binds to ET_A and ET_B leading to increased intracellular calcium concentration and causing vasoconstriction (45, 46). In vascular endothelial cells, binding of endothelin-1with ET_B leads to production of NO, prostacyclin and EDHF which cause vasorelaxation (45, 46). Moreover, endothelin-1 could reduce its own production (45, 46).

2.5.3.2 Thromboxane A2 and prostaglandin H_2

Thromboxane A2 and prostaglandin H_2 are secreted from vascular endothelial cells. Both of them activate vascular smooth muscle cells and platelets via thromboxane receptor, which causes vasoconstriction and platelet aggregation (45).

2.5.4 Endothelial dysfunction

In normal arteries, infusion of acetylcholine or bradykinin causes vasodilation. However, if vasoconstriction occurs instead upon exposure to acetylcholine, endothelial dysfunction is suggested (44-47). Not only vasoconstriction is a manifestation of endothelial dysfunction, but also vasospasm, immoderate thrombosis, and unnatural vascular proliferation can be elicited (45). The dysfunctions are associated with imbalance release of vasodilators, vasoconstrictors, pro-coagulant, anti-coagulant, cell growth factors and cell proliferation mediators, respectively (45). Endothelial dysfunction is a risk factor of atherosclerosis and contributes to cardiovascular diseases, such as cardiac failure, coronary artery disease, myocardial ischemia, chronic heart failure, hypertension, and others diseases including peripheral artery disease, diabetes, and chronic renal failure (44, 45).

2.5.5 Mechanism of endothelial dysfunction

Pathophysiology of endothelial dysfunction is much more complex and involves different mechanisms.

2.5.5.1 NO

Decrement of NO production or bioavailability is a major reason of endothelial dysfunction (44, 46, 47). Aging is the most important cause of turnover and regeneration of human endothelial cells, whose life span is around 30 years (46, 50). This is consistent with a clinical observation that acetylcholine-induced vasodilation is impaired in subjects over 30 years of age (50). Regenerating endothelial cells lose the ability to synthesize NO and can cause vasoconstriction, platelet aggregation and vascular smooth muscle cell proliferation, leading to atherosclerosis and cardiovascular diseases (44, 46). Additionally, decreased NO

production may be due to reduced eNOS activity, by inhibitors or unavailability of L-arginine, and prolonged shear stress (44, 46).

2.5.5.2 Hypercholesterolaemia and atherosclerosis

Impairment of endothelium-dependent relaxation was found in both animals and humans with hypercholesterolaemia (46). Oxidized low-density-lipoprotein (oxidized LDL) caused inhibition of NO formation and increased endothelin-1 which led to endothelial dysfunction (46). Endothelial dysfunction and NO impairment coupled with oxidized LDL increment resulted in acetylcholine-induced vasoconstriction, leading to atherosclerosis (46, 51), especially in large and medium arteries which could cause ischemia and infarction in various organs, such as brain, heart and extremities (51). Cardiovascular disease, a result of atherosclerosis, is a most common cause of death and disability worldwide (52). In coronary artery disease, atherosclerosis is mostly found at coronary artery branch points (46). The first stage of the atherosclerotic process starts with an injury of endothelial cells or endothelial dysfunction (51). This disturbs the homeostatic activity of endothelium and causes enhanced endothelial permeability, leading to increased production of intercellular adhesion molecule 1 (ICAM-1), vascular cell adhesion molecule 1 (VCAM-1), platelet endothelial-cell adhesion molecule 1 (PECAM-1), cytokines, growth factors and E-selectin, as well as recruitment of leukocytes, monocytes, and T-lymphocytes (44, 51, 53). T lymphocytes and monocytes with oxidized LDLs migrate into the intima of arterial walls and become foam cells causing an inflammation (44, 51, 53). The inflammation activates peptide growth factors and leads to stimulation of platelet aggregation, smooth-muscle cells migration, smooth-muscle cells proliferation, collagen synthesis, fibrous cap formation, necrotic core formation and lipid uptake (44, 51, 53). These thicken the arterial walls (44, 51, 53), which may cause subsequent obstruction of the arterial lumen and decreased blood flow seen in cardiovascular events (51).

2.5.5.3 Asymmetric dimethylarginine

Asymmetric dimethylarginine (ADMA) is an endogenous competitive inhibitor of eNOS, which causes inhibition of NO production (44, 49). Elevation of ADMA is one of the markers associated with endothelial dysfunction and atherosclerosis (49). ADMA is eliminated by urine excretion via kidney and

metabolized by the enzyme dimethylarginine dimethylaminohydrolase (DDAH) to citrulline (44). These are the reasons why ADMA is found to increase in patients with chronic renal failure and hepatic dysfunction (44).

2.5.5.4 Oxidative stress

Reactive oxygen species (ROS) bind to NO and convert the latter to peroxynitrite ($ONOO^-$) (44), itself a free radical which can damage proteins and cells leading to apoptosis and endothelial dysfunction, respectively (44). In hypertension and chronic renal failure, where oxidative stress is high, the decrement of NO bioavailability is found, which contributes to endothelial dysfunction and cardiovascular complication (44).

2.5.5.5 Angiotensin II

Angiotensin II (Ang II) causes vasoconstriction and promotes smooth muscle cell proliferation (49). Ang II is associated with endothelial dysfunction by its activation of NAD(P)H oxidase and stimulation of vascular inflammation (44).

2.5.5.6 Hyperhomocysteinemia

Hyperhomocysteinemia is an abnormally high level of homocysteine in the blood which is believed to cause an oxidative excess leading to impairment of NO bioavailability and increment of oxidized LDL levels (44, 54). Moreover, homocysteine can inhibit DDAH and leads to ADMA accumulation (44).

2.5.5.7 Diabetes

Diabetes mellitus (DM) is a disease with high blood glucose, or hyperglycemia, which causes formation of advanced glycation end products (AGE) (44). AGE is a cause of NO impairment and endothelial dysfunction in these patients (44). Moreover, AGE induces the formation of reactive oxygen species (ROS) and activates vascular inflammation, resulting in enhanced interleukin-6, VCAM-1and monocyte chemotactic protein-1 (MCP-1) production (44).

2.5.6 Treatment of endothelial dysfunction

Endothelial dysfunction can be alleviated by employing different mechanisms, some of which may address the cause of the disease.

In impairment of NO, treatment with L-arginine, the precursor for the NO synthesis, enhanced endothelium-dependent relaxation and restored left ventricular wall and pericapillary extracellular matrix thickness in hamsters with experimental hyperlipemia-hyperglycemia (47). In rabbits fed with cholesterol-enriched diet, intimal plaques of the left main coronary artery and aorta was found; however, plaques were not present in animals fed with cholesterol-enriched diet and dietary arginine (55, 56). Moreover, the dietary arginine could reduce platelet aggregation, reduce LDL oxidizability and maintain histological structure of myocardium (56). In human, oral L-arginine supplement decreased blood pressure and systolic pulmonary artery pressure in patients with heart failure (57). In hypercholesterolaemia patients, oral administration of L-arginine could restore acetylcholine-activated coronary blood flow increase (58).

ADMA increase has been reported in hyperglycemia, hypercholesterolemia, hyperhomocysteinemia, hypertension, coronary artery disease and heart failure, causing inhibition of NO (59). Treatment with antioxidants, estrogen, vitamin A, angiotensin receptor blockers (ARB) and angiotensin-converting enzyme (ACE) inhibitors could decrease the ADMA levels (59).

Enhancement of ROS caused decreased NO bioavailability and endothelial dysfunction. Treatment with vitamin C increased acetylcholine-induced vasodilation of resistance vessels in chronic renal failure patients (60). Furthermore, vitamin C could enhance endothelial function in forearm resistance vessels of humans with hypercholesterolemia and chronic smokers (45). In coronary artery disease patients, vitamin C improved brachial artery endothelium-dependent vasodilation (61). Vitamins C and E supplement increased flow-mediated dilation (FMD) of brachial artery in children with hyperlipidemia (62).

ARB and ACE inhibitors restored endothelial function in hypertensive humans and reduced oxidative excess and inflammation (44). Pretreatment with lisinopril (ACE inhibitor) and fluvastatin improved histamine, serotonin and acetylcholine-induced vasoconstriction in atherosclerotic human coronary arterioles (63). Pretreatment with statins or HMG CoA reductase inhibitors in human coronary artery endothelial cells (HCAECs) reduced upregulation of LOX-1, an oxidized low-density lipoprotein (ox-LDL) receptor 1, and induced eNOS expression (64).

Supplementation with folic acid could reduce total homocysteine, decrease LDL sensitivity to oxidation, and improve endothelial function in chronic renal failure children (54). In hyperhomocysteinemic cystathionine beta synthase heterozygote (CBS-/+) mice, folic acid supplementation reduced vasoconstriction in response to acetylcholine and induced NO production of coronary artery (65). FMD of brachial artery in coronary artery disease patients were increased after treatment with folic acid; moreover, incubation of porcine aortic endothelial cells with folic acid could increase eNOS dimer-to-monomer ratio (66).

A new strategy in the treatment of endothelial dysfunction is by employing endothelial progenitor cells (EPCs). EPCs are primitive bone marrow cells which circulate in the blood and are responsible for endothelial differentiation and angiogenesis (67). NOS3 knockout mice had impaired neovascularization and vascular endothelial growth factor (VEGF)-induced endothelial progenitor cells mobilization (68). Treatment with intravenous administration of progenitor cells could improve neovascularization in the mice (68). Expression profile of EPC genes in type-1 DM patients was restored to resemble that of healthy controls after treatment with folic acid supplementation (69). More interestingly, transferring EPCs is a novel procedure for treating endothelial dysfunction and cardiovascular disease. In a case study, EPCs injection could increase left ventricular ejection fraction in acute myocardial infarction patients (70).

2.6 Ion channels in human coronary artery endothelial cells (HCAECs)

Ion channels found in the surface membrane of HCAECs consist of inwardly rectifing K^+ (K_{ir}) channels, nonselective cation (NSC) channels, ATP-sensitive K^+ (K_{ATP}) channels and Ca^{2+}-dependent K^+ (K_{Ca}) channels, and Cl^- channels. No voltage-dependent Ca^{2+} channel is present in these cells (71-75). Endothelial expression of ion channels reported in the literature may vary, even though cells have been derived from the same source, because of the culture conditions, growth conditions, experimental conditions and cell confluence (18, 74).

The channels which influence the resting membrane potential in endothelial cells are K_{ir}, K_{ATP}, Cl^- and NSC channels (18, 74, 76-78). Endothelial cells, when stimulated by acetylcholine, bradykinin and histamine (77), for example, have subsequent increase in $[Ca^{2+}]_i$, leading to enhanced K_{Ca} channel open probability with increased K^+ efflux and hyperpolarization (18, 77), thus increasing cation, especially Ca^{2+}, influx through NSC channels; this may reverse the initial hyperpolarization, causing cell depolarization later (18, 77).

2.6.1 Ca^{2+}-activated K^+ (K_{Ca}) channels

K_{Ca} channels are classified by the single-channel conductance into three types: high-conductance (BK_{Ca}), intermediate-conductance (IK_{Ca}) and small-conductance (SK_{Ca}) Ca^{2+}-activated K^+ channels (18, 77).

2.6.1.1 High-conductance Ca^{2+}-activated K^+ (BK_{Ca}) channel

BK_{Ca} channel has a single channel conductance of about 100-250 pS (18, 77-79). The open probability of these channels is both voltage- and Ca^{2+}-dependent. Inhibitors of channel opening include tetraethylammonium (TEA, 100% block at 10 mM), charybdotoxin, iberiotoxin, d-tubocurarine, paxilline and quinine (18, 77, 80). The BK_{Ca} channels structure is composed of four α-subunits for pore-forming and four β-subunits which contribute to voltage- and Ca^{2+}-sensitivity (18, 79, 80). The α-subunit consists of seven transmembrane domains (S0-S6) and four hydrophobic domains in the cytoplasm (S7-S10). The N-terminus is located in the extracellular space and the α-subunit is coupled with the β-subunit by the way the C-terminus located in cytoplasm (18, 78, 80). The α-subunit can act as voltage- and Ca^{2+}-dependent by itself when β-subunit is absent (18, 78, 80). The voltage sensitivity of the α-subunit is dependent on S4 segment, or the voltage sensor, which contains positive charges of amino acids (18, 80). Moreover, the Ca^{2+}-sensitivity in the α-subunit is found at the "Ca^{2+} bowl," located between S9 and S10 segments, containing negative charges of amino acids (18, 78, 80). In addition, the Ca^{2+} sensitivity of BK_{Ca} channel is found also in the regulator of conductance for K^+ (RCK) domain, which is located between S6 and S7 segments (80). Like all channels in the Pore-loop family, the pore of BK_{Ca} channel is created by the conjugation of four pore-forming regions, from four α-subunits found between S5 and S6 segments (80). The β-subunit is

composed of two transmembrane domains (S1-S2) with N- and C-termini located in cytoplasm (80). The β-subunit interacts with the S0 domain and N-terminus of the α-subunit, leading to potentiation of voltage and calcium sensitivity (80).

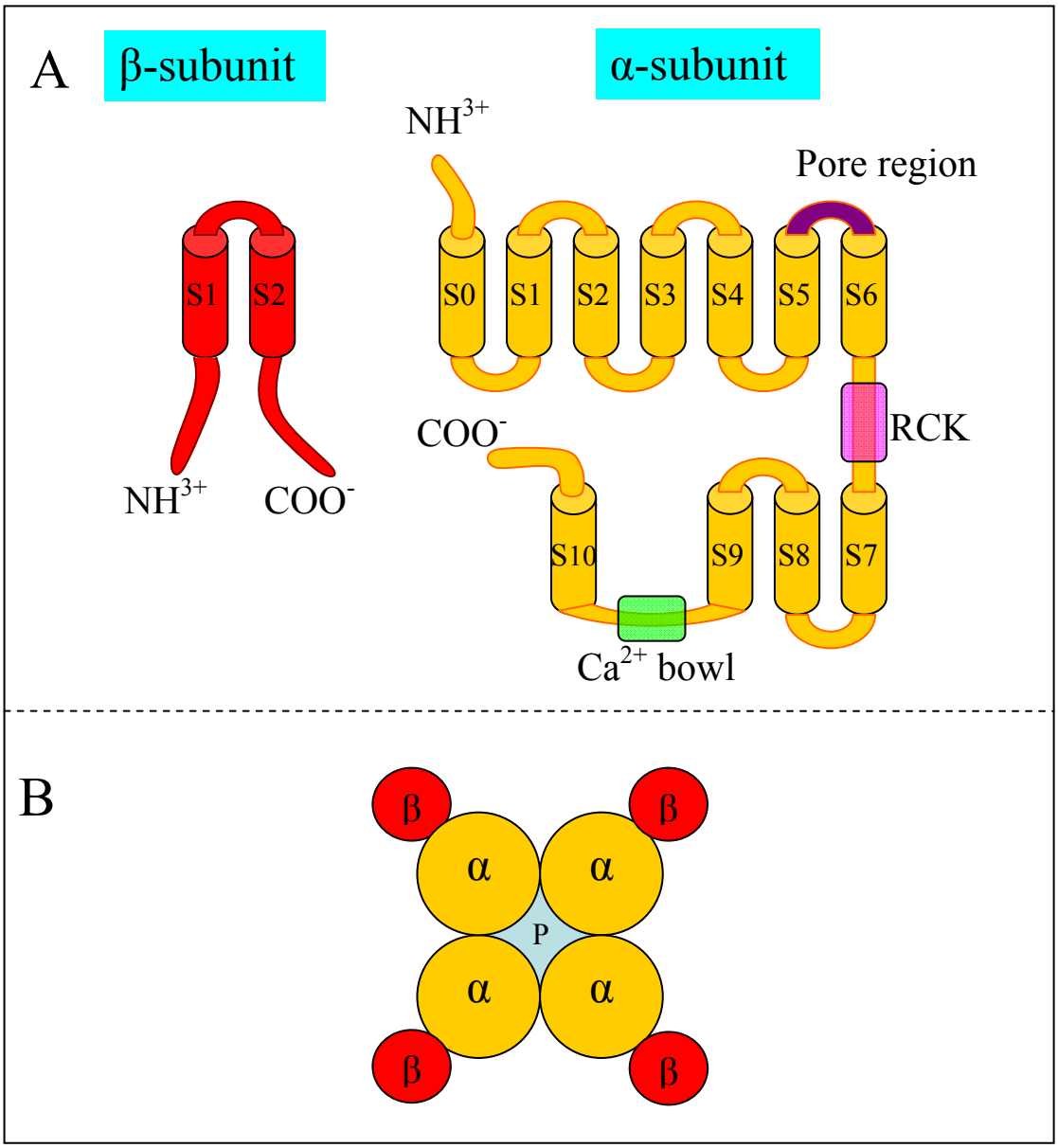

Figure 2.6 BK_{Ca} channel structure (18, 79, 80).

A: The α- and β-subunit structure of the BK_{Ca} channel. The α-subunit consists of eleven hydrophobic domains (S0-S10), pore (p) region, RCK domain and Ca^{2+} bowl. The β-subunit consists of two transmenbrane domain.

B: Postulated BK_{Ca} channel structure containing four α-subunits and four β-subunits.

2.6.1.2 Intermediate-conductance Ca^{2+}-activated K^+ (IK_{Ca}) channel

IK_{Ca} channel has a single-channel conductance of about 20-80 pS (18, 77, 78). The channel is activated by bradykinin, acetylcholine and ATP and blocked by charybdotoxin, quinine, clotrimazole, TRAM-34, tetrabutylammonium (TBA) and TEA (18, 77, 80). IK_{Ca} structure consists of four subunits of six transmembrane domains and pore-forming region between S5 and S6 segments, similar to SK_{Ca} channels (18, 80). Both N- and C-termini are intracellular (18, 80). IK_{Ca} channel is Ca^{2+}-dependent and not voltage-dependent, but it does not have Ca^{2+}-bowl (18). Recently, the Ca^{2+}-binding protein calmodulin (CaM) has been found at the C-terminus which is sensitive to $[Ca^{2+}]_i$ and controls the opening of IK_{Ca} channel (80). Morover, CaM plays important roles in inhibition of voltage-dependent and assembly of IK_{Ca} channel (18, 78, 80).

2.6.1.3 Small-conductance Ca^{2+}-activated K^+ (SK_{Ca}) channel

SK_{Ca} channel has a single-channel conductance of about 4-20 pS (77, 78). This channel is Ca^{2+}-dependent but not voltage-dependent and blocked by apamin, TBA, TEA, clotrimazole, and D-tubocurarine (18, 77, 80). The structure of SK_{Ca} channel consists of four subunits, each having six transmenbrane domains with cytoplasmic N- and C-termini (18, 80). The pore-forming region is also found between S5 and S6 segments (80). The S4 segment has some charged amino acids, but they do not exhibit a voltage sensitivity (80). Similar to IK_{Ca} channel, SK_{Ca} channel structure does not have a Ca^{2+} bowl for Ca^{2+} sensitivity, but CaM is present at the C-terminus to control the channel opening (18, 78, 80).

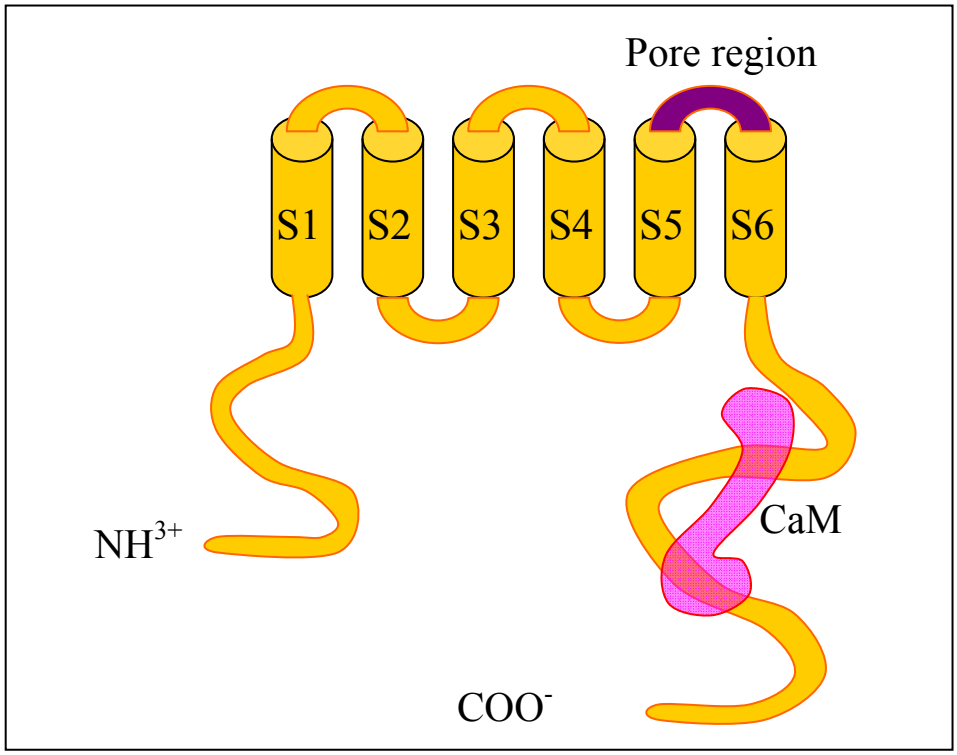

Figure 2.7 IK_{Ca}/SK_{Ca} subunit structure (80).

An IK_{Ca}/SK_{Ca} subunit consists of six transmembrane domains, with pore forming region between S5 and S6 segment. N- and C-termini are located in the cytoplasm. Calmodulin (CaM) is associated with this channel at the C-treminus.

2.6.2 Inwardly rectifying K^+ (K_{ir}) channel

The single-channel conductance of K_{ir} channel is 23-30 pS which is increased upon hyperpolarization and decreased with depolarization (18, 77, 78). The permeability profile of this channel is $P_K > P_{Rb} > P_{Cs}$, and blockers include extra-cellular Ba^{2+}, TEA, TBA, LP-805 (a NO releaser) and Cs^+ (18, 77). K_{ir} channel has four subunits, each of which contains two transmembrane domains (M1-M2; pore-forming region) with both N- and C-termini in the cytoplasm (18, 76, 78). This channel is believed to determine the resting membrane potential of many non-excitable cells (18, 78). At potentials more negative than the K^+ equilibrium potential, large K^+ influx passes through K_{ir} channel, while less K^+ efflux occurs at comparable positive potentials (18, 76, 78). K_{ir} channel acts as a K^+ sensor because a small

increment of extracellular K^+ ($[K^+]_o$) causes a positive shift of K^+ equilibrium potential and increased K_{ir} channel conductance which leads to hyperpolarization of cell membrane (18, 78).

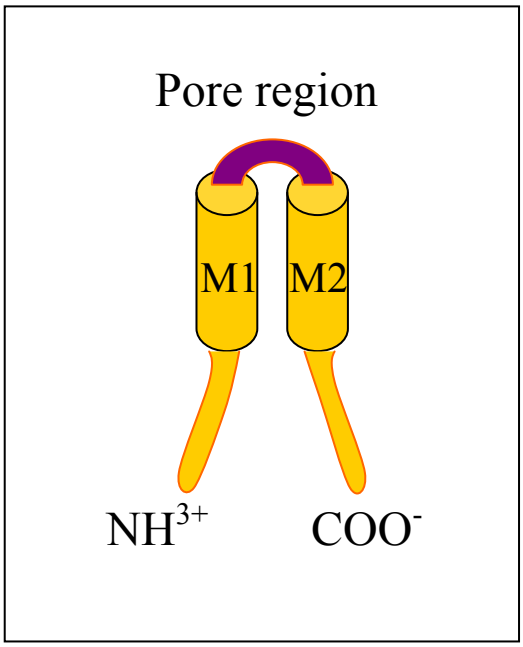

Figure 2.8 K_{ir} channel structure (18).

A K_{ir} subunit consists of two transmembrane domains which act as pore forming region. Both of N- and C-terminal are located in cytoplasm. One K_{ir} channel comprises four subunits.

2.6.3 ATP-sensitive K^+ channels (K_{ATP}) channel

K_{ATP} channel consists of four subunits of two transmembrane domains for pore formation and four subunits of sulfonylurea receptors (SUR) for ATP sensing (73, 76, 78, 79). The pore-forming region of this channel is a member of K_{ir} channel family, while SUR subunit is a member of the ATP-binding cassette (ABC) superfamily (73, 76). In HCAECs, K_{ir} and SUR subunits of K_{ATP} channel are Kir6.1 or Kir6.2 and SUR2B subunits (76). K_{ATP} channel is activated by levcromakalim and pinacydil, and blocked by glibenclamide, increased intracellular ATP concentration, intracellular pH increment, tolbutamide, and TEA (18, 77). In rabbit aortic endothelial

cells, K_{ir} single channel conductance was 25 pS when a K^+ channel activator was applied (18).

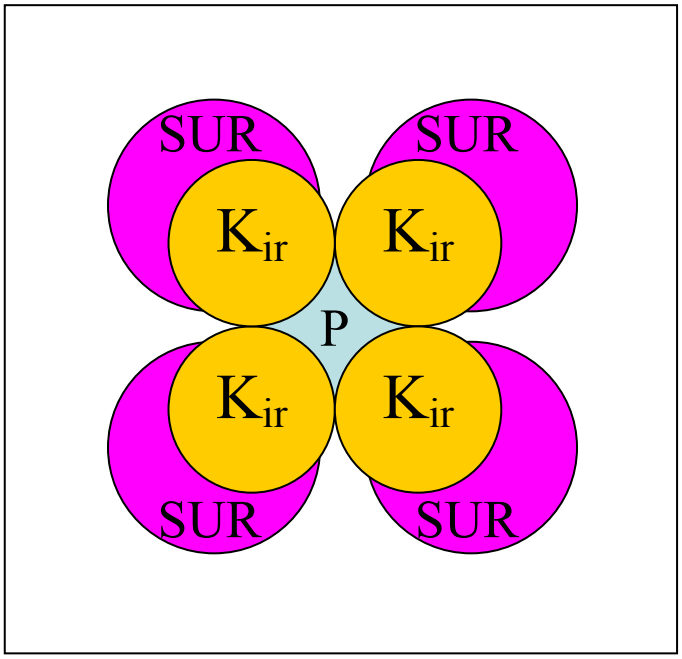

Figure 2.9 K_{ATP} channel structure (79).
A diagram of the top view of K_{ATP} channel which consists of four K_{ir} subunits for pore formation and four sulfonylurea receptor (SUR) subunits for ATP sensing.

2.6.4 Transient receptor potential (TRP) channel

TRP channel superfamily is encoded by *trp* gene which was first discovered in Drosophila photoreceptors (18, 81-83). TRPC or canonical TRP channels are a group of mammalian Ca^{2+}-permeable, nonselective cation channels, which can be divided into three subfamilies, i.e., TRPC (short TRPC), TRPM (long TRPC or melastatin), TRPV (osm-9-like TRPC or vanilloid) (18, 71, 72, 82, 84). In HCAECs, TRPC1, 3-7 were identified by RT-PCR, in situ hybridization and immunohistochemistry (71, 72). TRPC channel consists of four subunits of six transmembrane domains (S1-S6) with cytoplasmic N- and C-termini (18, 71, 81-84). These four subunits of TRPC channel can be either homotetrameric or heterotetrameric (71, 81). The N-terminus contains three or four ankyrin repeats for

protein-protein interaction and a caveolin-binding region for Ca^{2+}-entry (18, 71, 81-84). The C-terminus contains a proline-rich region for protein-protein interaction, a calmodulin-binding region for Ca^{2+} binding and 25 amino acids segment of TRP domain (no known function) (18, 71, 81-84). The pore-forming region is located between S5 and S6 segments (18, 71, 81, 82, 84). The S4 segment does not have positive charges for voltage sensor which is important for voltage-gated Ca^{2+}channels (18, 81, 82, 84). Therefore, Ca^{2+} entry via TRPC channels is dependent on the membrane potential and electrical driving force of Ca^{2+} (81). TRPC channels are activated by histamine, serotonin, bradykinin, substance P, ATP, thrombin and endothelin 1, while blocked by lanthanum (La^{3+}), 2-aminoethoxydiphenylborate (2-APB), SKF-96365, gadolinium (Gd^{3+}) and nickel (Ni^{2+}) (77, 82, 84).

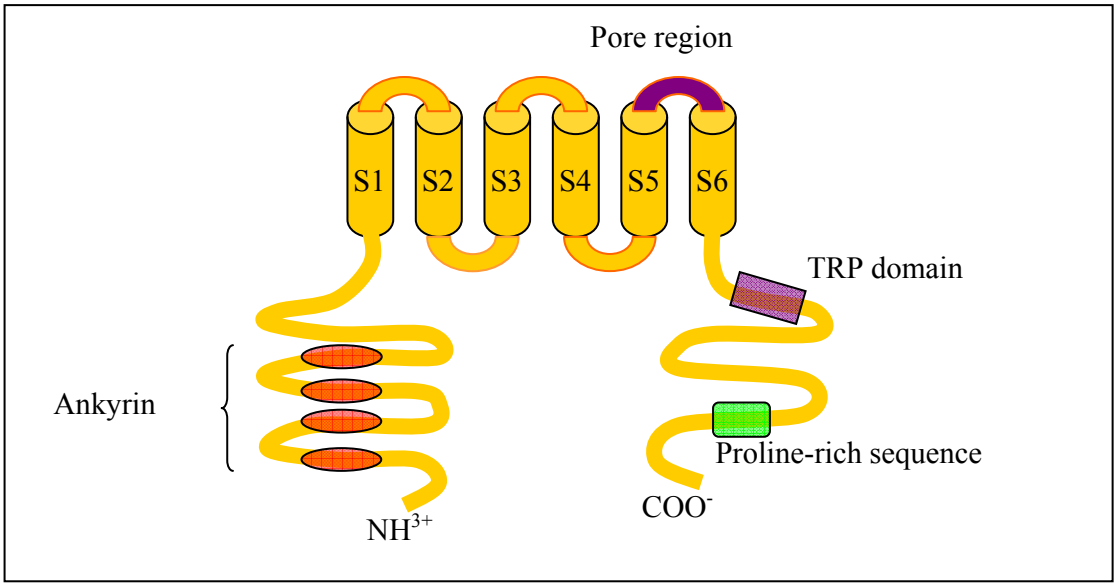

Figure 2.10 TRPC channel structure (18, 71, 81-83).

A TRP subunit consists of six transmembrane domains with cytoplasmic N- and C-termini. The N-terminus has three or four ankyrin repeats and a caveolin-binding region while the C-terminus has a proline-rich sequence, a caveolin-binding region and TRP domain.

2.6.5 Chloride (Cl^-) channels

Three types of Cl^- channels have been described in endothelial cells, i.e., volume-activated Cl^- channel (Cl_{vol} channel), Ca^{2+}-activated Cl^- channel (Cl_{Ca} channel) and high-conductance Cl^- channel (B_{Cl} channel) (77, 85). Classical Cl^- channel blockers are, e.g., 9-AC, anthracene-9-carboxylic acid (DIDS), N-phenylanthranilic acid (NPA), 9-aminocamptothecic acid (9-AC), NPPB, niflumic acid, and Zn^{2+} (18, 77, 78). In human umbilical vein endothelial cell (HUVEC), two types of Cl^- channels were found, i.e., Cl_{vol} channel and Cl_{Ca} channels. However, the Cl^- channel type in HCAEC remains to be characterized (85). The structure of Cl^- channels has not been clearly resolved.

The Cl_{vol} channel is activated by cell swelling, shear stress and cell shape alteration, while inhibited by cell shrinkage (18, 77, 85). Cell volume changes is detected by cytoskeleton element connected with plasma membrane, in response to stress (78). Blocking of Cl_{vol} channel leads to membrane hyperpolarization, driving force increse and Ca^{2+} influx, respectively (18). Cl_{vol} channel is permeable for $I^- > NO_3 \text{-> } Br^- > Cl^-$ and shows outward rectification (18, 77). Single-channel conductance at positive potentials is 40-50 pS, whereas it is 10-20 pS at negative potentials (78). The Cl_{Ca} channel is activated by Ca^{2+} and calmodulin kinase II (CaMK II) and shows outward rectification as well (18, 77, 78, 86). Its open probability is increased by $[Ca^{2+}]_i$ rise and depolarization (78). Moreover, this channel is inactivated at negative potential, but activated at positive potential, with a single-channel conductance around 25 pS (18, 86). The permeability sequence of Cl_{Ca} channel is $I^- > NO_3 \text{-> } Br^- > Cl^-$ (78, 86).

The B_{Cl} channel has a single-channel conductance around 113 to 400 pS, showing outward rectification and activated by stimulation of β-adrenergic and inhibition of protein kinase C (PKC) (18, 77). PKC activation and Zn^{2+} can inhibit the activation of this channel (18, 77). The open probability of B_{Cl} channel is increased at positive potential (77).

2.6.6 K_{Ca} channel expression and localization in endothelial cells

In endothelial cells, BK_{Ca} channels are poorly expressed and may be involved in regulation of NO production (87). On the other hand, the expression of

SK_{Ca} and IK_{Ca} channels are well expressed, but they have different localization (88). SK_{Ca} channels are two or three times more abundant than IK_{Ca} channels (88), and are located in caveolae which are found at homocellular endothelial gap junction sites (87, 88). Moreover, it has been found that endothelial nitric oxide synthase, G protein-coupled receptors and TRP channels are located in the same place with SK_{Ca} channels (88). These strongly suggest the association between SK_{Ca} channels, endothelial hyperpolarization, Ca^{2+} entry and NO production (87, 89). IK_{Ca} channels are not located in caveolae and are found at endothelial projection sites which are associated with myoendothelial gap junctions (87), (88). IK_{Ca} channels are activated by local Ca^{2+} release because they co-localize with endoplasmic reticulum. Activating IK_{Ca} leads to increased Ca^{2+} influx and subsequent smooth muscle hyperpolarization (87), (89).

Reduced expression of endothelial SK_{Ca} and IK_{Ca} channels could be found in conditions with dysfunction of the endothelium (88, 89). Decrement of SK_{Ca} channels causes lowered NO production and high blood pressure (87, 89). IK_{Ca} channels are reduced in endothelial dysfunction, causing attnuation of hyperpolarization responses to acetylcholine in both endothelial cells and vascular smooth muscle cells (89).

2.7 Principles of patch clamp technique

2.7.1 Basic membrane electrophysiology

2.7.1.1 Membrane Biology

Cell membrane is a group of phospholipid bilayers that act as a barrier, controlling exchange of substances between intracellular and extracellular fluid. Phospholipids consist of hydrophilic heads, which facing water, and hydrophobic tails which are kept within the membrane. Many proteins are embedded in the cell membrane, such as ion channels, receptors, cytoskeletal filaments, ionic pumps and enzymes (90).

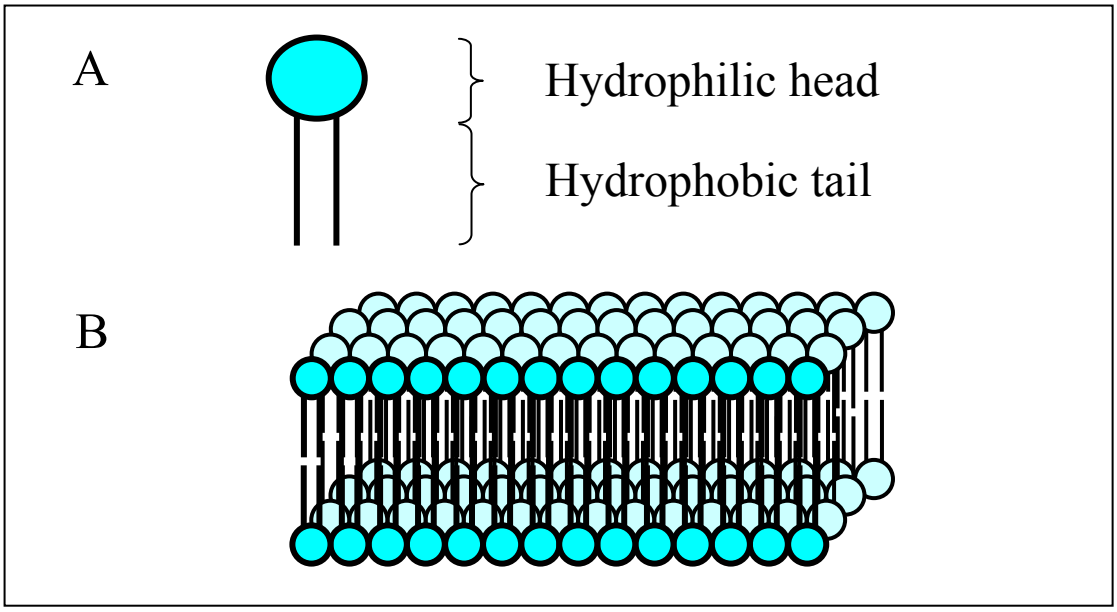

Figure 2.11 Cell membrane structure (90).
A. A phospholipid molecule consists of a hydrophilic head and hydrophobic tails.
B. Phospholipid bilayers

2.7.1.2 Nernst equation

Under physiological conditions, difference in solute concentrations exists between the intracellular and extracellular fluids (90). Therefore, each ion tends to diffuse down its concentration gradient across the cell membrane until it is in equilibrium (90). At the same time, the intracellular side of all cells is more negatively charged than the extracellular side, causing an electrical gradient across the cell membrane; the potential difference between the two sides of the membrane is termed the transmembrane potential or the membrane potential (91). When an ion's chemical and electrical gradients are in balance, there is no net flux of the ion across the cell membrane; i.e. the ion is in equilibrium. The membrane potential at which this happens is called the equilibrium potential. At rest, the resting membrane potential is near the equilibrium potential of potassium ion (E_K), because the membrane is most permeable to potassium ion in this condition (90, 91). The equation describing the equilibrium potential of an ion is the Nernst equation (90). (Figure 2.13)

$$E = \frac{RT}{zF} \ln \frac{[ion]_o}{[ion]_i}$$

Figure 2.12 Nernst equation (78, 90).

E = equilibrium potential of the ion under consideration (V, volts)

R = gas constant (8.31 J mol^{-1} K^{-1})

T = temperature in Kelvin

z = charge of the ion under consideration

F = Faraday constant (9.65 x 10^4 $Cmol^{-1}$)

$[ion]_o$ = extracellular concentration of the ion under consideration

$[ion]_i$ = intracellular concentration of the ion under consideration

2.7.1.3 Ohm's law

In electrophysiology, Ohm's law (figure 2.14) is the most important equation for describing the flow of current through an ion channel which is driven by the electrical potential difference between the membrane potential and the ion's equilibrium potential (78, 90-92).

$$\Delta V = IR = \frac{I}{G}$$

Figure 2.13 Ohm's law (78, 90-92).

ΔV = $V-V_R$ or electrical driving force; when V is the membrane potential and V_R is the equilibrium potential (V, volts)

I = current (A, amperes)

R = cell resistance (Ω, ohms)

G = conductance (S, siemens)

2.7.1.4 Equivalent circuit of the cell membrane

The relationship between the membrane and ion channels can be described as a simple electrical circuit diagram. In this circuit, cell membrane is a capacitor, an ion channel is a conductor or a resistor, and membrane potential is a battery (78, 90). The membrane acts as a capacitor because it is a lipid insulator located between the intracellular and extracellular fluids which contain conductive ions (90). The membrane potential exerts an electric field across the membrane (90). Negative charges are arranged inside and positive charges are arranged outside of the membrane (90). This is much like the situation of a capacitor in an electrical circuit. Since the area of a capacitor is directly proportional to its capacitance, it follows that the cell membrane surface area can be calculated from the cell membrane capacitance (90). The specific capacitance of most biological membranes is 1 $\mu F/cm^2$ (90).

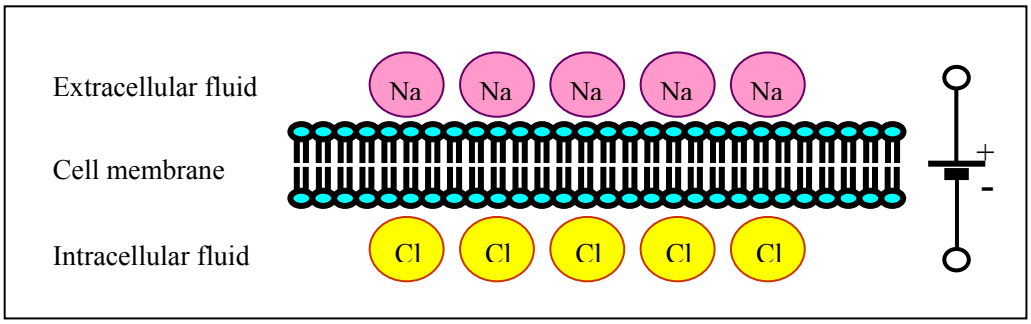

Figure 2.14 Cell membrane as a capacitor (90).
Membrane potential is caused by arrangement of positive charges on the extracellular side and negative charges on the intracellular side of cell membrane

Having electrically conductive pathways, i.e., ion channels, in the membrane in parallel with the membrane capacitor, results in an equivalent circuit of the membrane as shown in figure 2.16. The circuit is divided into two branches, the conductive and capacitive branches (78). (Figure 2.16)

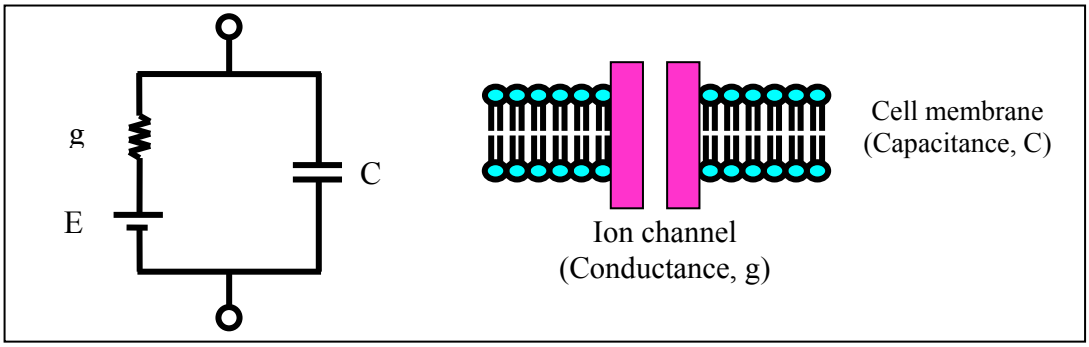

Figure 2.15 Diagram showing an equivalent circuit of the membrane (78, 90, 91). This circuit consists of a conductor (g) representing an ion channel, a capacitor (C) representing a cell membrane and a battery (E), in this case representing the equilibrium potential of the permeating ions of channel in the diagram.

2.7.2 Patch clamp technique

Patch clamp technique is a method for measuring ionic current flow of a small cell (< 20μm) under voltage clamp (93). Voltage clamping is a condition where the membrane voltage is maintained at a constant value to record membrane currents for studying ion channel activity (90-93). Another possible recording mode, current clamping, on the other hand, is where membrane currents are clamped constant for studying changes in membrane potential, e.g., action potential (90-92). When voltage clamping was first developed, two electrodes were needed, one for membrane voltage sensing, the other for current injection (90, 93). These electrodes interacted with each other through a feedback amplifier (93). Opening of ion channels caused increased membrane conductance, increased membrane currents and a change in membrane voltage from the set potential (command voltage, e.g. holding potential) which would be detected by the voltage-sensing electrode. The feedback amplifier would inject a current through the current-injecting electrode to maintain the membrane potential at the set value (90, 93). The injected currents would have the same magnitude but opposite in direction with the currents through the ion channels and would be proportional to the change in the conductance of the cell (90, 91, 93). Two-electrode method has a disadvantage because it cannot be used with small cells (< 20μm), where piercing membranes with two electrodes would cause too much injury to the cell.

Nevertheless, this method is still in use today for electrophysiological study of very large cells, such as *Xenopus* oocytes. This limitation has led to the development of single-electrode recording methods (90, 93).

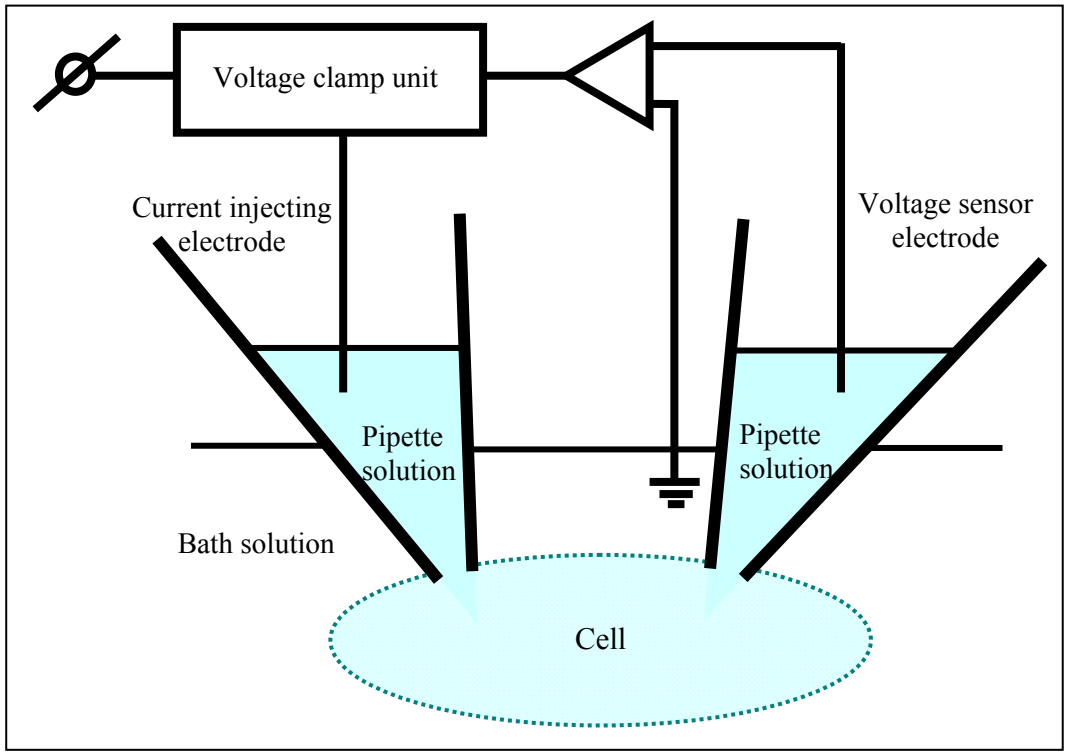

Figure 2.16 Two recording electrodes of voltage-clamp configuration (90).
Voltage change is detected by a voltage sensor electrode and sent to an amplifier in voltage clamp unit. The amplifier will send the current back to the cell via current injecting electrode to stable the membrane potential.

Discontinuous single-electrode voltage clamp uses only one electrode for voltage detecting and current injecting (93). The switching amplifier receives the voltage change signal and compares to the command voltage, then sends the currents back to the same electrode within a short period (93). The disadvantage of this method is that alternate voltage and current switching lead to unstable membrane potential (91, 93). Moreover, both the discontinuous single-electrode and two-electrode voltage

clamp have the same disadvantage, an unknown or unstable voltage drop by series resistance (93).

Continuous single-electrode voltage clamp or patch clamp employs only one electrode with continuous voltage detecting and current injecting (91, 93). Any voltage change will be compared with the holding potential by the feedback amplifier in the current-voltage converter (93). Then, the amplifier adjusts the voltage by passing the different voltage to a high impedance resistor and sends the currents back to the cell (93). This technique yields more satisfactory results than the two-electrode and discontinuous single-electrode voltage clamp methods (93). A blunt and low resistance micropipette is used in this method for forming a high-resistance seal (more than 1 GΩ) or gigaseal between the glass microelectrode's tip and the cell membrane by gently touching the cell and a gentle suction (91-93). This condition has been shown to cause a small current leakage (not more than 10 pA) which dose disturb the whole currents of ion channels (92).

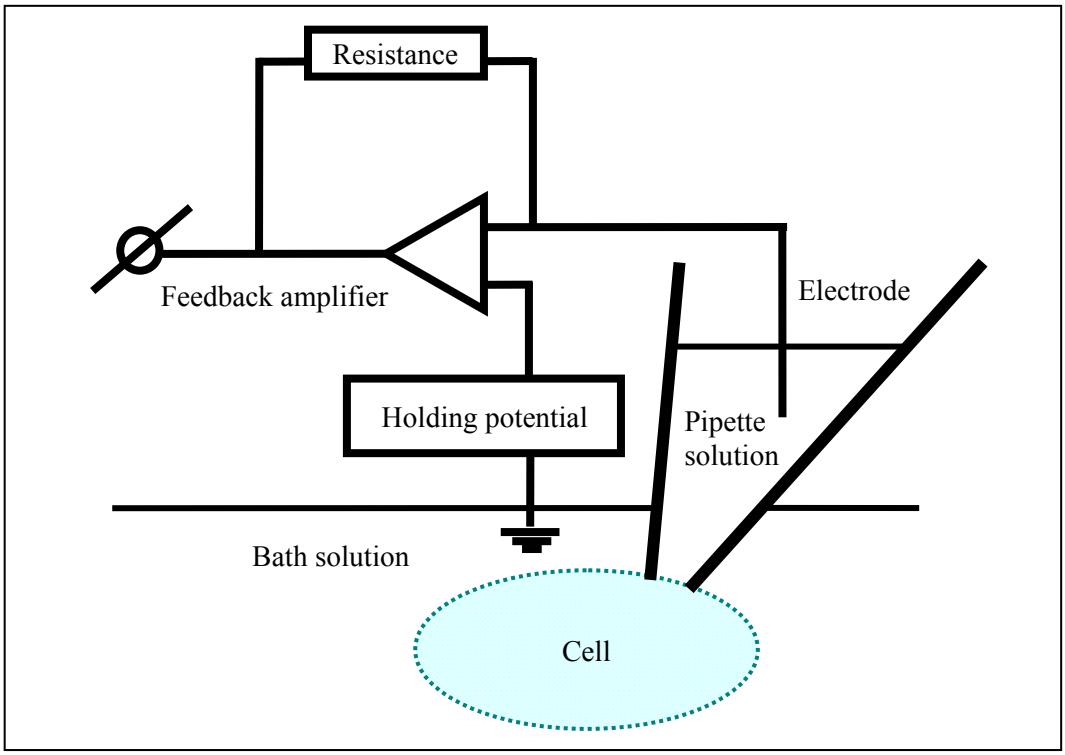

Figure 2.17 Continuous single-electrode voltage clamp or patch clamp (90, 93).

Both continuous voltage recording and current injection are accomplished through the use of only one electrode. The voltage is compared with the holding by the feedback amplifier and the voltage difference would be changed to current by a resistor.

2.7.3 Configurations of patch clamping

2.7.3.1 cell-attached configuration

Cell-attached configuration is a non-invasive technique which leaves the cell and the intracellular environment intact (94). This technique involves touching the cell membrane with the micropipette tip, making a high resistance seal (90, 94). Ion channel activity in the membrane patch under the tip of the micropipette is recorded (90). Single channel activity can be recorded in this configuration (single-channel recording) (90).

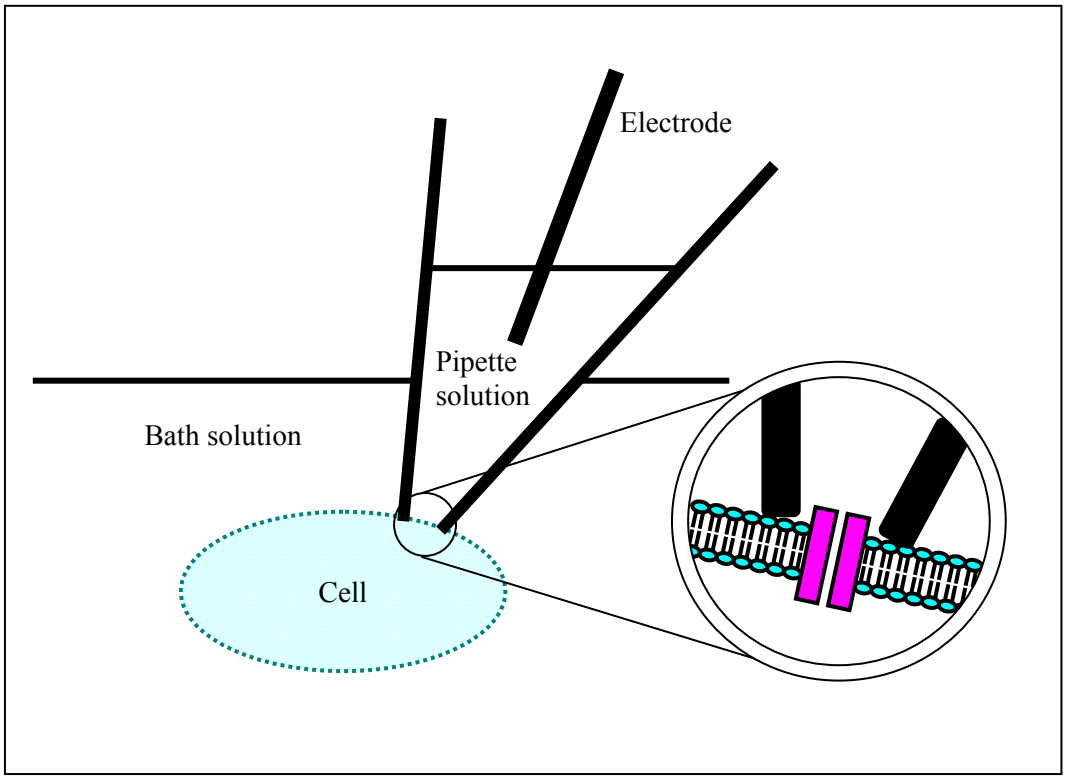

Figure 2.18 Cell-attached configuration (90).

2.7.3.2 whole-cell patch clamp configuration

Whole-cell patch clamp configuration starts with the cell-attached configuration and then the patch area under the micropipette tip is ruptured by voltage or gentle suction (90, 92, 94). The rupture leads to a connection between the cytoplasm and the pipette solution (90, 92, 94). Because of the very small volume of the cytoplasm, it is completely replaced by the pipette solution after cell rupture (90, 92, 94). If physiological condition is required, the pipette can be filled with ionic components that mimic cytoplasmic components (90). Whole-cell patch clamp configuration allows studying ionic currents flowing through all channels of the individual cell (92, 93). To study currents going through one type of ion channels, the ionic composition of the bath and pipette solution can be manipulated, or known channel inhibitors can be employed (94). Moreover, this technique can be used for studying cell capacitance, exocytotic activities, signaling pathways and gating of ion channels (92, 94).

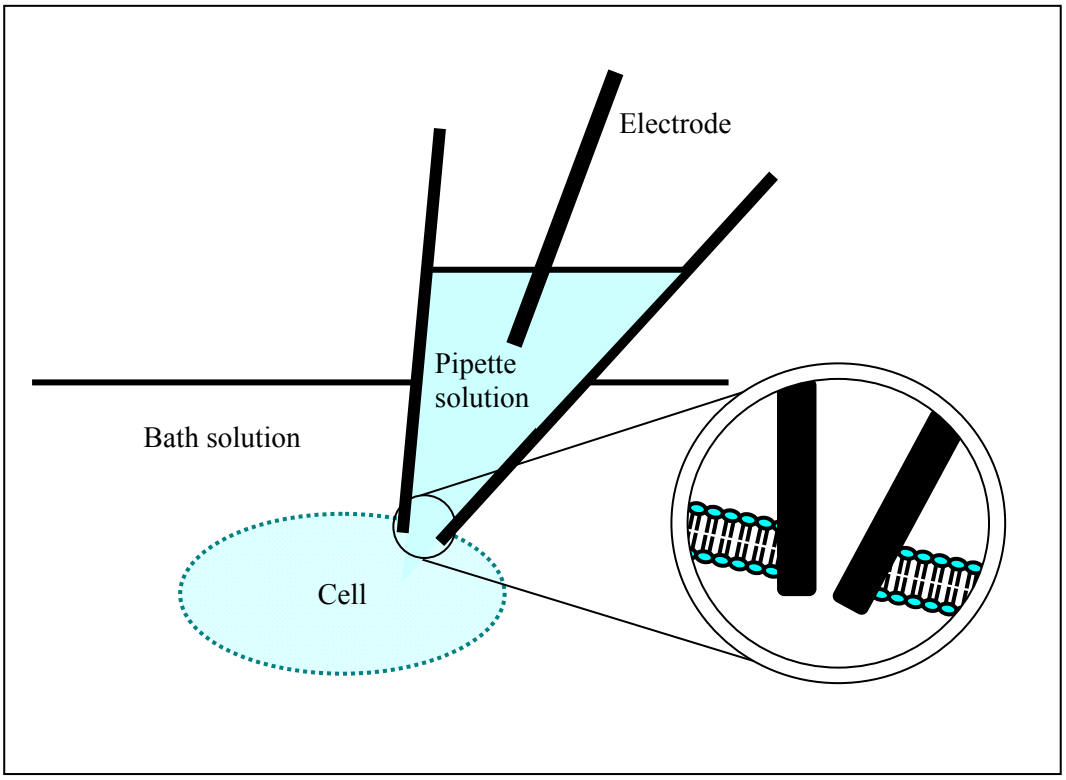

Figure 2.19 Whole-cell patch-clamp configuration.

2.7.3.3 Perforated patch clamp configuration

The washout (dialysis) of cytoplasm in the whole-cell patch clamp configuration becomes a trouble for studying cytosolic factors and intracellular signaling (90). Moreover, the dialysis can cause impairment of ion channel property and function which leads to a decrease in ion channel currents (94). To solve this problem, the perforated patch clamp technique has been developed, achieving good electrical contact and intact cytoplasmic composition (90, 94). In this technique, a membrane-perforating agent, such as nystatin or amphotericin B, is added into the pipette solution (90, 94). These agents create some pores in the membrane patch under the micropipette tip which are permeable to ions but not for larger particles, such as second messenger molecules (90, 94).

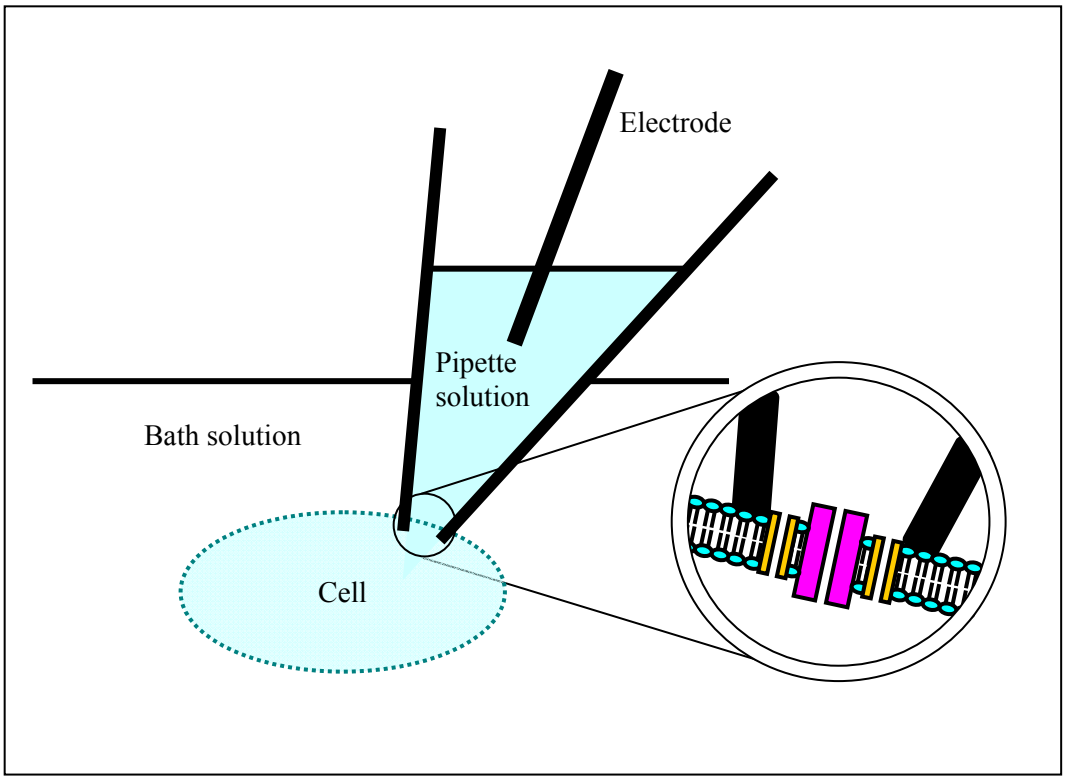

Figure 2.20 Perforated patch-clamp configuration.

2.7.3.4 outside-out patch clamp configuration

Outside-out patch clamp configuration starts with the whole-cell patch clamp configuration (90). Then the micropipette is withdrawn from the cell, taking with it small membrane around the micropipette tip (90, 94). The free margins of the torn membranes can reseal, forming a vesicle and allowing the outside of the membrane to contact with the bath solution (90, 94). This technique can provide excellent control of both the intracellular and extracallular environments (90, 94). Outside-out patch clamp configuration is suitable for studying the effect of extracellular ligand on the ion channels (90, 94).

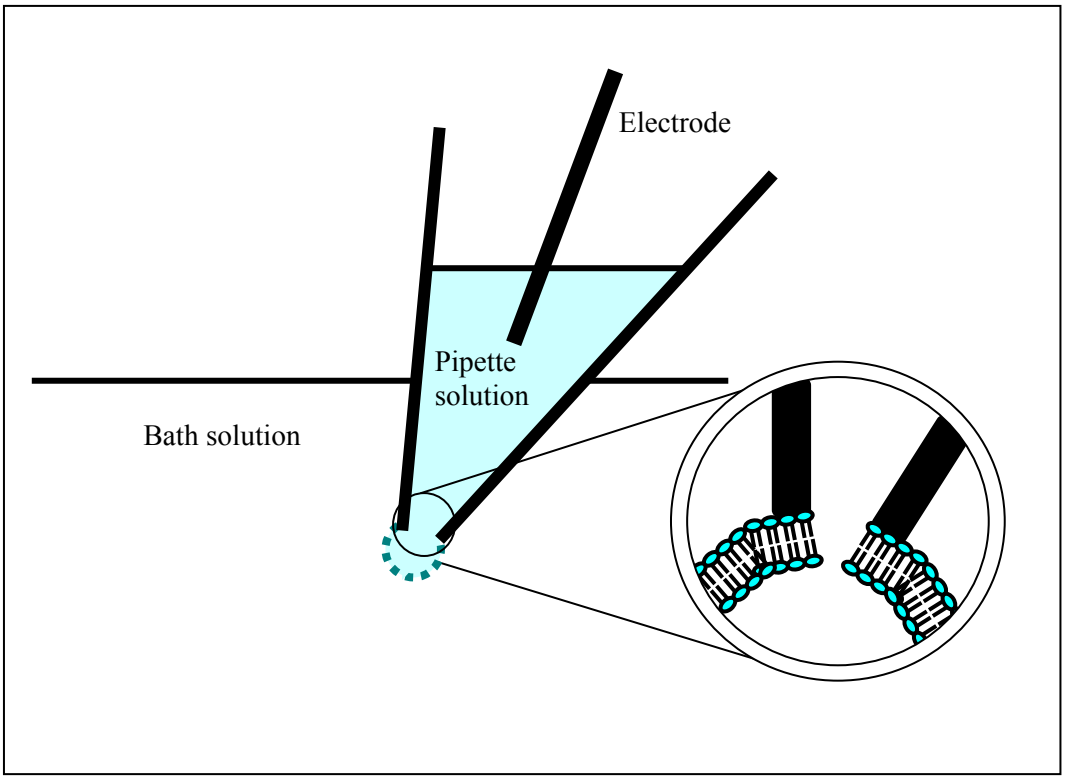

Figure 2.21 Outside-out patch-clamp configuration.

2.7.3.5 inside-out patch clamp configuration

Inside-out patch clamp configuration starts with the cell-attached patch clamp configuration (90). The micropipette is pulled away from the cell, and the torn membrane reseals, forming a vesicle at the tip of micropipette, similar to the outside-out patch clamp configuration (90). The vesicle is broken by exposure to the air, leading to a direct contact between the inside of the cell membrane under the micropipette tip and the bath solution (90). This technique is suitable for studying the regulation of ion channels by cytosolic ligands (90, 94).

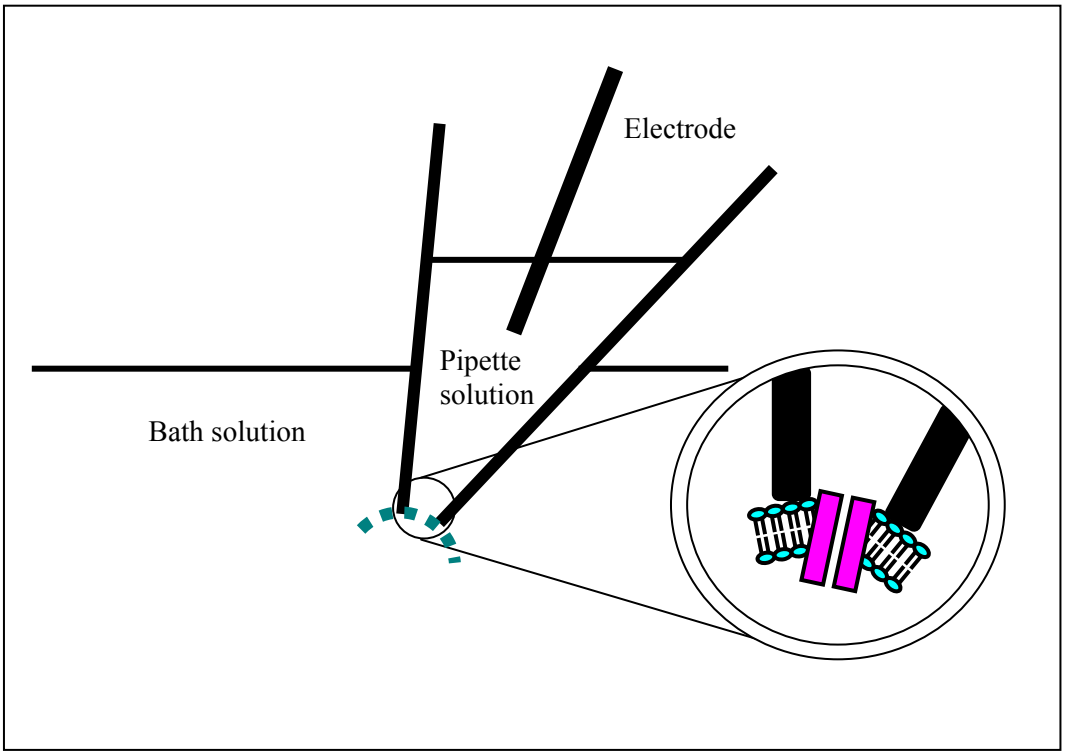

Figure 2.22 Inside-out patch-clamp configuration.

CHAPTER III
MATERIALS AND METHODS

3.1 Cell preparations

3.1.1 Cell culture

Cultured human coronary artery endothelial cells (HCAECs), third passage, were obtained from Lonza Walkersville Inc., USA. Routine characterization of HCAECs performed by the cell provider included immunofluorescent staining. Cells were stained positive for acetylated LDL and von Willebrand (Factor VIII) antigen, but negative for smooth muscle α-actin. Cells of fourth to eighth passages were plated on coverslips for electrophysiological experiments. Aliquots of cells were preserved in cryovials for future experiments.

3.1.2 Culture medium

Culture medium was composed of endothelial cell basal medium (EBM), 5% fetal bovine serum (FBS), 0.1% antibiotic (gentamycin sulfate amphotericin-B, GA-1000), 0.1% endothelial growth factor (rhEGF), 0.1% hydrocortisone and 0.4% bovine brain extract (BBE). All components were obtained from Lonza Walkersville Inc., USA.

3.1.3 Enzyme and substances for cell isolation

HEPES-buffered saline solution (containing 30 mM HEPES), trypsin/EDTA (containing 0.25 mg/ml trypsin) and TNS (trypsin-neutralizing solution) were obtained from Lonza Walkersville Inc., USA. (EDTA, ethylenediaminetetraacetic acid; HEPES, 4-(2-hydroxyethyl)-1-piperazineethanesulfonic acid)

3.1.4 Preparing cells for electrophysiology

HCAECs of the third passage were stored in liquid nitrogen. Fourth to tenth passages were subcultured from the third passage, and any unused cells were kept in a -70°C freezer until needed. The subcultured cells were stored in flasks containing the culture medium which were changed every 2-3 days. A flask with maximum cell growth (around 80% density) was selected for an experiment. Culture medium were removed and the remaining cells were washed with HEPES-buffered saline solution. HCAECs were isolated into single cells by incubating with 0.5 ml trypsin/EDTA for 2-5 minutes. The isolation was completed when 90% of the cells were round and floating, after which 0.5 ml TNS was added for neutralizing trypsin and the solution was then removed to contain in an eppendorf for centrifugation at 1000 rpm, 4°C, for 5 minutes. Then the supernatant was discarded and 1 ml cell medium was added and mixed with the cells. Finally, cells were plated on coverslips in 35 mm petri dishes for the experiments. Some cells were plated in a new flask for the next culture passage. All cells were kept at 37°C in a humidified incubator with 5% CO_2. Cells were ready for an electrophysiological experiment after 4-5 hours of incubation.

3.1.5 Coverslips preparation

Coverslips (18 x 18 mm; Menzel GmbH & Co KG, Braunschweig, Germany) were cut into eight pieces (4.5 x 9 mm). They were cleaned by incubation in 2 mM NaOH for 2 hours, followed by a thorough washed with dH_2O. They were next stored in 70% ethanol for one night. Finally, the coverslips were dried in a 40^oC oven and sterilized by ethylene oxide (EO) gas. Throughout the cleaning process, care was taken not to touch the glass coverslips directly, to avoid contamination with organic materials from skin, which could prevent effective poly-L-lysine coating (3.1.6).

3.1.6 Poly-L-lysine coating

All steps were done under sterile conditions. Poly-L-lysine (Sigma Chemicals, St Louis, MO, USA) was prepared as a 1:10 solution (poly-L-lysine:water, v/v). One day before an experiment, coverslips were immersed for ten minutes in

poly-L-lysine solution in a 35 mm petri dish. Then the coverslips were left to dry overnight at room temperature.

3.2 Electrophysiological experiments

3.2.1 Patch-clamp setup

Whole-cell patch clamp configuration was used in all the experiments. Cells were visualized under 400-fold magnification of a phase-contrast, inverted microscope (Nikon Eclipse TE 2000-u, Tokyo, Japan). Cells were placed in a 150-µl recording chamber (RC-26, Warner Instrument, Hamden, Connecticut, USA) mounted on the microscope stage. Solutions in the recording chamber were grounded by an agar bridge. A headstage (a current-voltage converter, CV 202B, Axon Instruments, Molecular Devices, Sunnyvale, California, USA) was mounted on a manual micromanipulator (MX-2, Narishige, Tokyo, Japan), and connected to a patch-clamp amplifier (Axopatch 200B, Axon instruments), an analog-to-digital converter (Digidata 1440A, Axon instruments) and a personal computer, respectively. A Faraday cage covered the inverted microscope, headstage, micromanipulator and the flow system to minimize extraneous electrical noise. In addition, power line noise going into the patch-clamp amplifier was mostly eliminated by using the line conditioner capability in the following components, respectively: an uninterrupted power supply (Powermetric, Bangkok, Thailand), a surge protector (Belkin, Gold series, Belkin International, Los Angeles, California, USA), and a power distributor with a power cable (Hydra Model-2 with Python cable, Shunyata Research, Poulsbo, Washington, USA). The microscope and the micromanipulator were placed on a handmade anti-vibration table which was supported by several doughnut-shaped balloon diaphragms (Newport Corporation, CA, USA). (Figure 3.1)

3.2.2 Electrophysiological recording

Cell membrane currents were collected by a Ag/AgCl electrode connected to the headstage, which converted the current to voltage signal. The signal was then sent to the patch-clamp amplifier, for filtering (5 kHz, low-pass Bessel filter), conditioning and amplification. Then the analog signals were sampled at 4 kHz by the

analog-to-digital converter. Data were displayed on a personal computer and analyzed by using the program pClamp version 10.0 (Axon Instruments). (Figure 3.1)

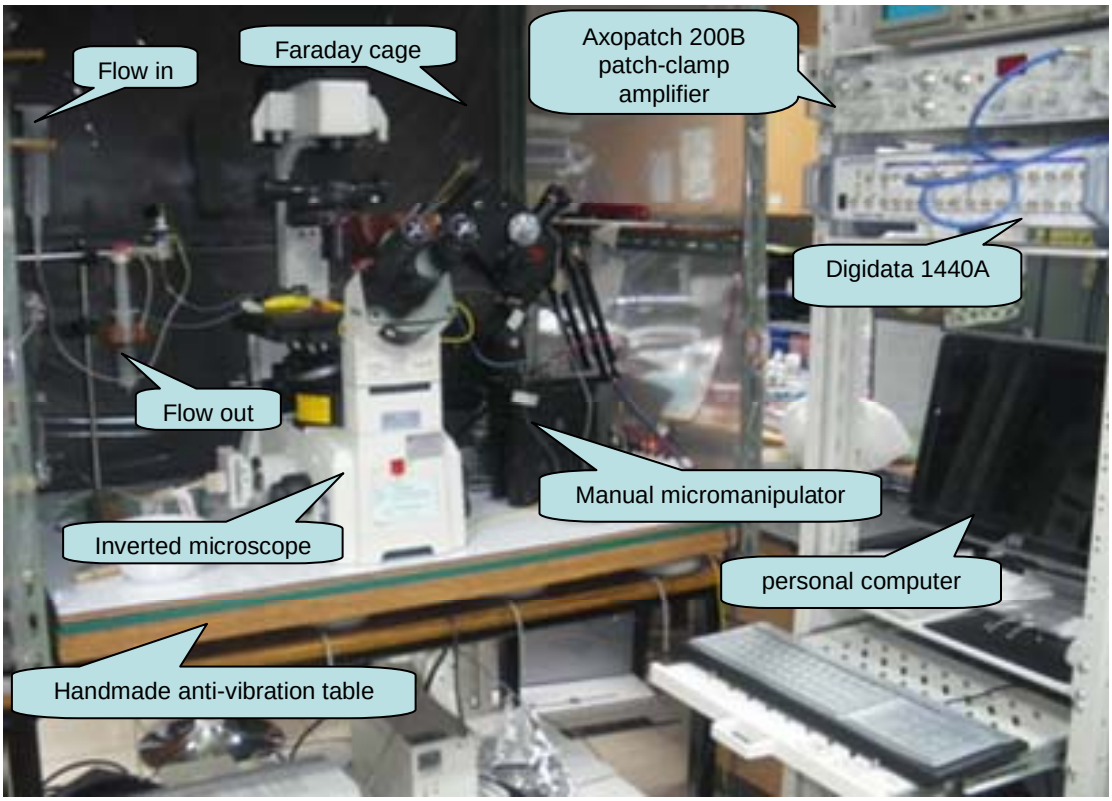

Figure 3.1 Patch-clamp setup for electrophysiological recording.

3.2.3 Silver/silver chloride electrodes

An electrode is a conductive wire which provides an electrical contact with an electrolyte solution (90). Ionic currents in the solution were converted to electron currents in the conductive wire by electron transfer (90, 91). A silver (Ag) wire coated with a compound of Ag and AgCl, as used in the present experiments, is commonly used in electrophysiological study (91). When a current is passed from the wire to the solution, Cl^- in the solution interacts with Ag, resulting in AgCl and an electron (e^-) is freed to move up the wire (to the headstage) (91). On the other hand, a current going from the solution to the wire causes an interaction between e^- and AgCl to produce Ag, freeing the Cl^- into the solution (91). The reversible reaction was a mechanism of

electron transfer (91). To prepare a Ag/AgCl electrode, a cleaned silver wire was immersed in a 6% sodium hypochlorite solution and kept in the dark for 2-4 days. The sliver wire was ready to use when the white, shiny appearance became dark, brownish grey. Re-chloriding was usually needed when increased electrical noise could be recorded.

The Ag/AgCl electrode in the agar bridge construction was made the same way as above.

3.2.4 Pipette preparation

A glass microelectrode or pipette filled with salt solution (internal or pipette solution) acted as a connector between a cell and the Ag/AgCl electrode. [90, 94] The quality of electrophysiological data, formation of gigaseal and low-noise recordings were all dependent on the quality of the pipette (93), (94). Pipettes in this study were fabricated from 15-cm borosilicate glass capillaries (1.2 mm outer diameter, 0.69 mm inner diameter, Sutter Instrument, Novato, California, USA), cut into three 5-cm pieces. Before pipette pulling, they were cleaned with 95% ethanol and fire-polished at the ends to blunt the sharp edges (90). Each glass capillary was pulled using a two-step pipette puller (PP-830, Narishige, Tokyo, Japan) yielding two pipettes. The sharp pipette tips may injure the cell during an experiment, and therefore they were also fire-polished with a microforge (MP-830, Narishige, Tokyo, Japan). The final tip diameter was 0.7-1.5 μm, resulting in 2-5 MΩ pipette resistance in the bath solution. The pipette was kept in dust-free conditions to prevent obstruction of the tip.

At the time of an experiment, the internal solution was filled up the tip by suction, and then back-filled using a pulled, tapered (until needle-like) plastic insulin syringe. Gentle tapping was used if air bubbles were found at the tip of the pipette.

3.2.5 Agar Bridge

The bath solution was grounded by connecting to a Ag/AgCl ground electrode via an agar bridge and a 1 M NaCl solution. Agar bridges were prepared by filling a warm solution, consisting of 1 M NaCl, 1 mM EGTA and 2% agar, into a polyethylene tube (PF 200, Intrammedic, New Jersey, USA). The tube was already

cooled down, it was cut into pieces, approximately two inches each, and kept in 1 M NaCl and 1 mM EGTA, at 4-8^{o}C (in a refrigerator).

To construct a ground electrode, a coiled Ag/AgCl wire was housed in a 1-ml plastic syringe filled with 1 M NaCl and 1 mM EGTA solution. The Ag/AgCl electrode was connected at one end to a gold-pin connector for the ground connection with the headstage. An agar bridge was fitted into the syringe's needle port and sealed. (Figure 3.2)

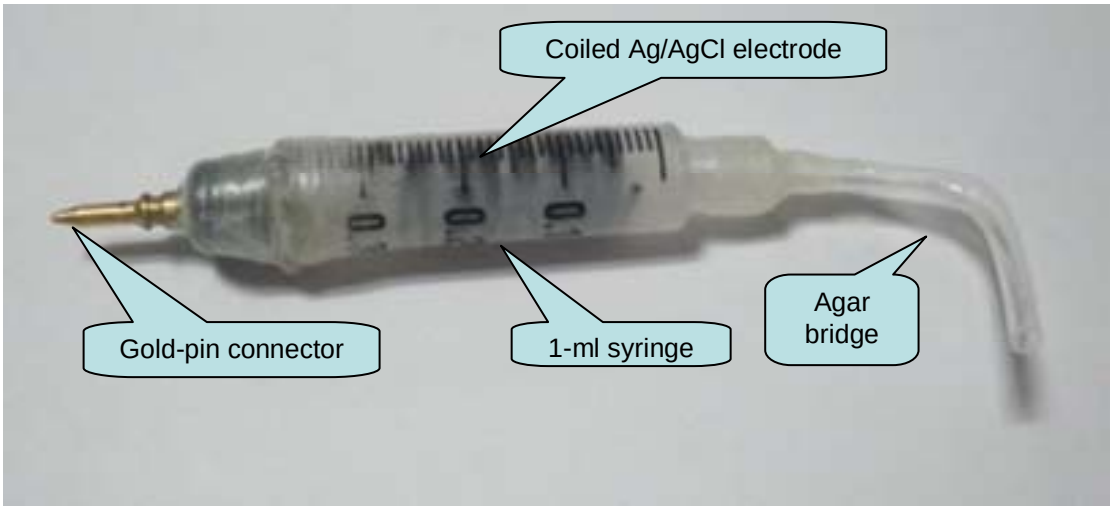

Figure 3.2 A ground electrode.

3.2.6 Flow system

Flow system was gravity-driven. Test solutions were kept in reservoirs connected to a four-inlet precision valve (Hamilton Company, Reno, Nevada, USA), for selecting solutions, and a flow control valve (FR-55S, Warner Instruments) for adjusting inflow rate going into a chamber. The outflow rate was adjusted by varying the height of the outflow tube from the chamber. (Figure 3.3)

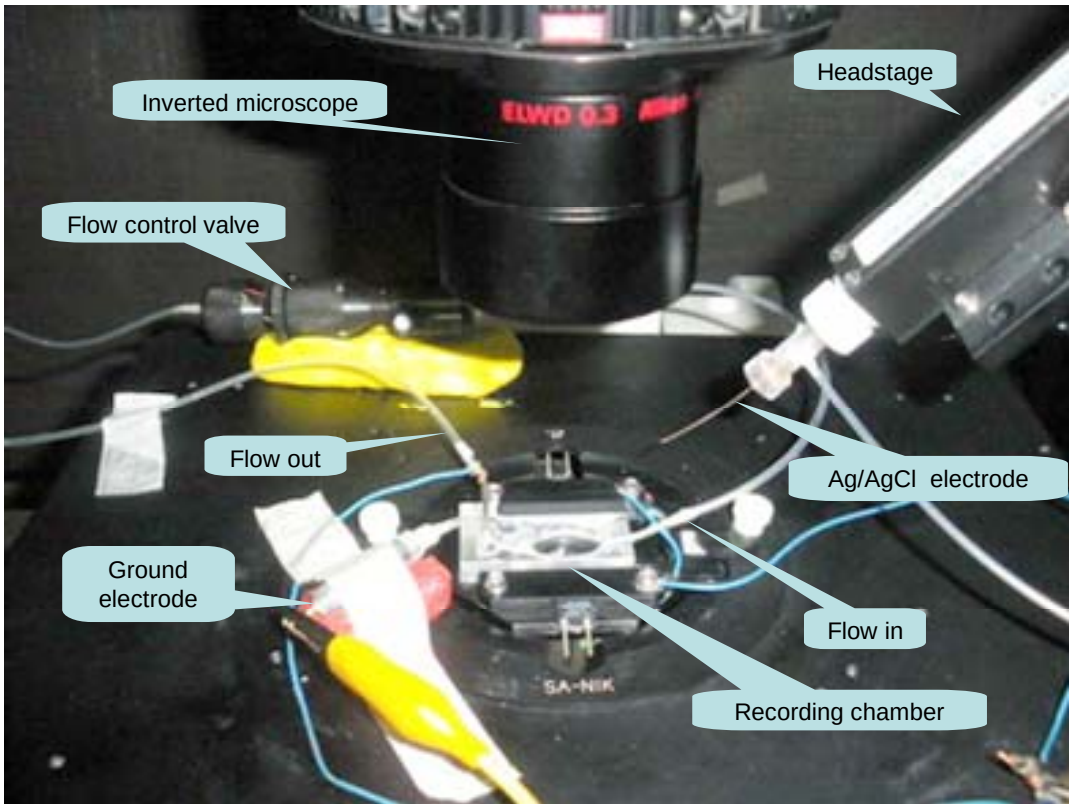

Figure 3.3 Recording chamber.

3.2.7 Solutions and chemicals

Unless otherwise noted, all chemicals were obtained from Sigma Chemicals (St Louis, MO, USA).

3.2.7.1 Solutions for whole-cell recording

Both external and internal solutions were modified from reference 17.

External (or bath) solution (mmol/l): 145 NaCl, 5.4 KCl, 1.8 $CaCl_2$, 1 $MgCl_2$, 5 HEPES, and 10 glucose; pH 7.3 (adjusted with NaOH). The osmolality was 320-325 mOsmol/kg.

Internal (or pipette) solution (mmol/L): 140 KCl, 1 $MgCl_2$, 4 $CaCl_2$, 5 HEPES, 10 EGTA, and 2 ATP; pH 7.2 (adjusted with KOH). The osmolality was 290-300 mOsmol/kg. The free Ca^{2+} concentration of this solution was calculated to be

115.4 nM (Patton C. CaMgATPEGTA Program version 1.0, using constants from NIST database. http://maxchelator.stanford.edu).

3.2.7.2 Ginsenoside Re preparation

Ginsenoside Re stock solution was prepared by dissolving 5 mg ginsenoside Re (equaled to 5.28 μmol; molecular weight = 947.2) in DMSO, making a 1-ml solution. The final concentration was 5.28 mM. Ginsenoside Re stock solution was kept at 4-8 °C in the refrigerator.

Table 3.1 Ginsenoside preparation

Ginsenoside Re concentration (μM)	Adding ginsenoside Re from stock solution (μM)	External solution (ml)	Final DMSO concentration (%)
0.1	0.95	50	0.002
0.3	2.84	50	0.006
1	9.47	50	0.02
3	28.41	50	0.06
10	94.69	50	0.19
30	284.09	50	0.57

3.2.7.3 Preparation of blocker solutions

10 μM Lanthanum (95) (La^{3+}, a nonselective cation channel or NSC blocker) was prepared by adding 50 μl of La^{3+} stock solution (0.1 M; dissolved in dH_2O) into 50 ml of external solution.

100 nM apamin (96) (a small-conductance calcium-activated potassium channels (SK_{Ca}) blocker) was prepared by adding 40 μl of apamin stock solution (125 μM; dissolved in l% acetic acid) into 50 ml of external solution. The final solution was pH-adjusted before using in an experiment.

"Four blockers" consisted of 10 μM La^{3+}, 10 μM clotrimazole (intermediate-conductance calcium-activated potassium channels (IK_{Ca}) blocker) (97),

1 mM TEA (tetraethylammonium, a large-conductance calcium-activated potassium channel, or BK_{Ca}, blocker) (78), and 2 mM Ba^{2+} (inward-rectifier potassium channels (K_{ir}) blocker) (98). Four-blocker solution was prepared by adding 50 µl of La^{3+} stock solution, 17.24 µl of clotrimazole stock solution (0.029 M; dissolved in DMSO), 0.0082855 g of TEA and 0.024428 g of Ba^{2+} into 50 ml external solution. The aim was to block most currents except for the SK_{Ca}.

Four-blocker solution with 1 µM ginsenoside Re was prepared by adding 9.47 µl of ginsenoside Re stock solution into 50 ml of four-blocker solution.

Four-blocker solution with 1 µM ginsenoside Re and apamin was prepared by adding 9.47 µl of ginsenoside Re stock solution and 40 µl of apamin stock solution into 50 ml of four-blocker solution.

3.2.8 Experimental procedure

On the experiment day, HCAECs was plated on petri-dishes containing poly-L-lysine-coated coverslips and then incubated for 4-5 hours, allowing time for cells to attach to the coverslips. Subsequently, a coverslip was taken from the petri-dish and immersed in the external solution-containing recording chamber. After a glass pipette was filled with the internal solution and put in the pipette holder connecting to the headstage, its tip was dipped into the external solution while positive pressure was applied to prevent influx of the bath solution into the pipette. Pipette resistance was read at this point and the pipette offset was adjusted to 0 mV. A round-shaped, isolated cell on the coverslip was selected, then the pipette was moved to the cell. A soft negative pressure was applied when the pipette touched the cell membrane, to facilitate gigaohm seal formation. Fast pipette capacitance was then adjusted. For patch membrane rupture and whole-cell access, a sudden negative pressure was applied. Finally, whole-cell capacitance and series resistance were compensated. (Figure 3.4)

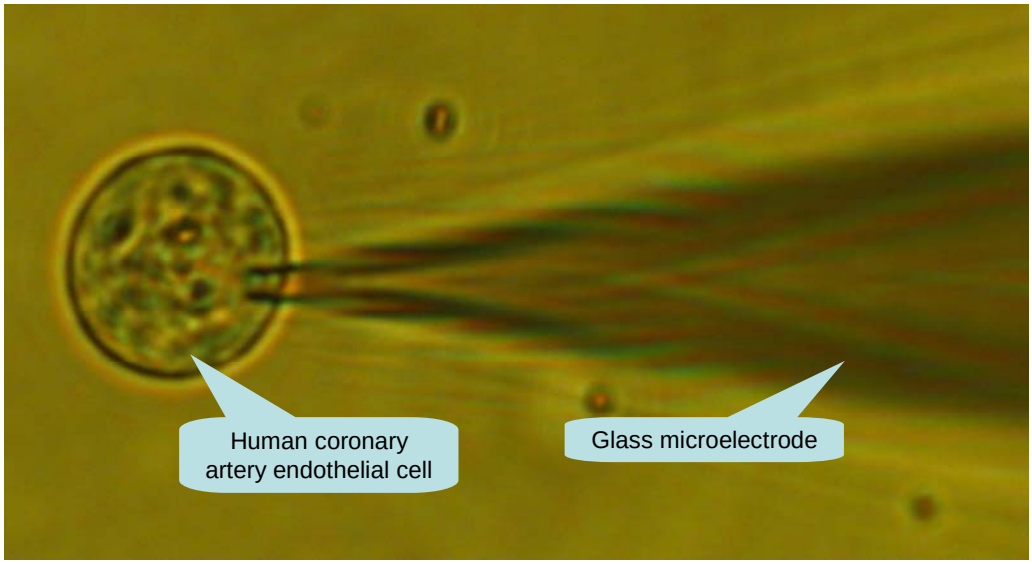

Figure 3.4 Human coronary artery endothelial cell attached to a glass microelectrode.

Studying dose-response relation. The cell was electrically stimulated with 600 ms voltage steps from -100 mV to +80 mV, increasing 20 mV per step (figure 3.5). After current recording in the external solution (control), the superfused fluid was switched to a test solution consisting of the external solution and one dose of ginsenoside Re. Three to five minute equilibration was allowed in a new solution before another stimulation and current recording. Washout currents, after returning to the control solution were recorded if stable recording could still be obtained. The lowest ginsenoside Re concentration that gave a maximal response was chosen as the optimal concentration of ginsenoside Re

Blocker experiments. The currents were first recorded in the external solution, followed by recording in a blocker solution. Then a test solution containing the blocker solution with the optimal concentration of ginsenoside Re was applied and the currents were recorded. If the cell was stable, recordings of washout currents in the blocker solution and the external solution were performed, respectively. Experiments were also done in the following sequence: external solution, ginsenoside Re (optimal dose), ginsenoside Re + a specific blocker, ginsenoside Re (washout) and external solution (washout).

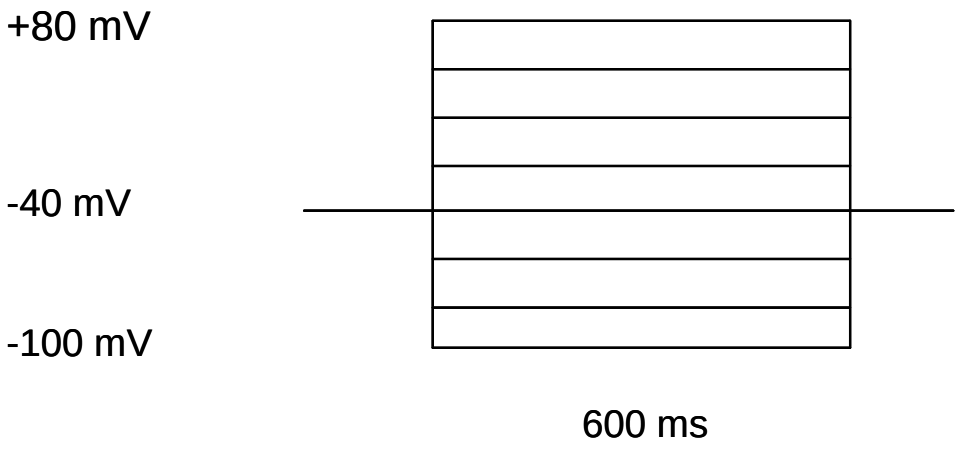

Figure 3.5 Pattern of stimulating voltage steps.

3.3 Experimental design

3.3.1 Effect of ginsenoside Re on HCAEC currents.

Control condition	external solution
Test condition	external solution + 1 μM ginsenoside Re
Washout	external solution

3.3.2 Effect of ginsenoside Re on HCAEC currents at different concentrations (0.1-30 μM) (dose-response curve)

Control condition	external solution
Test condition	external solution + (0.1-30 μM) ginsenoside Re
Washout	external solution

3.3.3 Effect of ginsenoside Re on SK_{Ca} currents of HCAECs: Apamin experiments

100 nM Apamin, a specific blocker of SK_{Ca} was used.

3.3.3.1 Effect of ginsenoside Re when SK_{Ca} was blocked

Control condition 1	external solution
Control condition 2	external solution + 100 nM apamin
Test condition	external solution + 100 nM apamin + ginsenoside Re (optimal concentration)
Washout 1	external solution + 100 nM apamin
Washout 2	external solution

3.3.3.2 Effect of apamin on ginsenoside Re-induced currents

Control condition 1	external solution
Control condition 2	external solution + ginsenoside Re (optimal concentration)
Test condition	external solution + 100 nM apamin + ginsenoside Re (optimal concentration)
Washout 1	external solution + ginsenoside Re (optimal concentration)
Washout 2	external solution

3.3.4 Effect of ginsenoside Re on SK_{Ca} currents of HCAECs: Four-blocker experiments.

Four-blocker solution was composed of specific blockers of NSC, BK_{Ca}, IK_{Ca} and K_{ir}. In the presence of this solution, SK_{Ca} channel was not inhibited and constituted the remaining currents.

3.3.4.1 Effect of ginsenoside Re in the presence of four-blocker solution

Control condition 1	external solution
Control condition 2	external solution + 4 blockers
Test condition	external solution + 4 blockers + ginsenoside Re (optimal concentration)
Washout 1	external solution + 4 blockers
Washout 2	external solution

3.3.4.2 Effect of apamin on ginsenoside Re-induced currents in the presence of four-blocker solution.

Control condition 1	external solution + 4 blockers
Control condition 2	external solution + 4 blockers + ginsenoside Re (optimal concentration)
Test condition	external solution + 4 blockers + ginsenoside Re (optimal concentration) + 100 nM apamin
Washout 1	external solution + 4 blockers + ginsenoside Re (optimal concentration)
Washout 2	external solution + 4 blockers

3.3.5 Effect of ginsenoside Re on NSC currents of HCAECs: La^{3+} experiments

10 μM La^{3+}, a specific blocker of NSC, was employed.

3.3.5.1 Effect of ginsenoside Re when NSC was blocked

Control condition 1	external solution
Control condition 2	external solution + 10 μM La^{3+}
Test condition	external solution + 10 μM La^{3+} + ginsenoside Re (optimal concentration)
Washout 1	external solution + 10 μM La^{3+}
Washout 2	external solution

3.3.5.2 Effect of La^{3+} on ginsenoside Re-induced currents

Control condition 1	external solution
Control condition 2	external solution + ginsenoside Re (optimal concentration)
Test condition	external solution + 10 μM La^{3+} + ginsenoside Re (optimal concentration)
Washout 1	external solution + ginsenoside Re (optimal concentration)
Washout 2	external solution

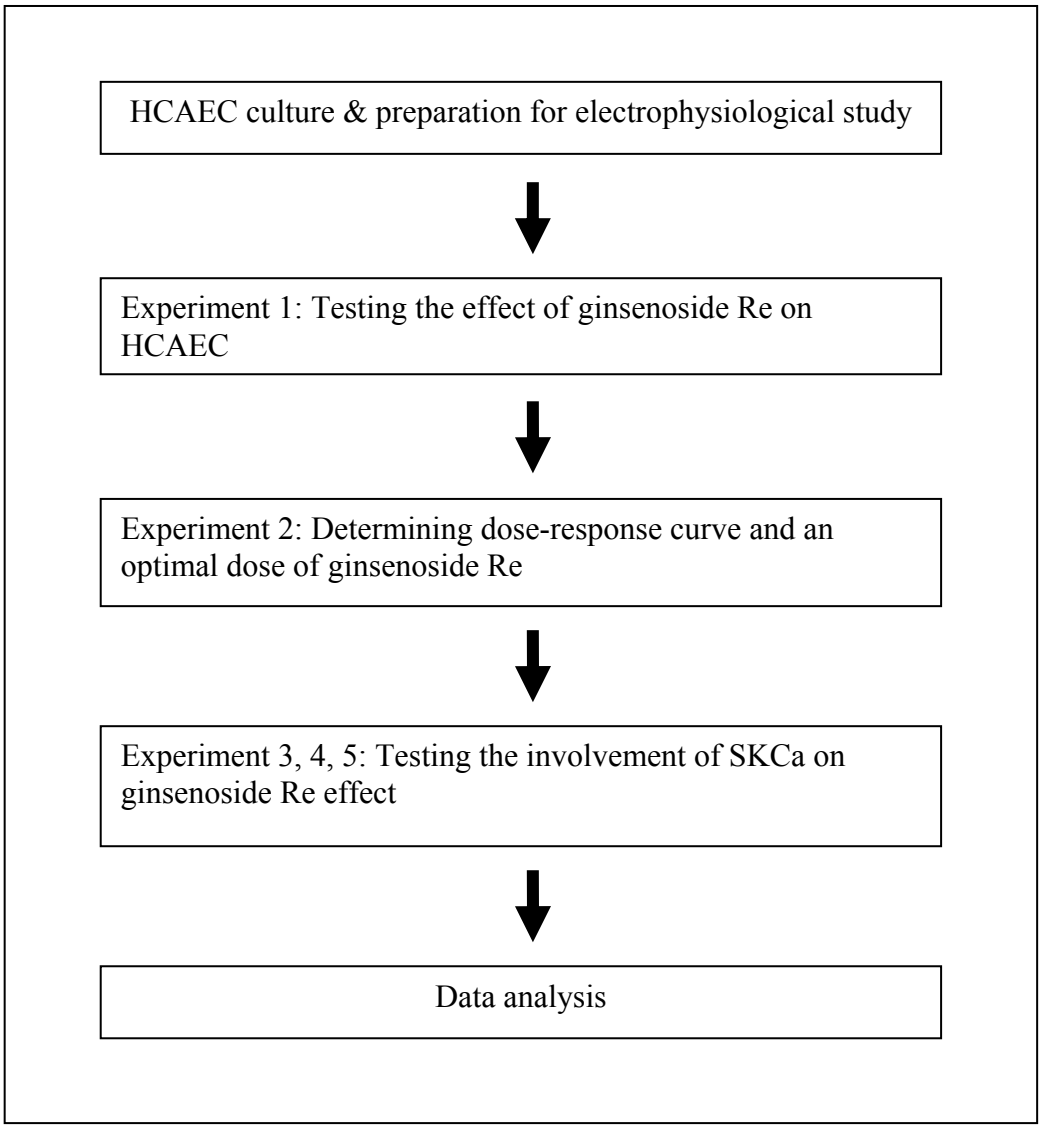

Figure 3.6 Experimental overview.

3.4 Data analysis

3.4.1 Series resistance and voltage error

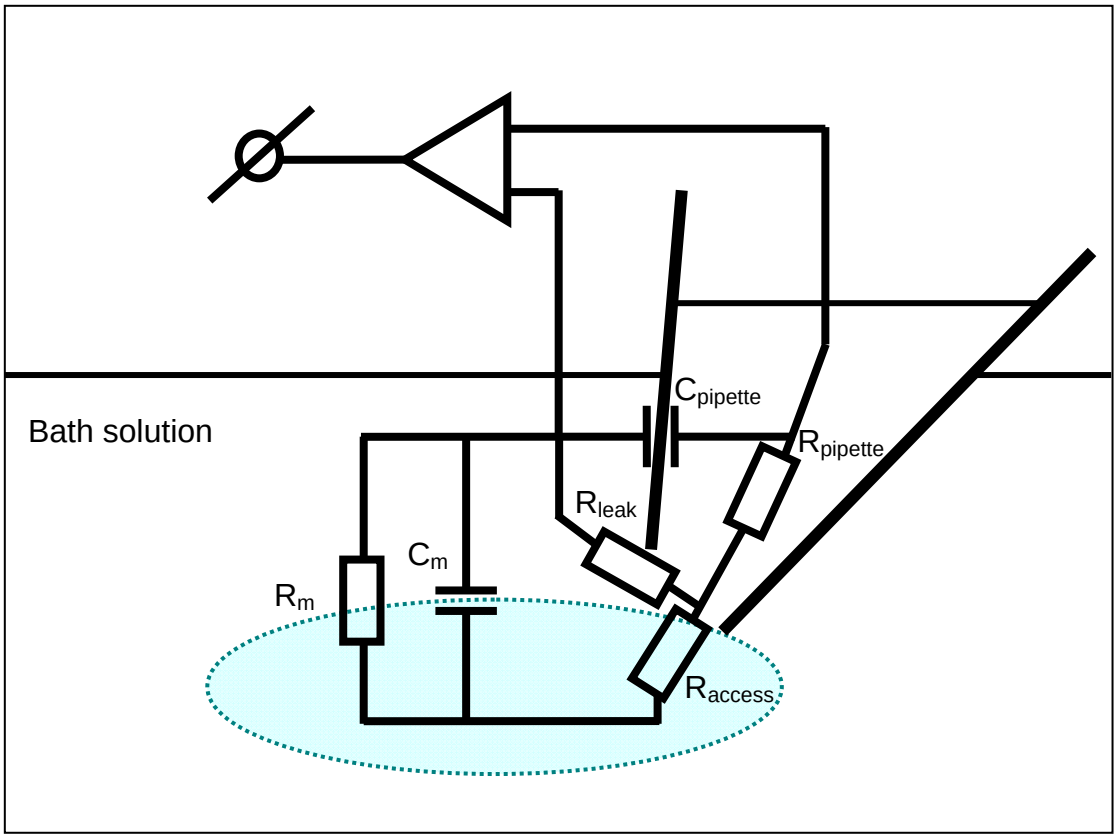

Figure 3.7 An equivalent circuit in a whole-cell experiment (see text for details).[99]

Figure 3.7 diagrams an equivalent circuit of the whole-cell patch clamp experiments in this study. The cell membrane is represented by the whole-cell membrane resistance (R_m) and capacitance (C_m). R_m represents all ion channels in the cell membrane; all channel currents pass through it and it is the largest resistor of this equivalent circuit. A pipette with a capacitance and a resistance of $C_{pipette}$ and $R_{pipette}$ is connected with the cell's interior via the tip of the pipette, which is represented by the access resistance (R_{access}). $C_{pipette}$ is usually very small and well compensated. Any

electrical connection between the bath and the pipette solution is depicted as the leak resistance (R_{leak}). High value of R_{leak} indicates the high quality of seal and ultra-low leakage current, which is desirable for optimum recording of the membrane current. access resistance (R_{access}).

Series resistance (R_s) represents all the resistance in series with R_m. In the equivalent circuit of figure 3.7, R_s consists of $R_{pipette}$ and R_{access}. Because R_s is in series with R_m, part of the command voltage intending to clamp the membrane will be reduced by a voltage error which can be calculated by Ohm's law (figure 3.8):

$$V = I_m \times R_s$$

Figure 3.8 Ohm's law.

V = voltage error

R_s = series resistance

I_m = membrane currents

[For maximum voltage error, I_m is substituted by the maximum currents of the cell.]

In addition, R_s will affect the time constant of membrane potential change because of it is in series with the membrane capacitance (C_m). Time constant of C_m charging is proportional to the series resistance (90).

3.4.2 Current analysis

All data were initially analyzed with pClamp version 10.0. Subsequent simple calculations were done in Microsoft Excel. Current density-voltage (I-V) curves and bar graphs were plotted using GraphPad PRISM 5 (GraphPad Solfware, San Diego, CA USA).

Currents at +60 mV were used for comparison between control and test solution because they were large but did not suffer from frequent leakage as much as those at +80 mV. Currents were normalized by division with the cell capacitance

(representing cell surface area), yielding current density in pA/pF. To calculate percentage of control current, the current at +60 mV in control conditions was taken as 100 %; other currents in the same cell were calculated as percentage of this 100 % current and the results were called % control. The difference of % control from 100 % was called % different. Subsequently, current-voltage (I-V) curves were plotted using % control data for comparison between control, test and washout currents.

3.4.3 Exclusion criteria

Data from a cell were discarded if the seal resistance was less than 800 MΩ or the maximum voltage error was more than 4 mV. Cells with less than 25 pA current amplitude at +60 mV were excluded.

3.4.4 Dose-response curve

Concentration-response curves were fitted with the dose-response equation (figure 3.9), using also GraphPad PRISM 5.

$$y = I_{max} \{1/ (1 + (EC50/x)^n)\}$$

Figure 3.9 Dose-response equation.

y = relative current

I_{max} = maximam current amplitude

X = agonist concentration

EC50 = half-effective concentration

n = Hill coefficient

3.4.5 Statistical analyses

All statistical analyses were performed using the program GraphPad PRISM 5.

Results were expressed as mean ± SEM.

Kolmogorov-Smirnov test was used for testing the normality of the data.

One-sample *t* test was used to test if the percentage blocked was significantly different from zero; i.e. significance indicated a block.

One-way analysis of variance (ANOVA) with Dunnett's multiple comparison test was used to test differences among more than two groups.

Differences were considered statistically significant at a *P* value of < 0.05.

CHAPTER IV
RESULTS

Altogether 245 cells were included in this project. The mean cell capacitance was 24.17 ± 1.13 pF. The mean outward current magnitude at +60 mV was 104.70 ± 3.80 pA. The mean normalized current was 6.84 ± 0.40 pA/pF. The mean series resistance was 7.50 ± 0.24 MΩ. The mean voltage error was 1.15 ± 0.05 mV. (Table 4.1)

Table 4.1 Average, minimum and maximum values of HCAEC capacitance, outward currents and normalized currents, together with series resistance and voltage error in the experiments of this study.

Characteristics	**n**	**min**	**max**	**Mean ± SEM**
Cell capacitance (pF)	245	3.81	85.25	24.17 ± 1.13
Outward currents at +60 mV (pA)	245	26.74	329.40	104.70 ± 3.80
Normalized currents (pA/pF)	245	0.57	37.25	6.84 ± 0.40
Series resistance (MΩ)	245	1.40	26.00	7.50 ± 0.24
Voltage error (mV)	245	0.12	3.99	1.15 ± 0.05

Normalized currents are outward currents/cell capacitance; n = number of cell, min = minimum, max = maximum, SEM = standard error of mean**.**

4.1 Dose-response curve

Experiments were carried out to examine the effects of ginsenoside Re on HCAEC currents at concentrations 0.1-30 μM, construct a dose-response curve and determine the EC50 of ginsenoside Re effect.

4.1.1 Effect of 1.8 % DMSO

Dimethyl sulfoxide (DMSO) is a solvent that dissolves both polar and nonpolar compounds. It was used in this study for dissolving ginsenoside Re. The maximum concentration of DMSO in external solution is 1.8 % v/v. Currents were recorded in 1.8 % DMSO in external solution to examine its effects in human coronary endothelial cells (HCAECs).

After establishing gigaseal and whole-cell access into a cell by the glass micropipette at the beginning of an experiments, the cell was clamped at a holding potential of -40 mV, which approximated the reported resting membrane potential of HCAEC. Then the cell was stimulated at 1 Hz with 600-ms pulses, amplitudes varying from -100 mV to +80 mV in 20 mV increments (Figure 4.1). Figure 4.2 shows raw current traces from a representative cell; the upper trace was recorded in the external solution (control) and the lower trace in external solution with 1.8 % DMSO v/v (DMSO 1.8 %). The resulting average current-voltage (I-V) curve from six cells is shown in figure 4.3A. When currents at +60 mV in 1.8 % DMSO were compared to control currents at the same voltage as % control (Figure 4.3B), no effect of DMSO on HCAEC currents could be demonstrated (91.43 ± 9.39 % compared with 100 % control, n = 6, $P = 0.4031$, one-sample *t* test).

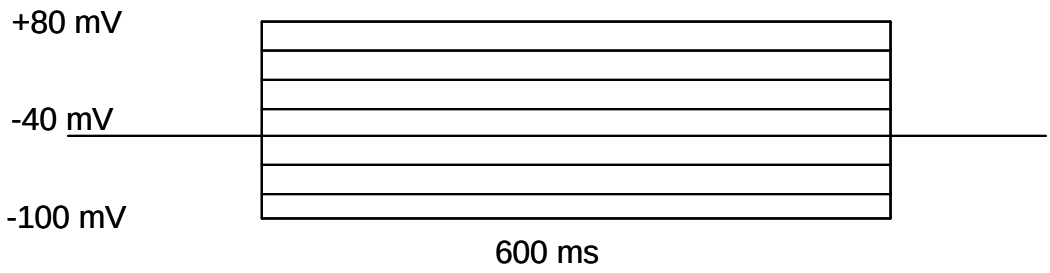

Figure 4.1 The voltage pattern for all experiments.

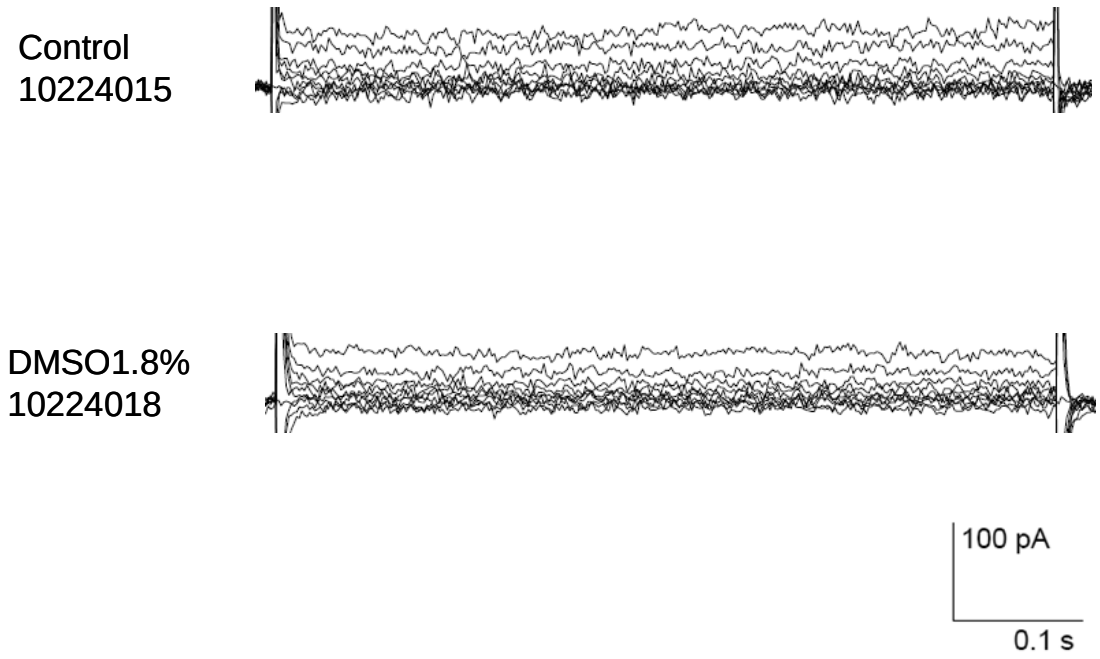

Figure 4.2 Current traces, with and without 1.8 % DMSO v/v, from a representative HCAEC (Cm = 38.18 pF, Rs = 26 MΩ, voltage error = 1.46 mV).

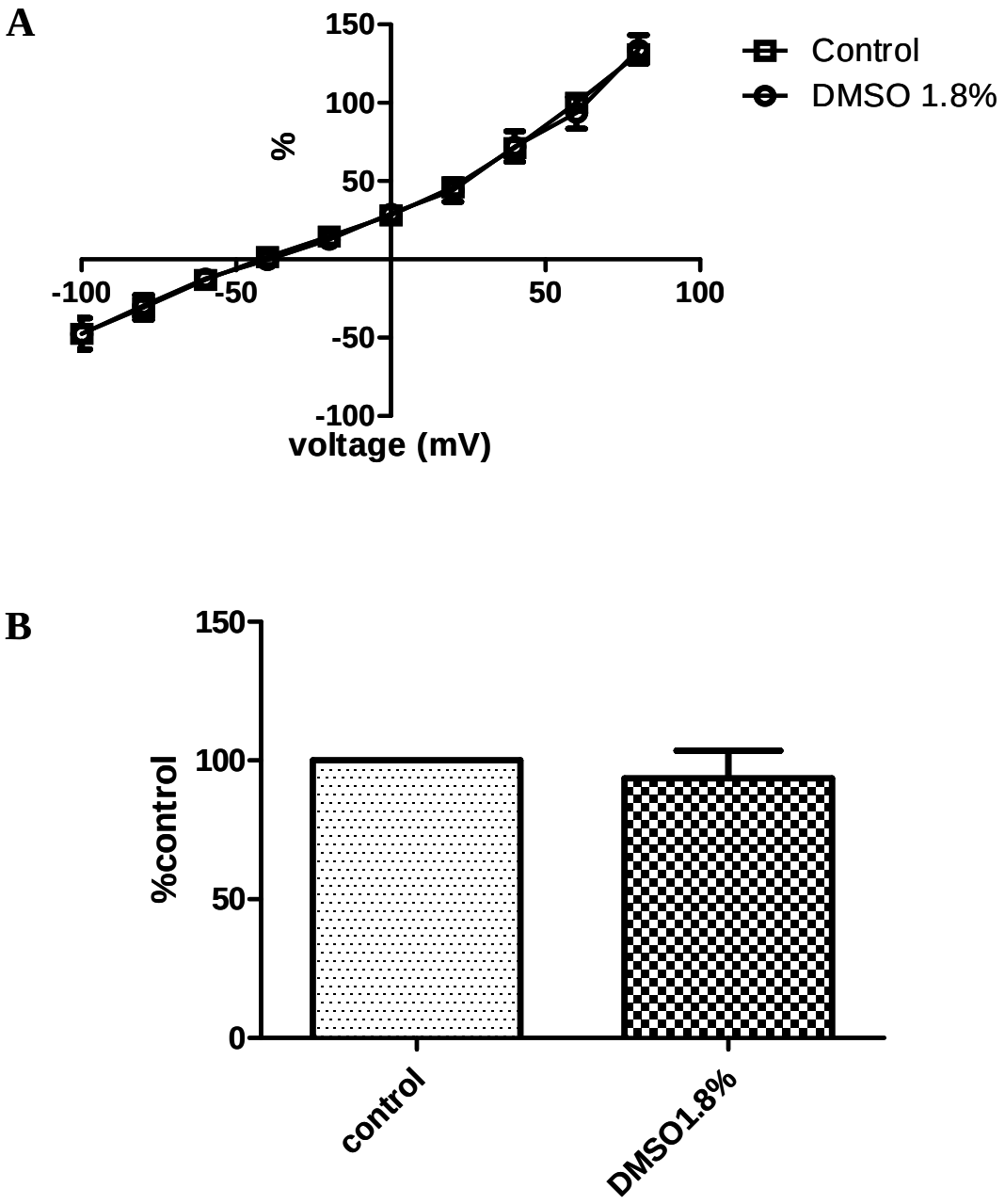

Figure 4.3 Effects of 1.8 % DMSO. Error bars are S.E.M.

A: The average current-voltage curves, plotted from % control data (n = 6).

B: Bar graphs comparing % control currents at +60 mV from all cells. No statistical difference was found between currents in control and 1.8 % DMSO (100 % *vs* 91.43 ± 9.39 %, n = 6, $P = 0.4031$, one-sample *t* test).

4.1.2 Effect of 100 nM Ginsenoside Re

Ginsenoside Re at 100 nM did not affect HCAECs currents, as shown in figures 4.4 and 4.5. Currents in 100 nM ginsenoside Re were 96.66 ± 1.90 % of control currents (n = 10, $P = 0.1123$, one-sample t test).

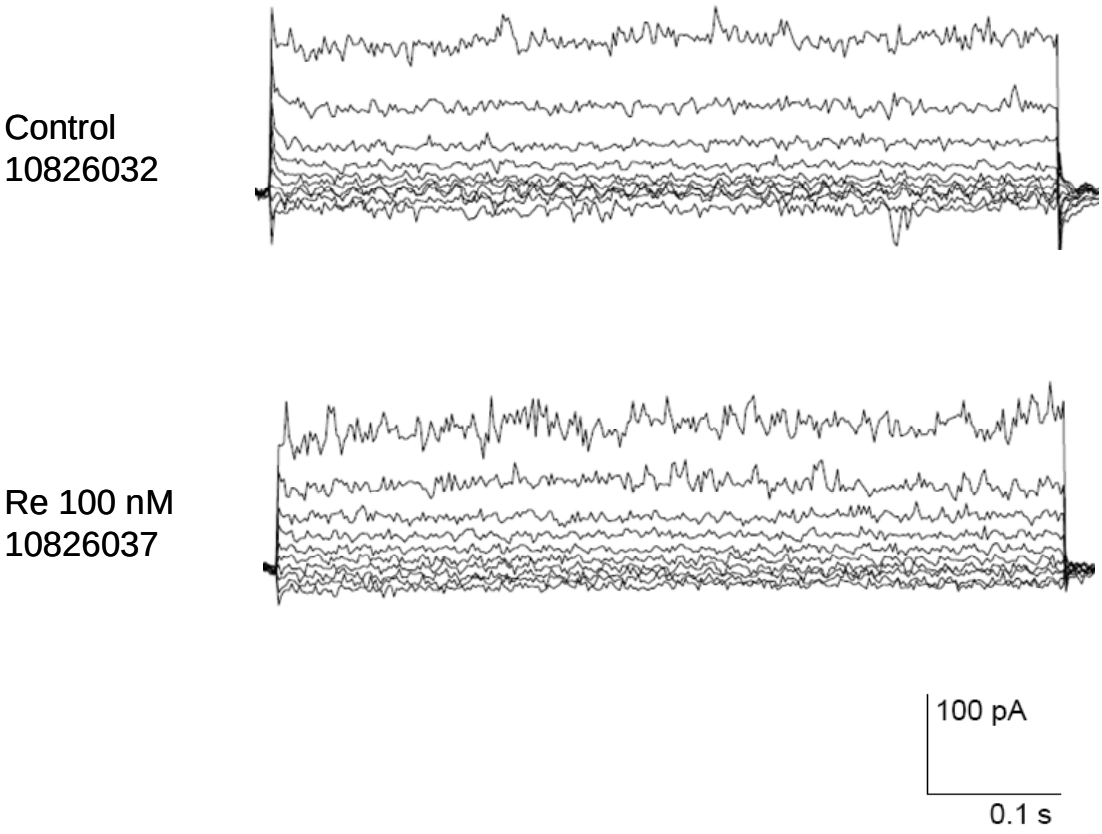

Figure 4.4 Current traces, with and without 100 nM ginsenoside Re, from a representative HCAEC (Cm = 8.79 pF, Rs = 18.2 MΩ, voltage error = 2.68 mV).

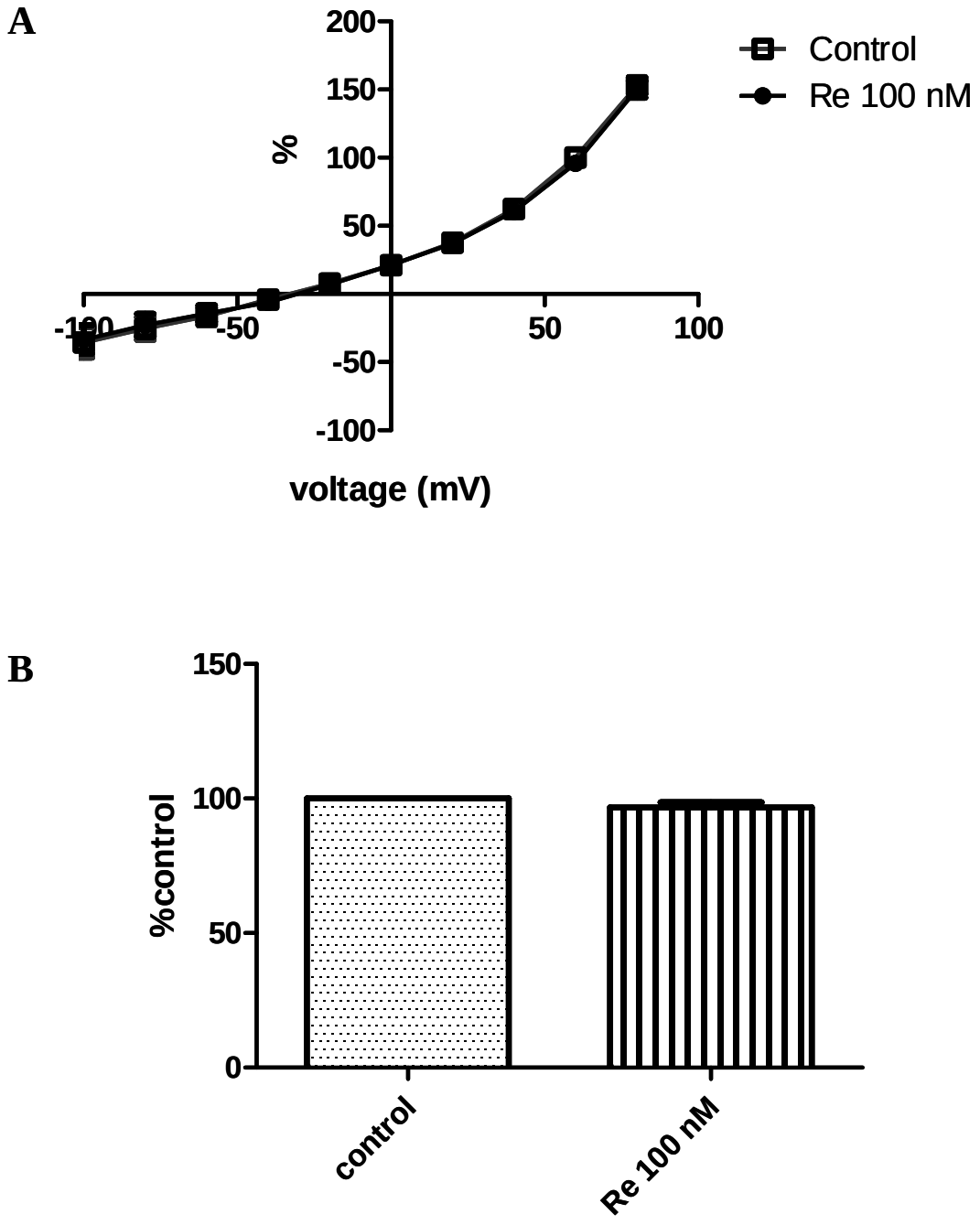

Figure 4.5 Effects of 100 nM ginsenoside Re. Error bars are S.E.M.

A: The average current-voltage curves, plotted from % control data (n = 10).

B: Bar graphs comparing % control currents at +60 mV from all cells. No statistical difference was found between currents in control and 100 nM ginsenoside Re (100 % *vs* 96.66 ± 1.90 %, n = 10, $P = 0.1123$, one-sample *t* test).

4.1.3 Effect of 300 nM Ginsenoside Re

Ginsenoside Re at 300 nM did not affect HCAECs currents, as shown in figures 4.6 and 4.7. Currents in 300 nM ginsenoside Re were 106.10 ± 3.05 % of control currents (n = 9, $P = 0.0812$, one-sample t test).

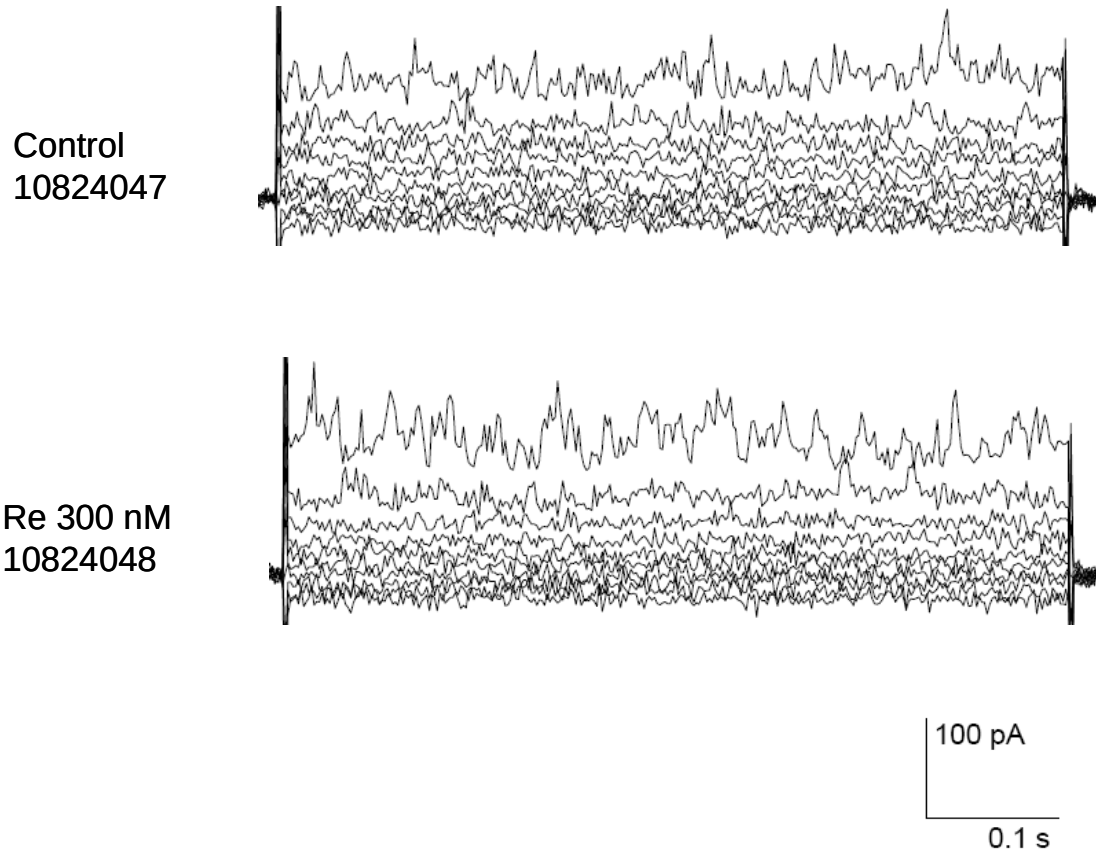

Figure 4.6 Current traces, with and without 300 nM ginsenoside Re, from a representative HCAEC (Cm = 61.08 pF, Rs = 3.9 MΩ, voltage error = 0.55 mV).

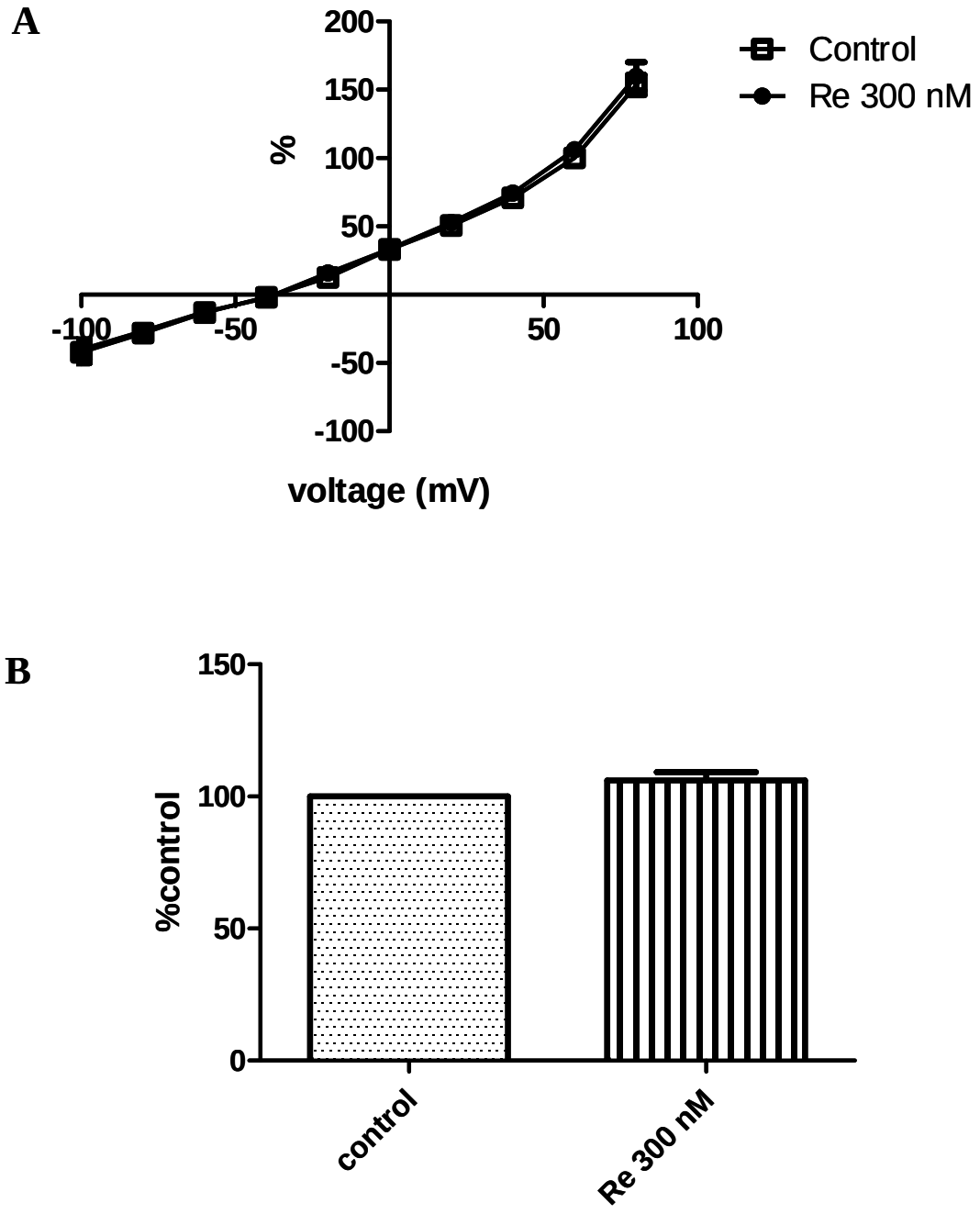

Figure 4.7 Effects of 300 nM ginsenoside Re. Error bars are S.E.M.

A: The average current-voltage curves, plotted from % control data (n = 9).

B: Bar graphs comparing % control currents at +60 mV from all cells. No statistical difference was found between currents in control and 300 nM ginsenoside Re (100 % *vs* 106.10 ± 3.05 %, n = 9, *P* = 0.0812, one-sample *t* test).

4.1.4 Effect of 1 μM Ginsenoside Re

Ginsenoside Re at 1 μM significantly increased outward currents of HCAECs, as shown in figures 4.8 and 4.9. Currents in 1 μM ginsenoside Re were 134.00 ± 8.11 % of control currents (n = 10, $P = 0.0023$, one-sample t test).

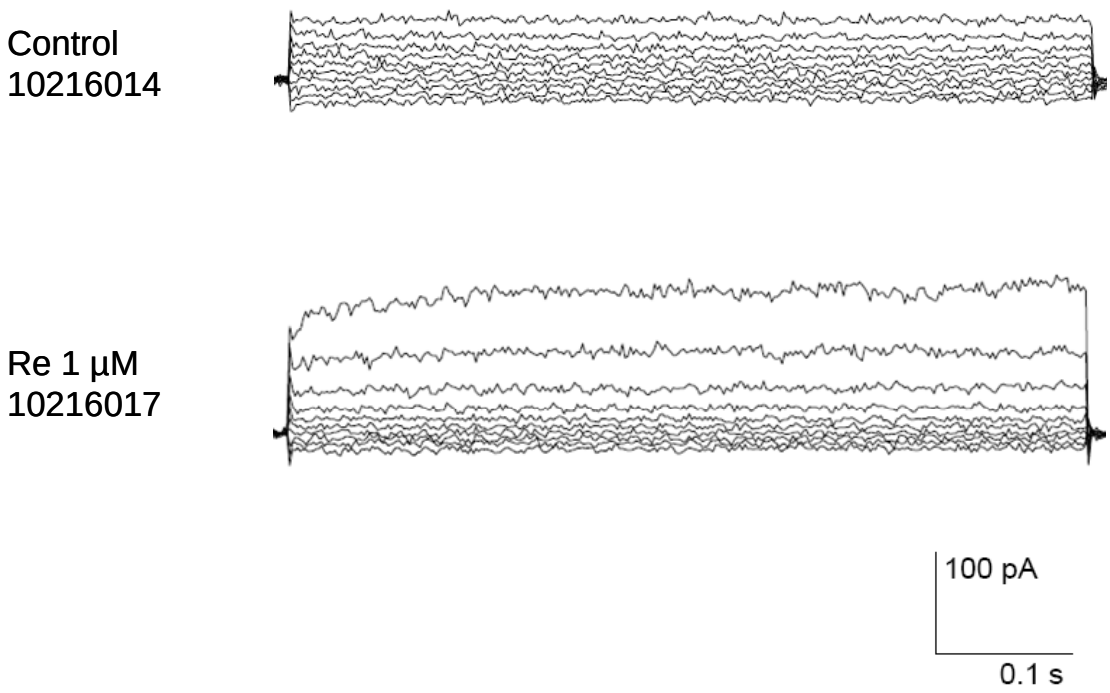

Figure 4.8 Current traces, with and without 1 μM ginsenoside Re, from a representative HCAEC (Cm = 11.72 pF, Rs = 9.5 MΩ, voltage error = 1.35 mV).

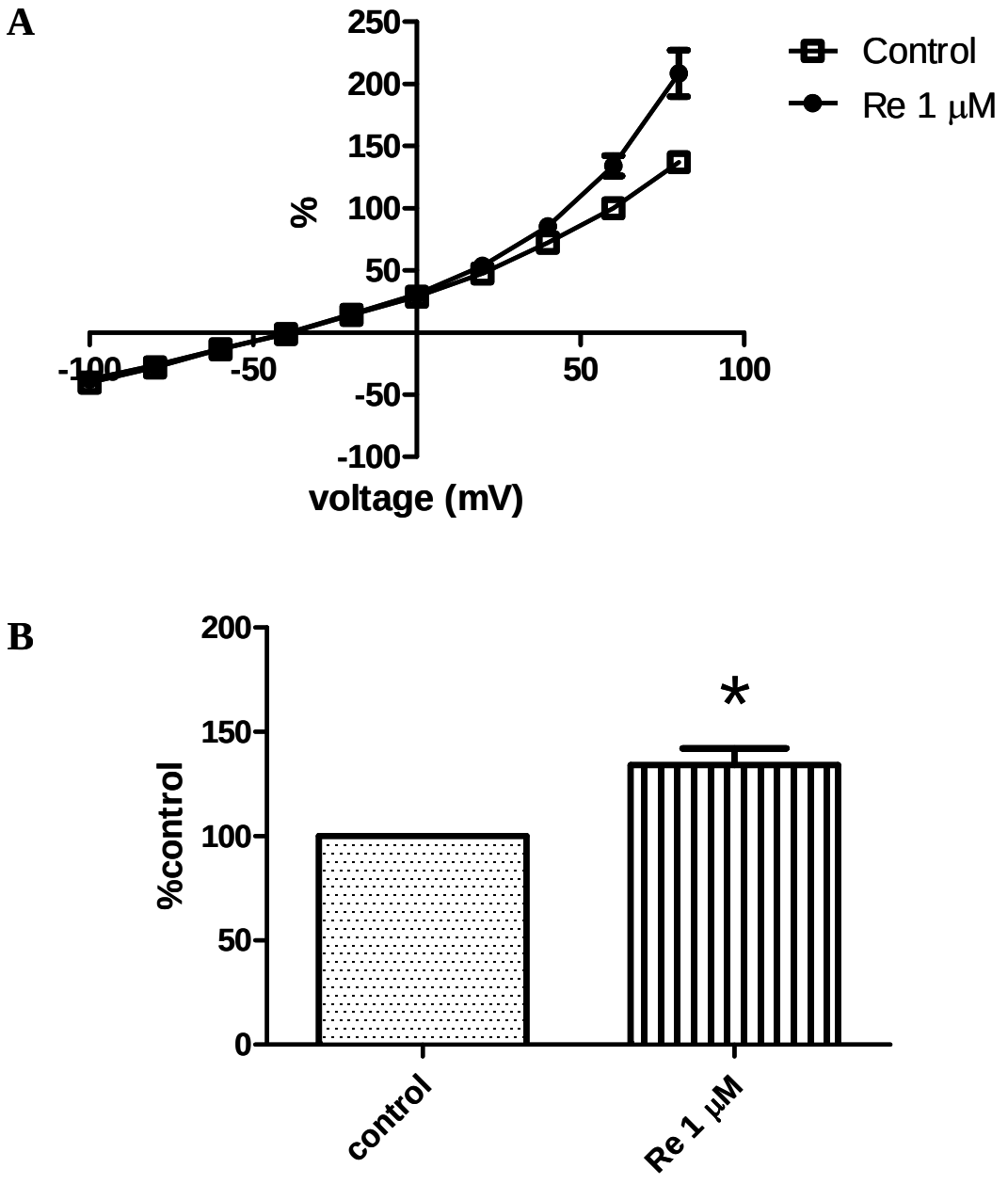

Figure 4.9 Effects of 1 μM ginsenoside Re. Error bars are S.E.M. An asterisk (*) represents a significant increase.

A: The average current-voltage curves, plotted from % control data (n = 10).

B: Bar graphs comparing % control currents at +60 mV from all cells. Significant difference was found between currents in control and 1 μM ginsenoside Re (100 % *vs* 134.00 ± 8.11 %, n = 10, $P = 0.0023$, one-sample *t* test).

Washout currents in control external solution could be recorded in four out of ten cells. Figure 4.10 shows the current traces with washout in a representative cell. Figure 4.11 shows the average current-voltage curves.

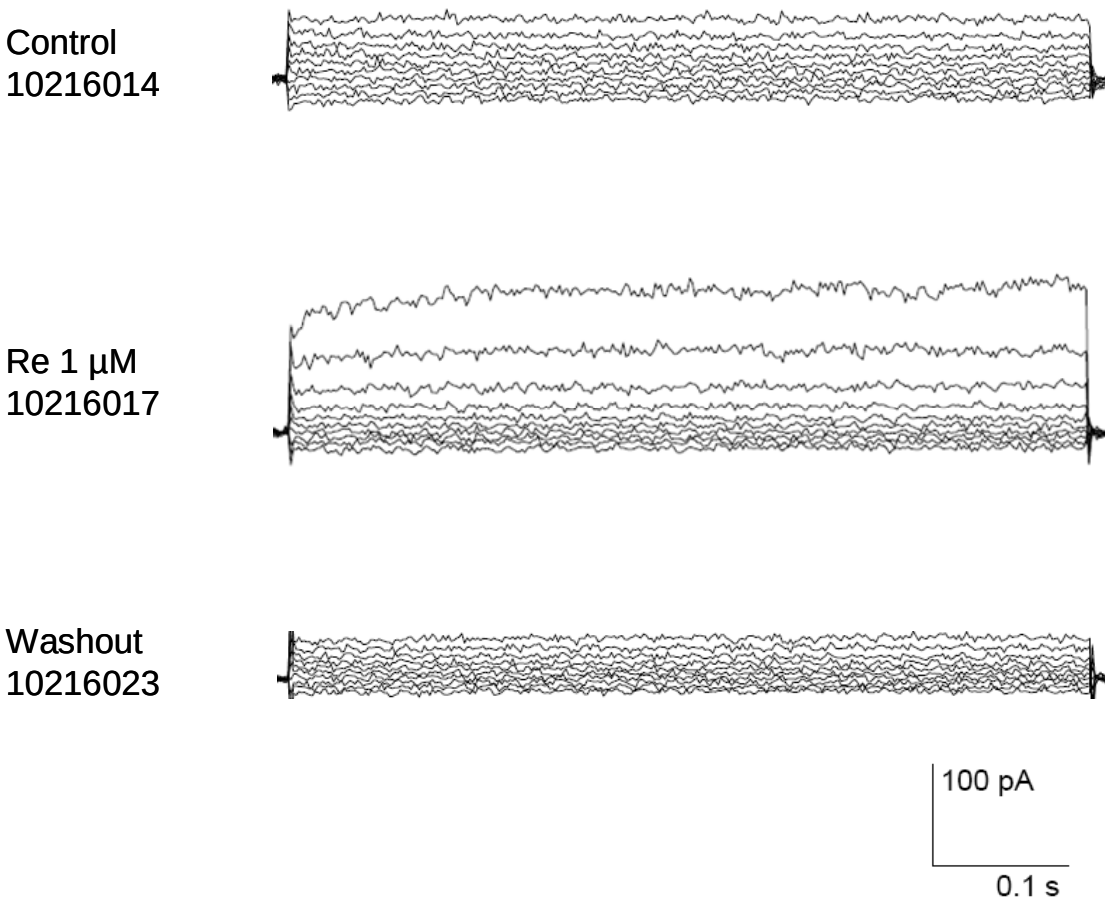

Figure 4.10 Current traces in control *vs* 1 µM ginsenoside Re, with washout currents, from a representative HCAEC (Cm = 11.72 pF, Rs = 9.5 MΩ, voltage error = 1.35 mV).

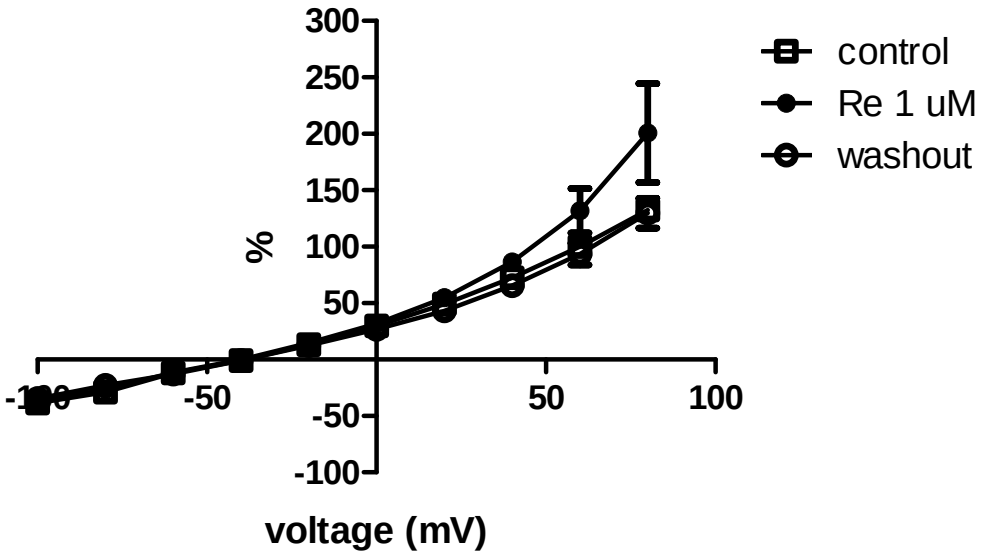

Figure 4.11 Average current-voltage curves in control *vs* 1 μM ginsenoside Re, with washout currents, plotted from % control data (n = 4).

4.1.5 Effect of 3 µM Ginsenoside Re

Ginsenoside Re at 3 µM significantly increased outward currents of HCAECs, as shown in figures 4.12 and 4.13. Currents in 3 µM ginsenoside Re were 131.50 ± 6.24 % of control currents (n = 7, $P = 0.0023$, one-sample t test).

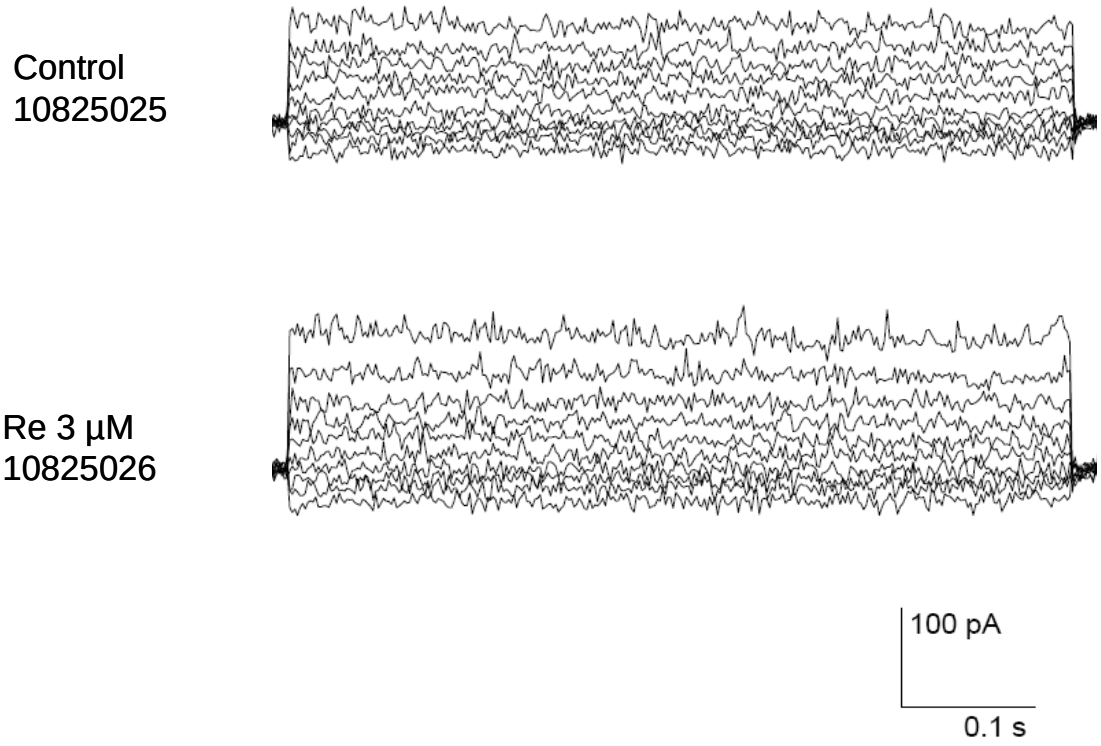

Figure 4.12 Current traces, with and without 3 µM ginsenoside Re, from a representative HCAEC (Cm = 39.79 pF, Rs = 5.7 MΩ, voltage error = 0.76 mV).

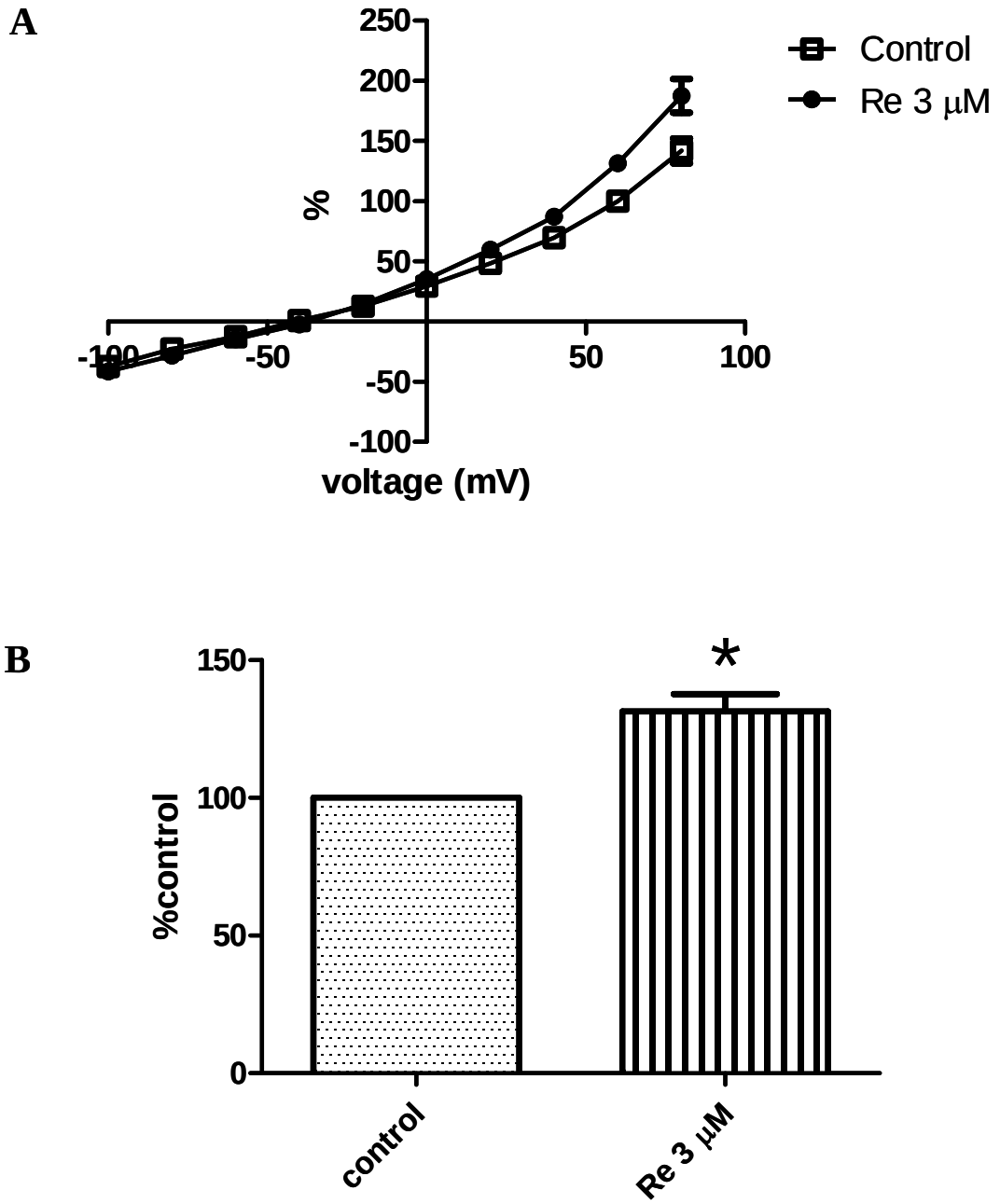

Figure 4.13 Effects of 3 μM ginsenoside Re. Error bars are S.E.M. An asterisk (*) represents a significant increase ($P < 0.05$, one-sample *t* test).

A: The average current-voltage curves, plotted from % control data (n = 7).

B: Bar graphs comparing % control currents at +60 mV from all cells. Significant difference was found between currents in control and 3 μM ginsenoside Re (100 % *vs* 131.50 ± 6.24 %, n = 7, $P = 0.0023$, one-sample *t* test).

Washout currents in control external solution could be recorded in one out of seven cells. Figure 4.14 shows the current traces with washout in a representative cell. Figure 4.15 shows the average current-voltage curves.

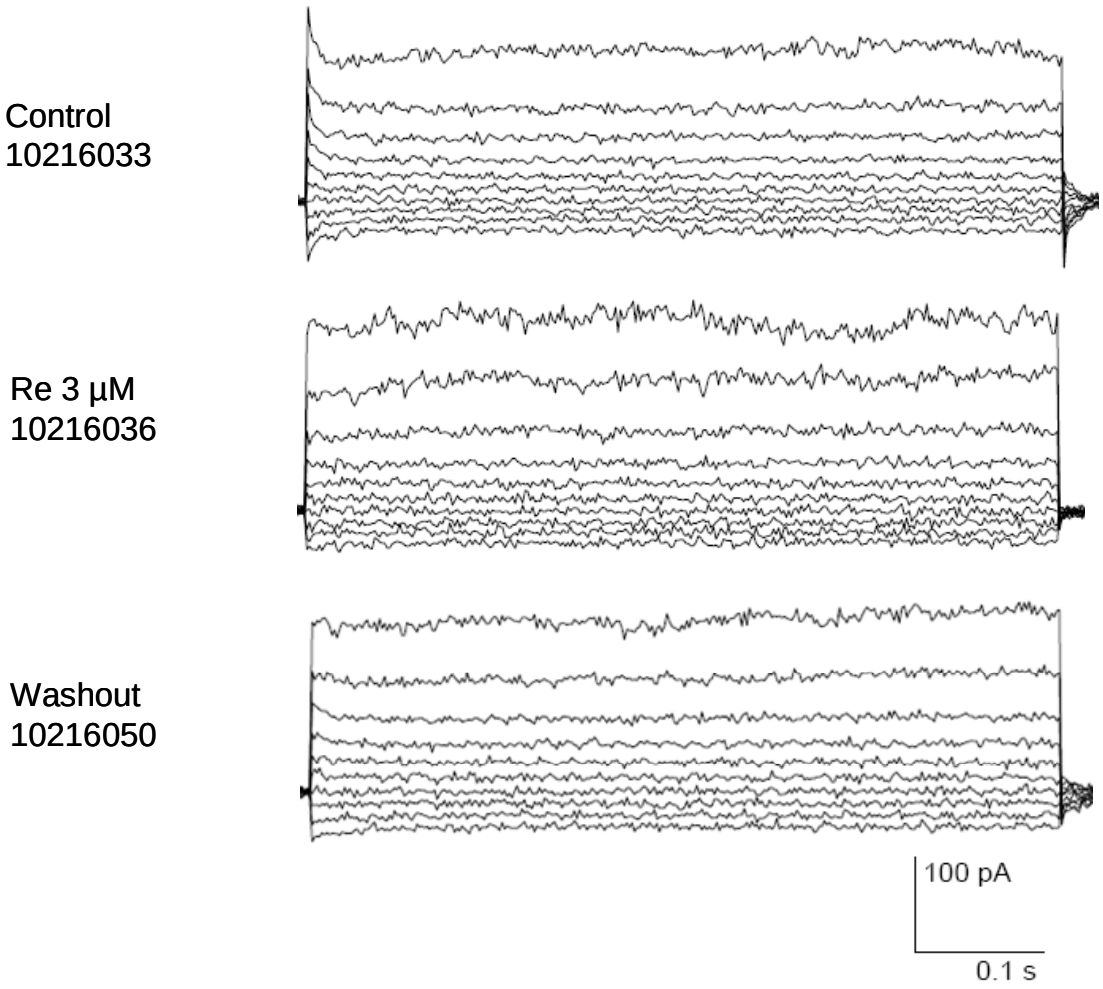

Figure 4.14 Current traces in control *vs* 3 µM ginsenoside Re, with washout currents, from a representative HCAEC (Cm = 8.59 pF, Rs = 9 MΩ, voltage error = 1.45 mV).

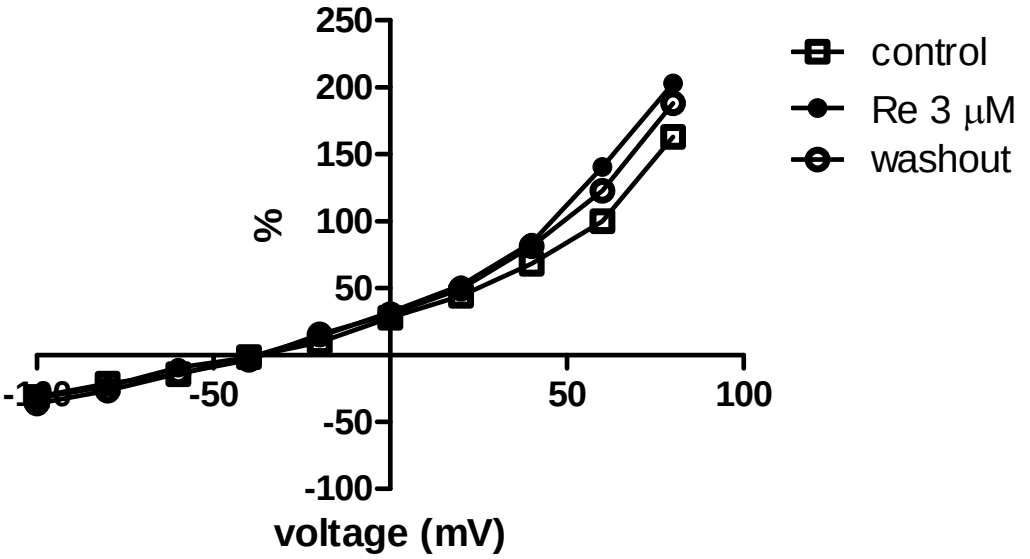

Figure 4.15 The average current-voltage curves in control *vs* 3 μM ginsenoside Re, with washout currents, plotted from % control data (n = 1).

4.1.6 Effect of 10 µM Ginsenoside Re

Ginsenoside Re at 10 µM significantly increased outward currents of HCAECs, as shown in figures 4.16 and 4.17. Currents in 10 µM ginsenoside Re were 127.70 ± 11.70 % of control currents (n = 9, $P = 0.0455$, one-sample t test).

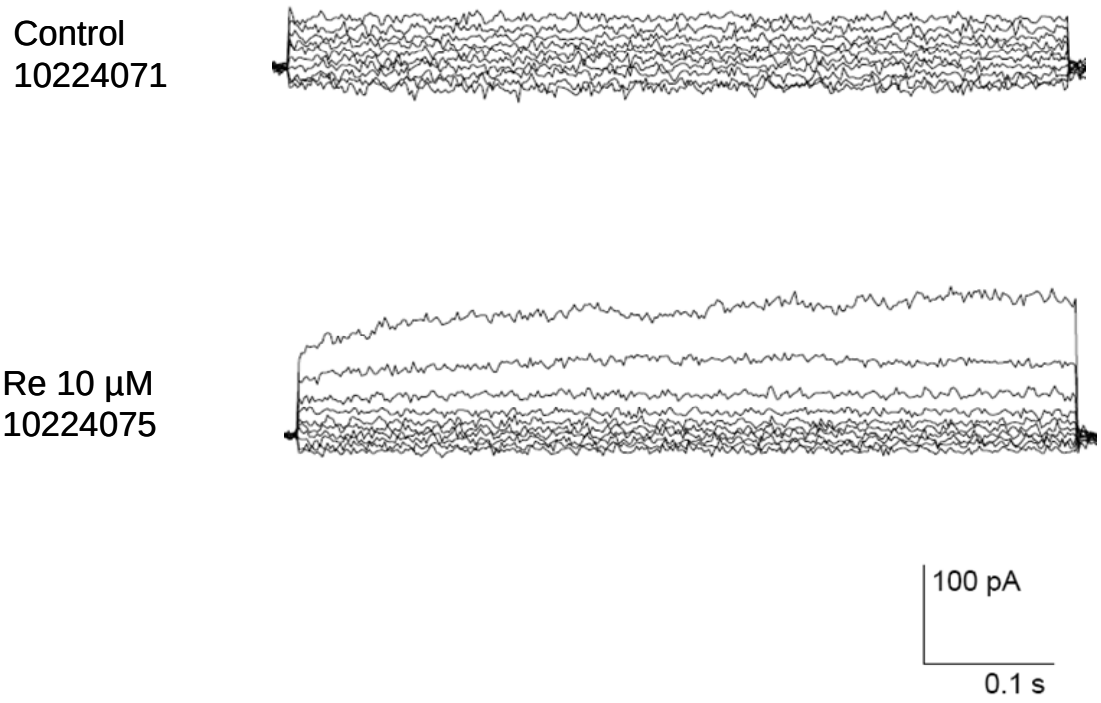

Figure 4.16 Current traces, with and without 10 µM ginsenoside Re, from a representative HCAEC (Cm = 5.66 pF, Rs = 4 MΩ, voltage error = 0.50 mV).

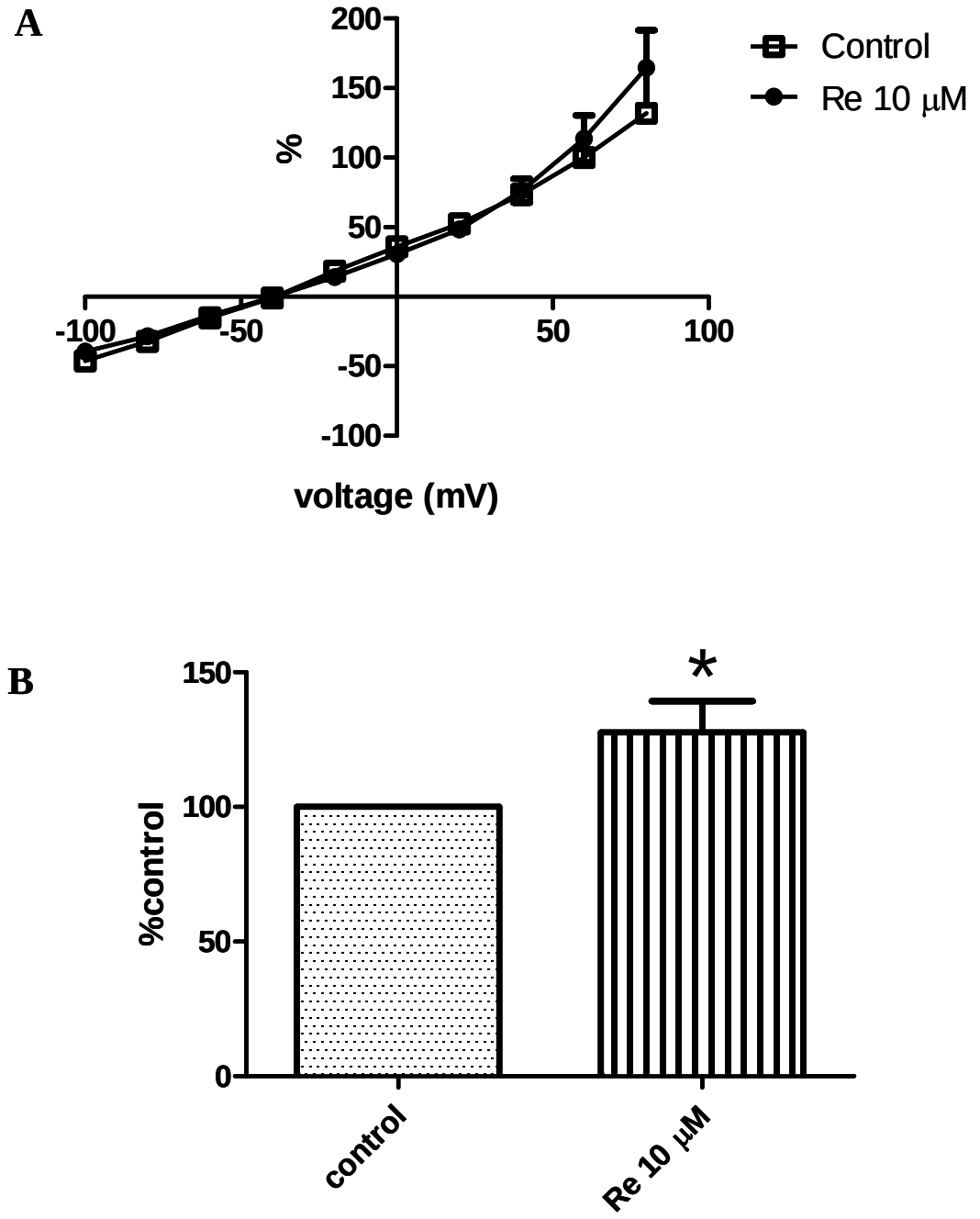

Figure 4.17 Effects of 10 μM ginsenoside Re. Error bars are S.E.M. An asterisk (*) represents a significant increase ($P < 0.05$, one-sample *t* test).

A: The average current-voltage curves, plotted from % control data (n = 9).

B: Bar graphs comparing % control currents at +60 mV from all cells. Significant difference was found between currents in control and 10 μM ginsenoside Re (100 % *vs* 127.70 ± 11.70 %, n = 9, $P = 0.0455$, one-sample *t* test).

Washout currents in control external solution could be recorded in seven out of nine cells. Figure 4.18 shows the current traces with washout in a representative cell. Figure 4.19 shows the average current-voltage curves.

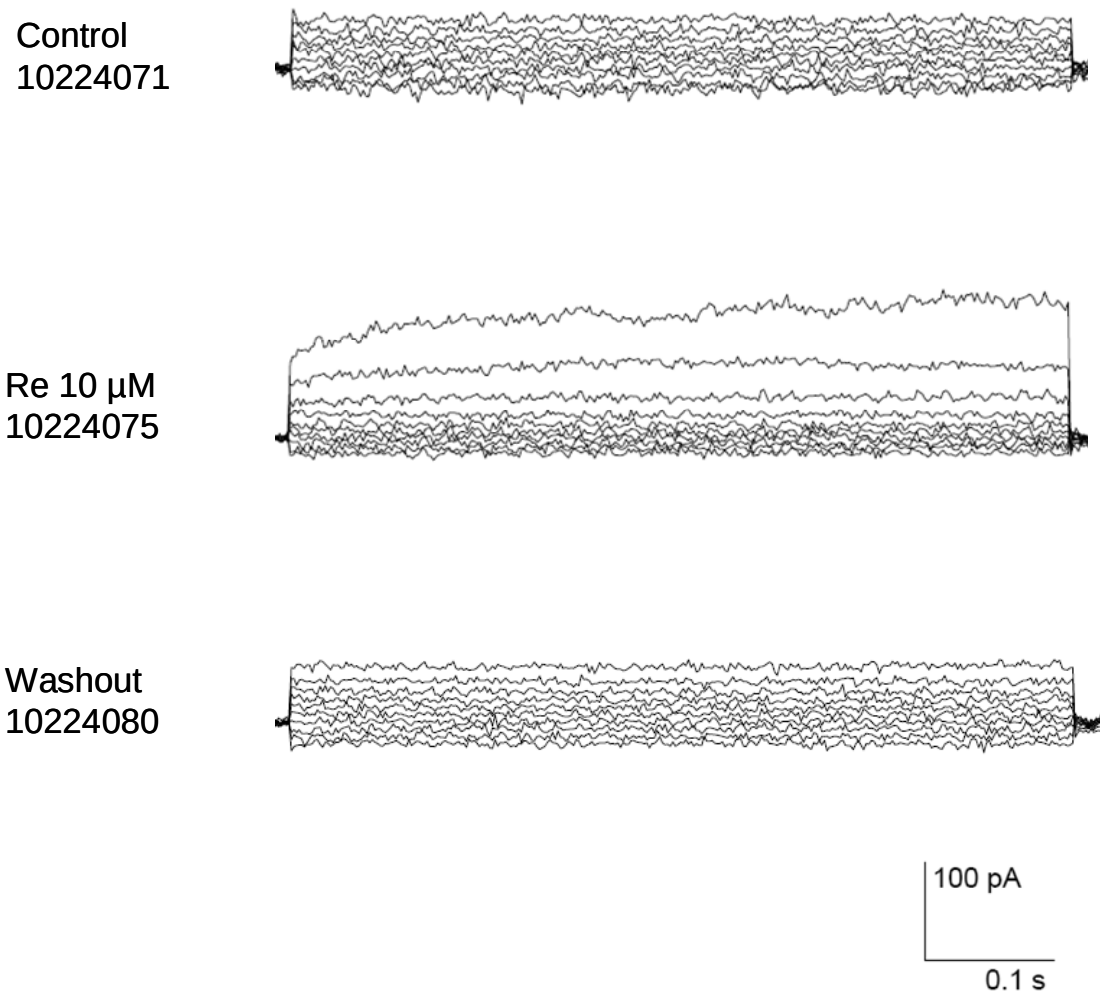

Figure 4.18 Current traces in control *vs* 10 µM ginsenoside Re, with washout currents, from a representative HCAEC (Cm = 5.66 pF, Rs = 4 MΩ, voltage error = 0.50 mV).

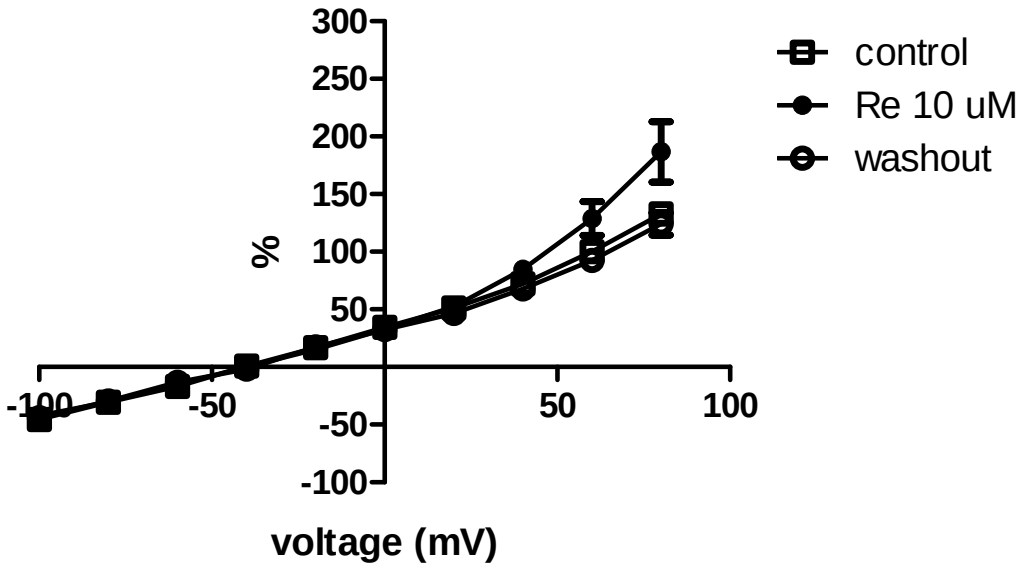

Figure 4.19 The average current-voltage curves in control *vs* 10 μM ginsenoside Re, with washout currents, plotted from % control data (n = 7).

4.1.7 Effect of 30 µM ginsenoside Re

Ginsenoside Re at 30 µM significantly increased outward currents of HCAECs, as shown in figures 4.20 and 4.21. Currents in 30 µM ginsenoside Re were 147.20 ± 16.13 % of control currents (n = 9, *P* = 0.0191, one-sample *t* test).

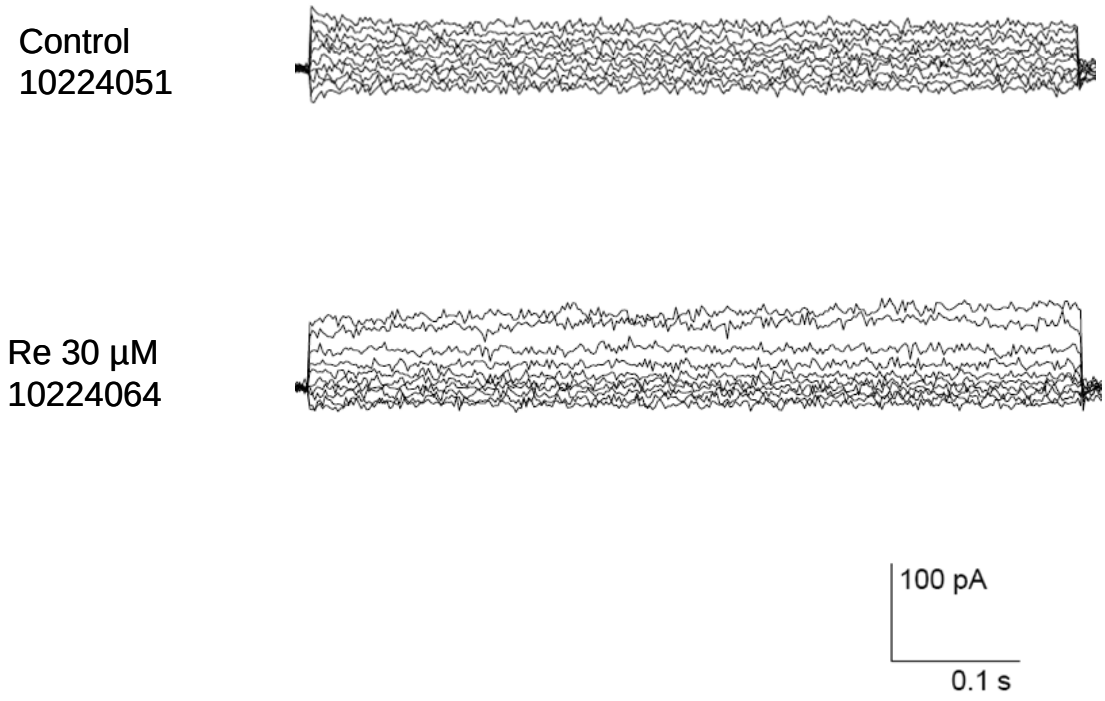

Figure 4.20 Current traces, with and without 30 µM ginsenoside Re, from a representative HCAEC (Cm = 5.66 pF, Rs = 4 MΩ, voltage error = 0.32 mV).

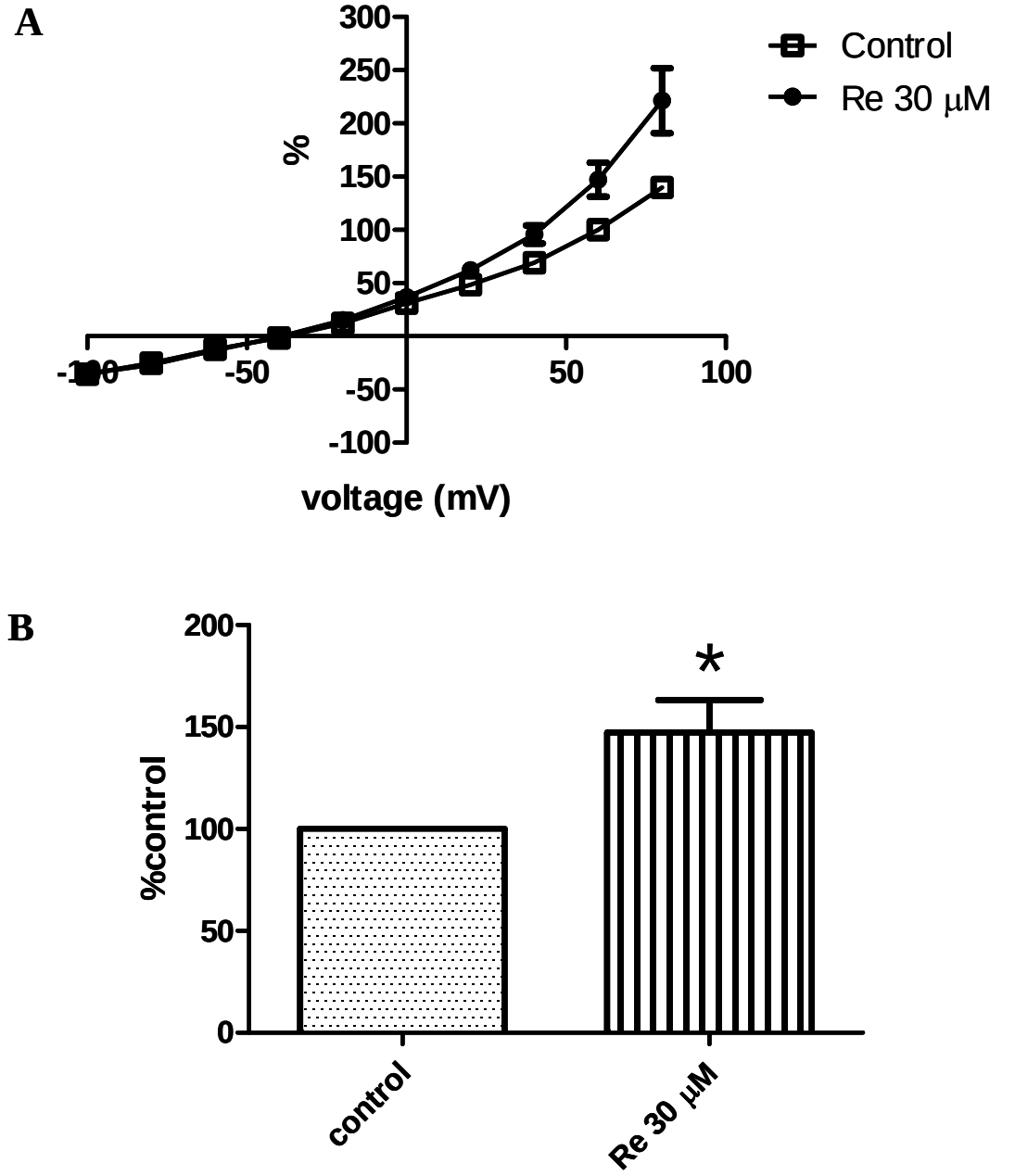

Figure 4.21 Effects of 30 μM ginsenoside Re. Error bars are S.E.M. An asterisk (*) represents a significant increase ($P < 0.05$, one-sample *t* test).

A: The average current-voltage curves, plotted from % control data (n = 9).

B: Bar graphs comparing % control currents at +60 mV from all cells. Significant difference was found between currents in control and 30 μM ginsenoside Re (100 % *vs* 147.20 ± 16.13 %, n = 9, $P = 0.0191$, one-sample *t* test).

Washout currents in control external solution could be recorded in three out of nine cells. Figure 4.22 shows the current traces with washout in a representative cell. Figure 4.23 shows the average current-voltage curves

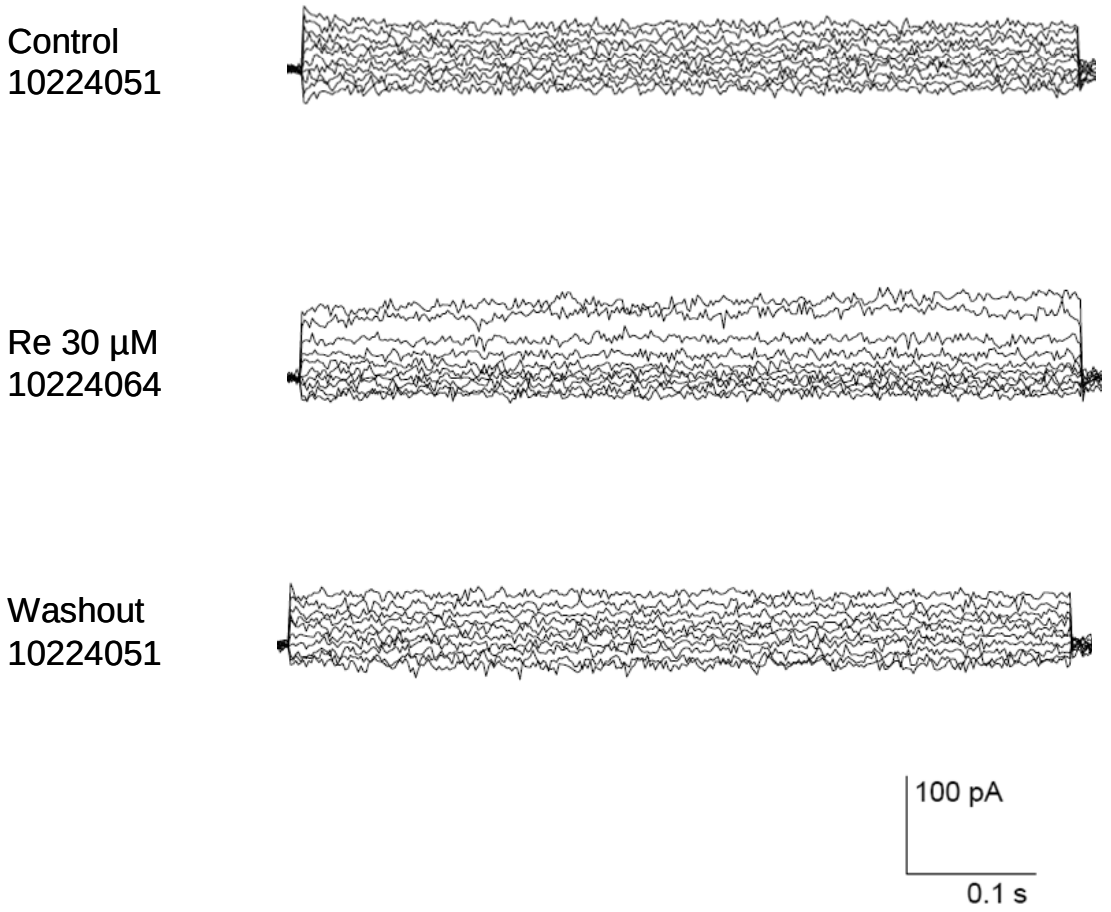

Figure 4.22 Current traces in control *vs* 30 µM ginsenoside Re, with washout currents, from a representative HCAEC (Cm = 5.66 pF, Rs = 4 MΩ, voltage error = 0.32 mV).

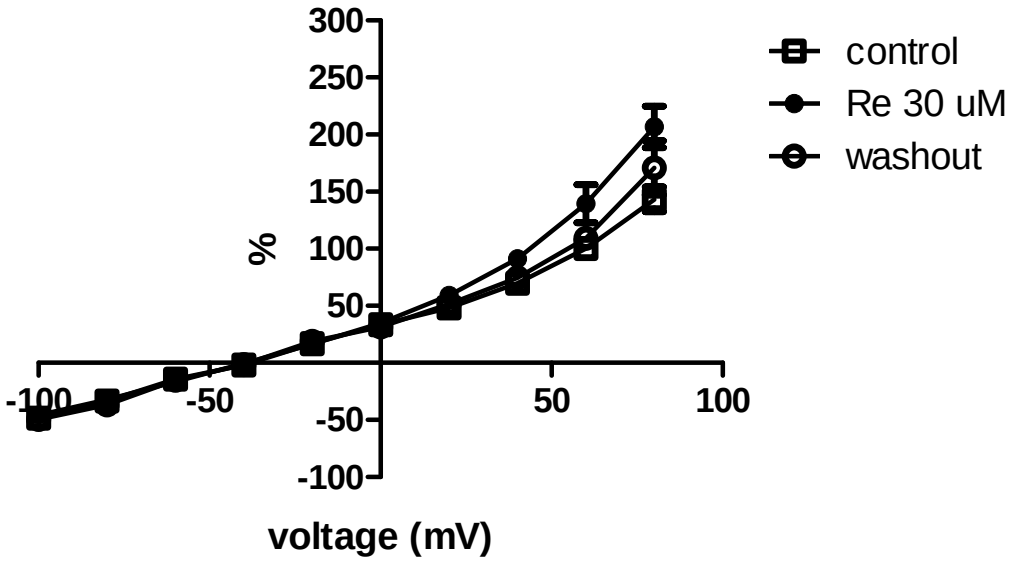

Figure 4.23 The average current-voltage curves in control *vs* 30 μM ginsenoside Re, with washout currents, plotted from % control data (n = 3).

4.1.8 Dose-response relationship

The total cell current amplitudes at +60 mV in control, DMSO, and ginsenoside Re were plotted as bar graphs, using % control (figure 4.24) and % different (figure 4.25) data. Ginsenoside Re at 1, 3, 10 and 30 μM significantly increased HCAEC total currents when compared with control ($P < 0.05$, one-way ANOVA with post hoc Dunnett's multiple comparison test, and also one-sample *t* test). The dose-response relation of % control *vs* log [ginsenoside Re] is shown in figure 4.26. Fitting the curve to the dose-response equation (see Materials & Methods, 3.4.4) yielded an EC50 of 408.90 ± 1.59 nM and a maximum increase of 36.20 ± 5.62 % from currents in control. Because 1 μM ginsenoside Re was the smallest dose that elicited maximal response, this concentration was used in the remaining experiments.

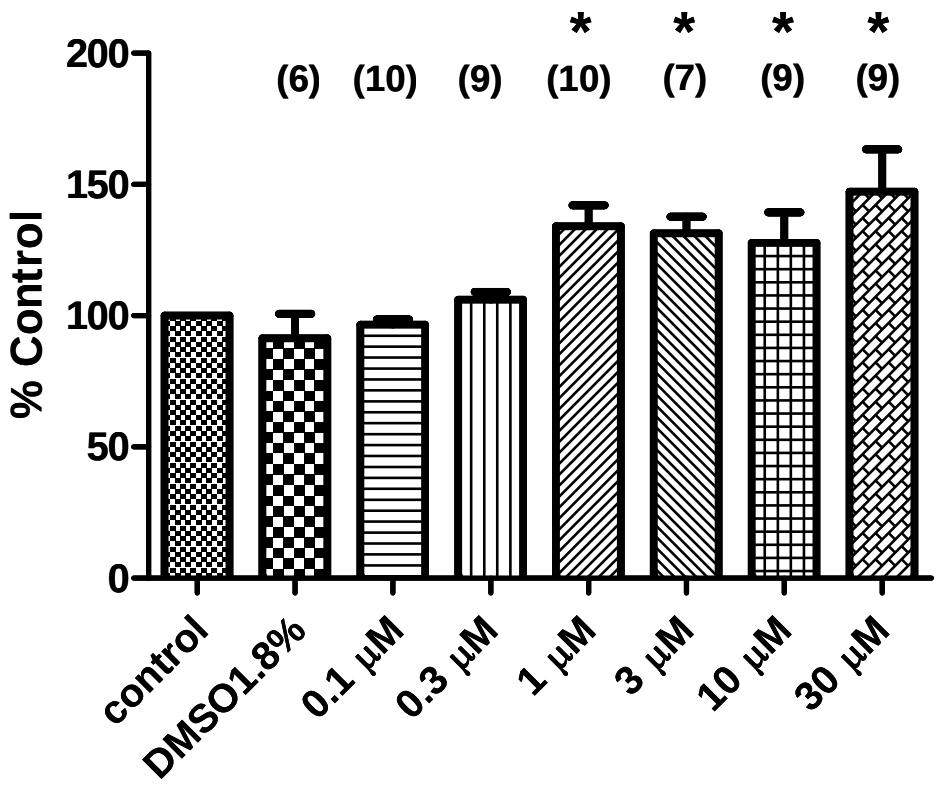

Figure 4.24 Bar graphs showing current amplitudes in % control, comparing in control (= 100%), DMSO, and various concentrations of ginsenoside Re. Error bars are S.E.M. Asterisks (*) represent significant increases ($P < 0.05$, one-way ANOVA with post hoc Dunnett's multiple comparison test, and also one-sample *t* test).

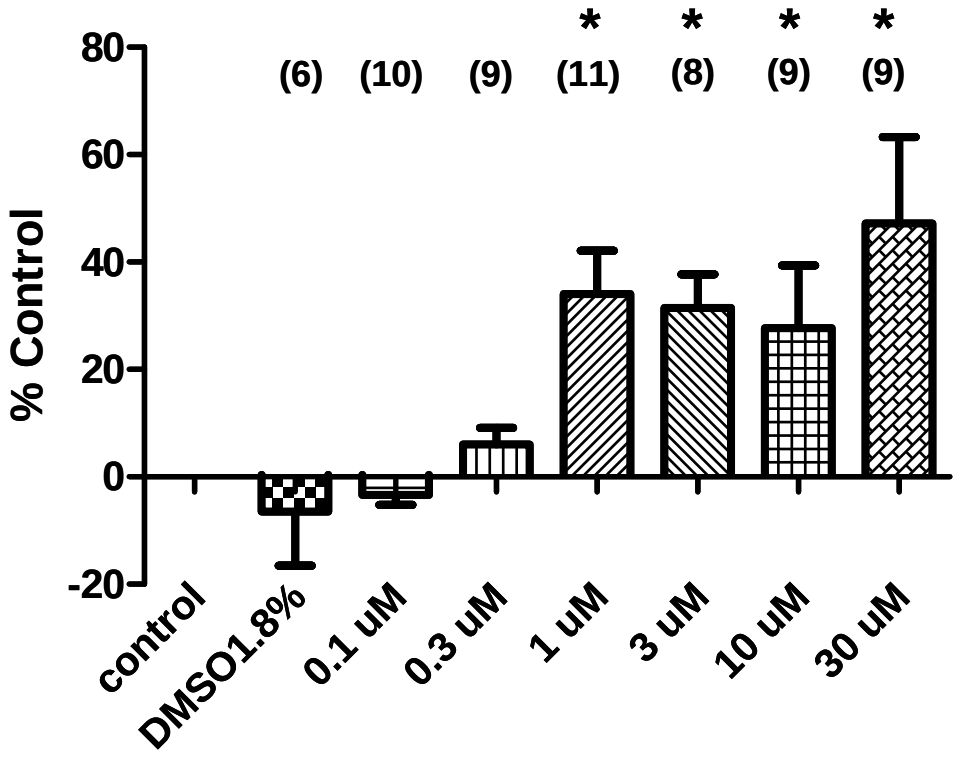

Figure 4.25 Bar graphs showing current amplitudes in % different, comparing in control (= 0%), DMSO, and various concentrations of ginsenoside Re. Error bars are S.E.M. Asterisks (*) represent significant increases ($P < 0.05$, one-way ANOVA with post hoc Dunnett's multiple comparison test, and also one-sample *t* test).

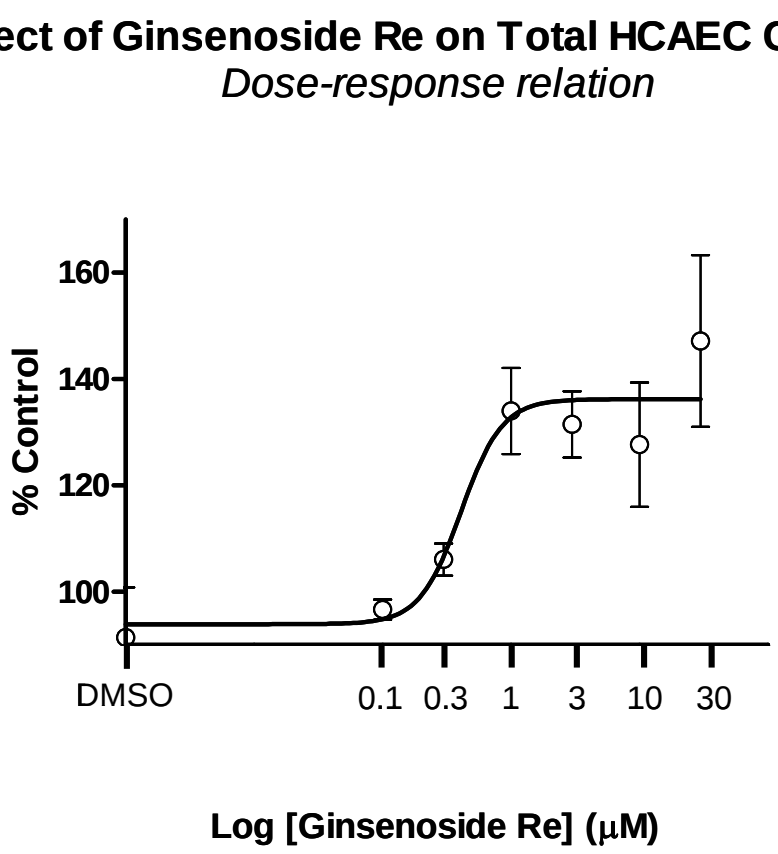

Figure 4.26 Dose-response relation.

Ginsenoside Re concentrations were plotted in a log scale on the X-axis, while % control of HCAEC currents at +60 mV were plotted on the Y-axis. Curve-fitting to the dose-response equation was done in GraphPad PRISM 5 program. The resulting EC50 was 408.90 $\pm$ 1.59 nM, with a maximum increase of 36.20 $\pm$ 5.62 %.

4.2 Effect of ginsenoside Re on small-conductance Ca^{2+}-activated K^+ channels in HCAECs: Apamin experiments

4.2.1 Effect of ginsenoside Re when SK_{Ca} was blocked

In this experiment, apamin, a specific blocker of small-conductance calcium-activated potassium (SK_{Ca}) channels, was added to the external solution. Currents were recorded in 100 nM apamin *vs* 100 nM apamin plus 1 μM ginsenoside Re. Raw data from a representative cell are shown in figure 4.27, with I-V curves and bar graphs in figure 4.28. In the presence of 100 nM apamin, 1 μM ginsenoside Re did not significantly affect the membrane currents (101.20 ± 6.56 % of control, 1.20 ± 6.56 % difference, n = 8, P = 0.8654, one-sample t test). Apparently, ginsenoside Re did not affect HCAEC currents when SK_{Ca} was blocked.

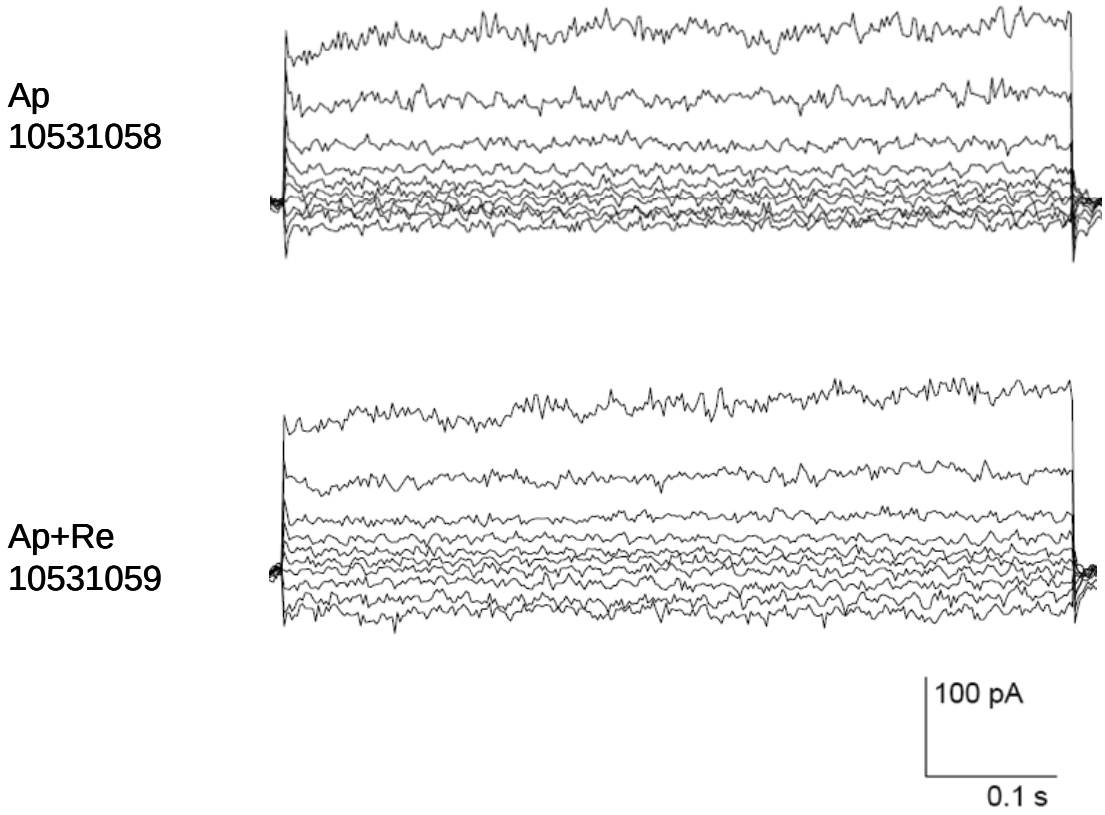

Figure 4.27 Current traces in 100 nM apamin, with and without 1 μM ginsenoside Re, from a representative HCAEC (Cm = 6.54 pF, Rs = 9.5 MΩ, voltage error = 1.78 mV).

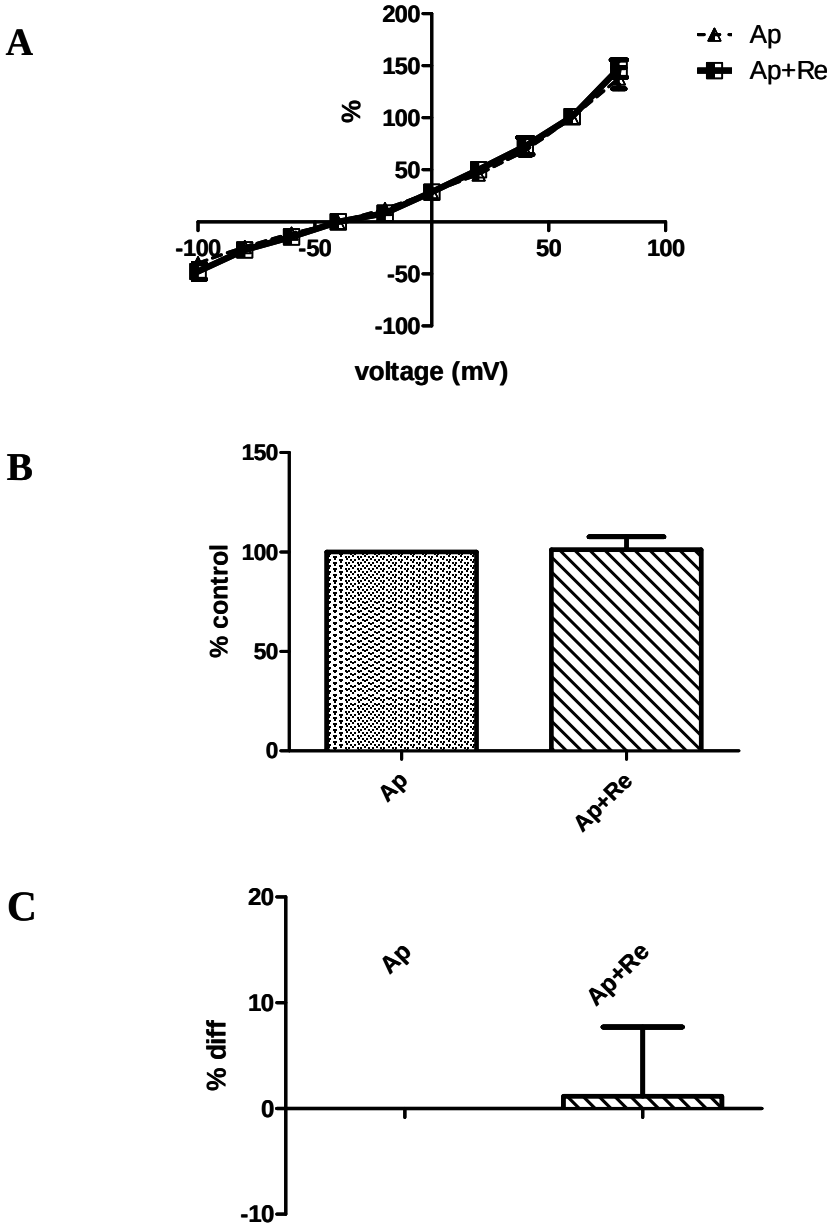

Figure 4.28 Effect of 1 μM ginsenoside Re in the presence of 100 nM apamin. Error bars are S.E.M.

A: The average current-voltage curves, plotted from % control data (n = 8).

B: Bar graphs comparing currents at +60 mV in % control from all cells. No difference between apamin and apamin with 1 μM ginsenoside Re was found (100 % vs 101.20 ± 6.56 %, $P = 0.8654$, one-sample t test).

C: Bar graphs comparing % different at +60 mV from all cells.

In three out of eight cells, currents in external solution only were also recorded before 100 nM apamin was added. An example of such recording is shown in figure 4.29. The corresponding I-V curves are shown in figure 4.30. On average, apamin could block 24.91 ± 11.04 % of control currents (n = 3)

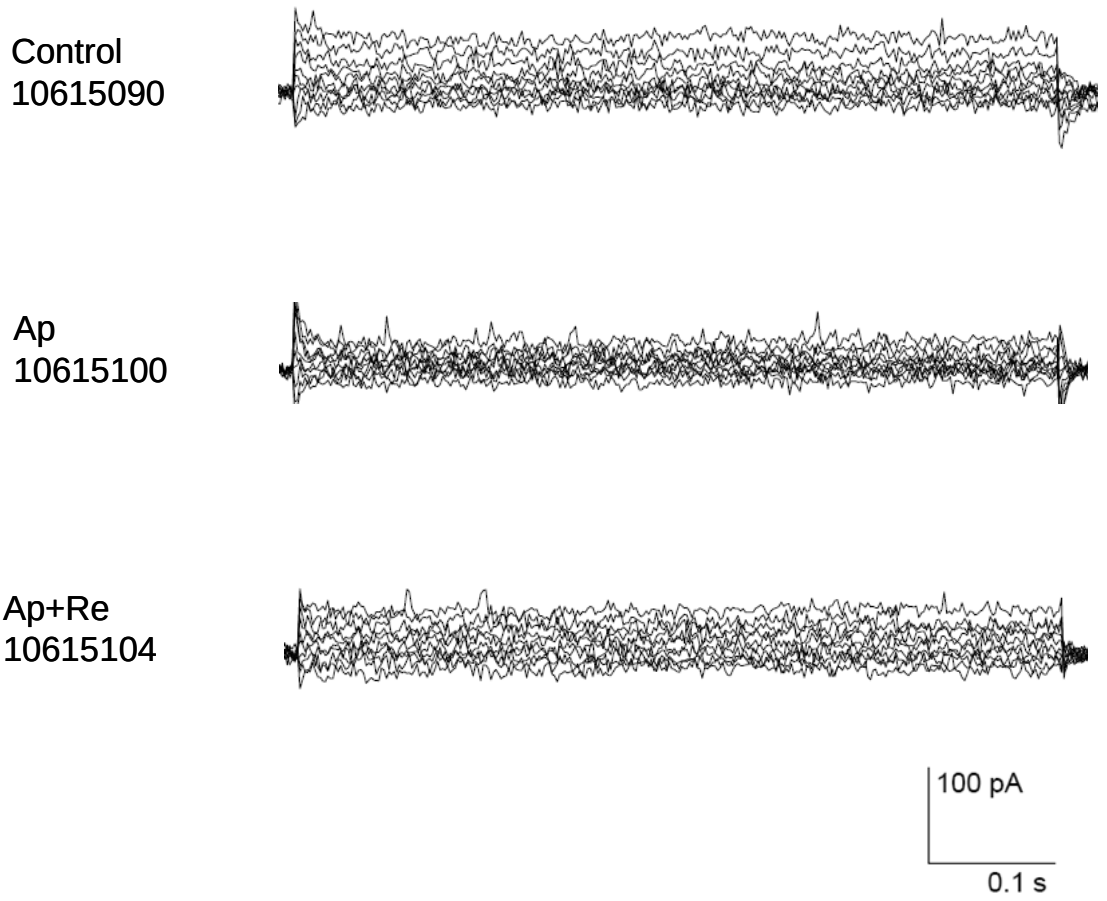

Figure 4.29 Current traces in control, 100 nM apamin and 100 nM apamin with 1 μM ginsenoside Re, from a representative HCAEC (Cm = 17.68 pF, Rs = 2.8 MΩ, voltage error = 0.12 mV).

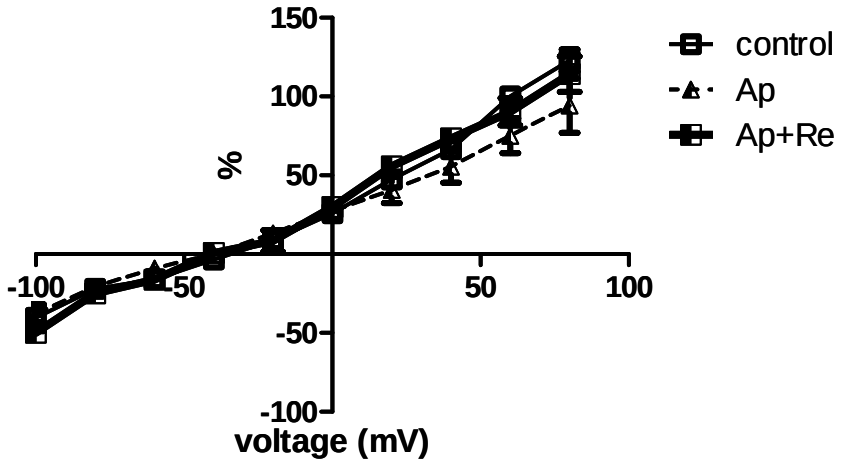

Figure 4.30 Average current-voltage curves from three cells where control currents were recorded before addition of 100 nM apamin and 100 nM apamin + 1 μM ginsenoside Re. Error bars are S.E.M.

4.2.2 Effect of apamin on ginsenoside Re-induced currents

In this experiment, currents were first recorded in 1 μM ginsenoside Re, followed by 1 μM ginsenoside Re with 100 nM apamin. Current traces from a representative cell are shown in figure 4.31. The average current-voltage curves and bar graphs are in figure 4.32. We found that the outward currents at +60 mV were significantly decreased after adding apamin, (remaining currents after apamin were 73.02 ± 4.76 % compared with ginsenoside Re alone, or 26.98 ± 4.76 % different, n = 8, $P = 0.0008$, one-sample *t* test).

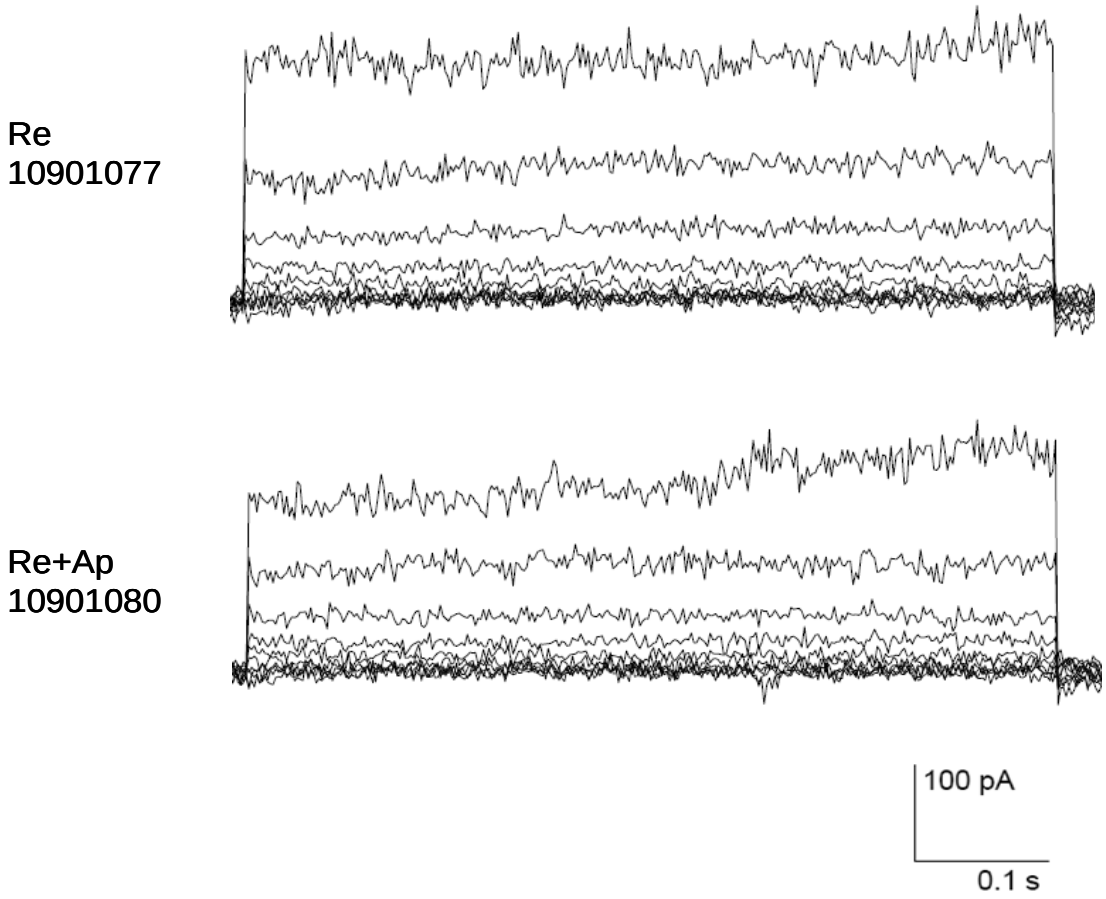

Figure 4.31 Current traces in 1 μM ginsenoside Re, with and without 100 nM apamin, from a representative HCAEC (Cm = 23.97 pF, Rs = 6 MΩ, voltage error = 1.24 mV).

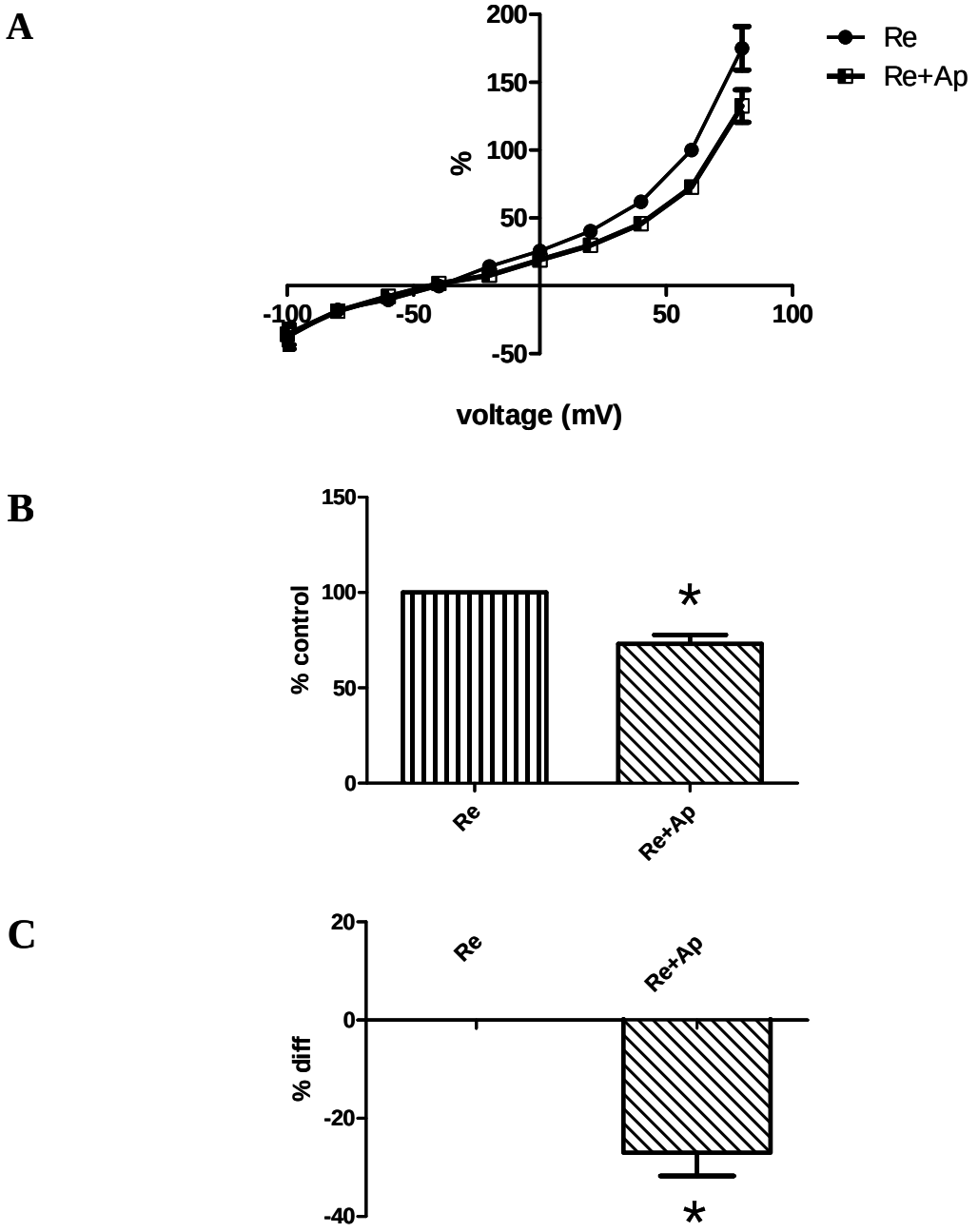

Figure 4.32 Effects of 100 nM apamin in the presence of 1 μM ginsenoside Re. Error bars are S.E.M. Asterisks (*) represent significant changes.

A: The average current-voltage curves, plotted from % control data (n = 8).

B: Bar graphs comparing % control currents at +60 mV from all cells. Significant difference between 1 μM ginsenoside Re and 1 μM ginsenoside Re with apamin was found (100 % vs 73.02 ± 4.76 %, n = 8, $P = 0.0008$, one-sample t test).

C: Bar graphs showing average % different of currents at +60 mV from all cells.

Reversibility of apamin blockade on ginsenoside Re-induced currents could be demonstrated in six out of eight cells. Figure 4.33 shows the current traces in 1 μM ginsenoside Re, 1 μM ginsenoside Re + 100 nM apamin, and 1 μM ginsenoside Re (washout) in a representative cell. Corresponding average current-voltage curves are shown in figure 4.34. The washout currents at +60 mV were 98.84 $\pm$ 4.46 % of control (both in ginsenoside Re). The difference was not significant (n = 6, P = 0.8050, one-sample t test).

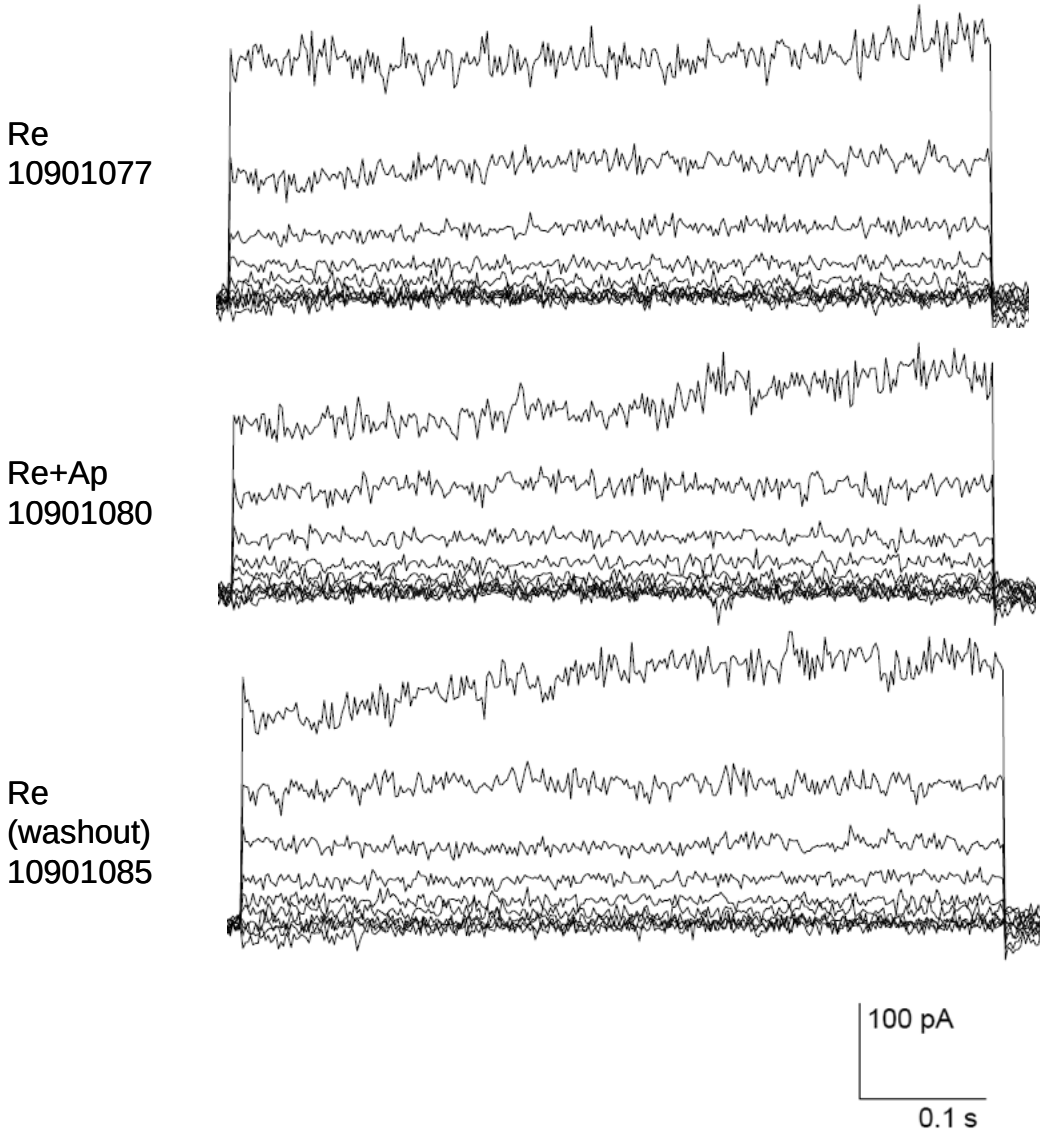

Figure 4.33 Current traces recorded in 1 μM ginsenoside Re ("Re"), 1 μM ginsenoside Re with 100 nM apamin ("Re+Ap") and on return to 1 μM ginsenoside Re ("Re (washout)"), from a representative HCAEC (Cm = 23.97 pF, Rs = 6 MΩ, voltage error = 1.57 mV).

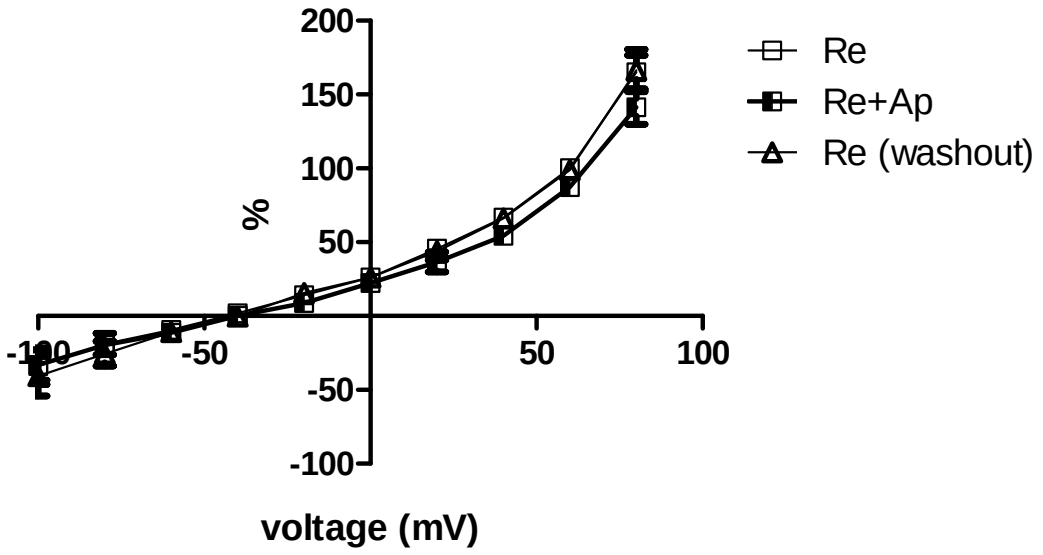

Figure 4.34 The average current-voltage curves, showing the effect of 100 nM apamin on ginsenoside Re-induced currents and washout (on return to 1 μM ginsenoside Re), plotted from % control data (n = 6). Re *vs* Re (washout) = 100 % vs 98.84 $\pm$ 4.46 % (*P* = 0.8050, one-sample *t* test).

4.3 Effect of ginsenoside Re on small-conductance Ca^{2+}-activated K^+ channels in HCAECs: Four-blocker experiments.

4.3.1 Effect of ginsenoside Re in the presence of four-blocker solution

Four-blocker solution contained 10 μM La^{3+}, 10 μM clotrimazole, 1 mM TEA and 2 mM Ba^{2+}, all mixed in external solution, for blocking nonselective cation (NSC) channel, intermediate-conductance calcium-activated potassium (IK_{Ca}) channel, large-conductance calcium-activated potassium (BK_{Ca}) channel, and inward-rectifier potassium (K_{ir}) channel, respectively. In the presence of four-blocker solution, control currents were significantly decreased to 41.47 ± 3.20 % (a -58.53 ± 3.20 % different, n = 6, $P < 0.0001$, one sample t test). Current traces from a representative cell are shown in figure 4.35, and the current-voltage curves and bar graphs are in figure 4.36.

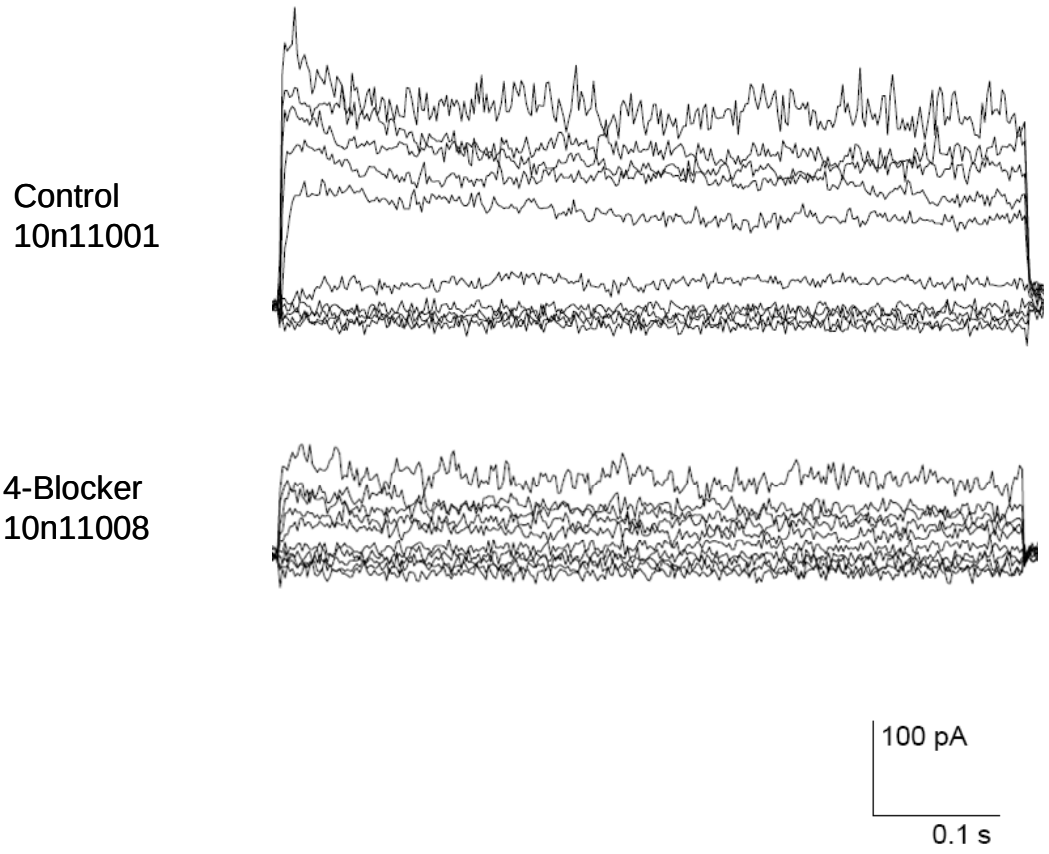

Figure 4.35 Current traces in control and four-blocker solutions, from a representative HCAEC (Cm = 64.99 pF, Rs = 6.5 MΩ, voltage error = 1.33 mV).

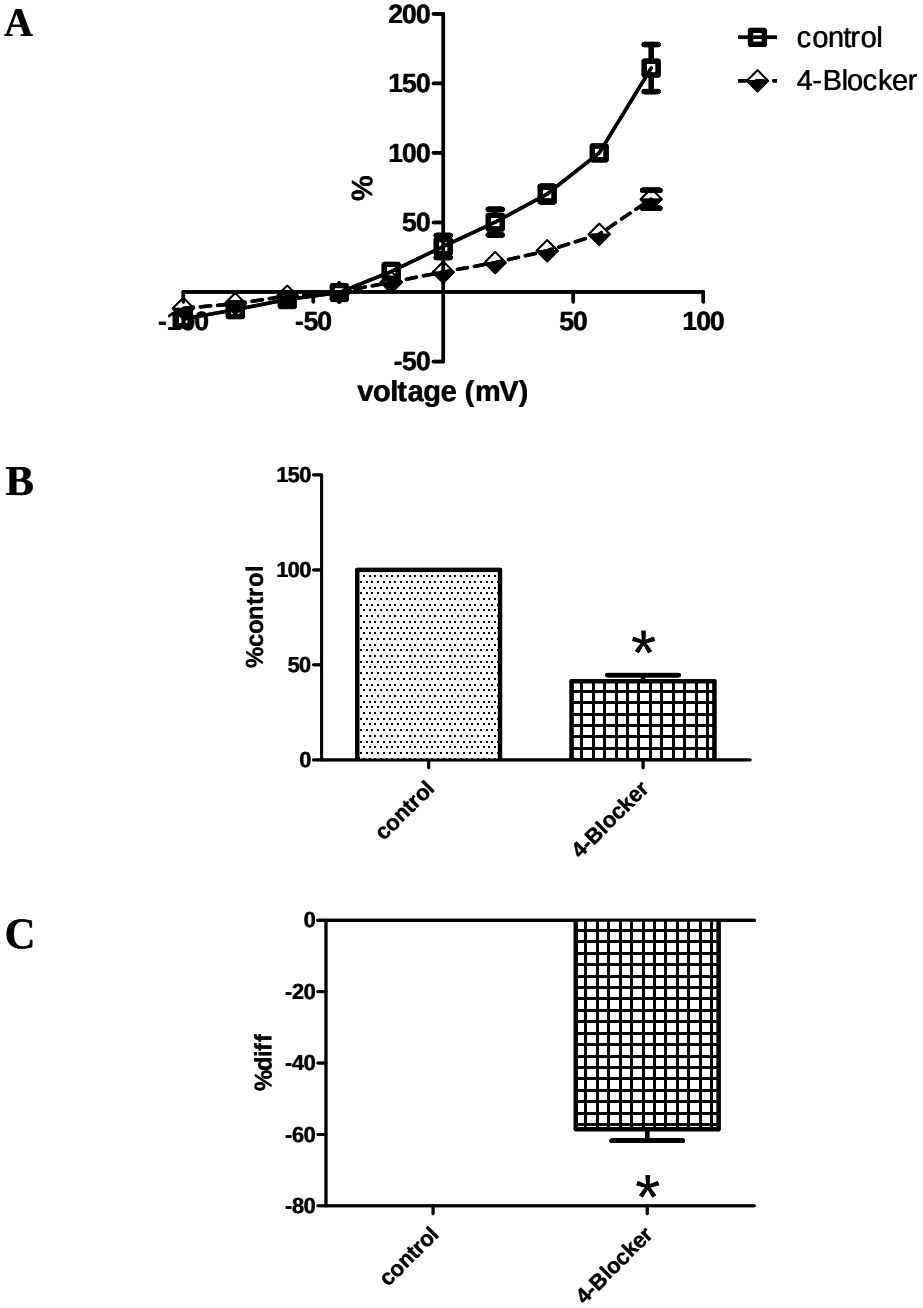

Figure 4.36 Effects four-blocker solution on total HCAEC currents. Error bars are S.E.M. Asterisks (*) represent significant changes ($P < 0.05$,).

A: The average current-voltage curves, plotted from % control data (n = 6).

B: Bar graphs comparing % control currents at +60 mV from all cells. Significant difference was found between currents in control *vs* four-blocker solutions (100 % *vs* 41.47 ± 3.20 %, $P < 0.0001$, one-sample *t* test).

C: Bar graphs showing average % different of currents at +60 mV (58.53 ± 3.20 %).

Addition of 1 μM ginsenoside Re in the four-blocker solution could significantly enhance the currents by 35.49 ± 4.22 % (n = 15, $P < 0.0001$, one-sample *t* test). Traces from a representative cell are shown in figure 4.37. The current voltage curves and bar graphs are in figure 4.38. Thus ginsenoside Re-induced currents may not be NSC, IK_{Ca}, BK_{Ca} or K_{ir} currents.

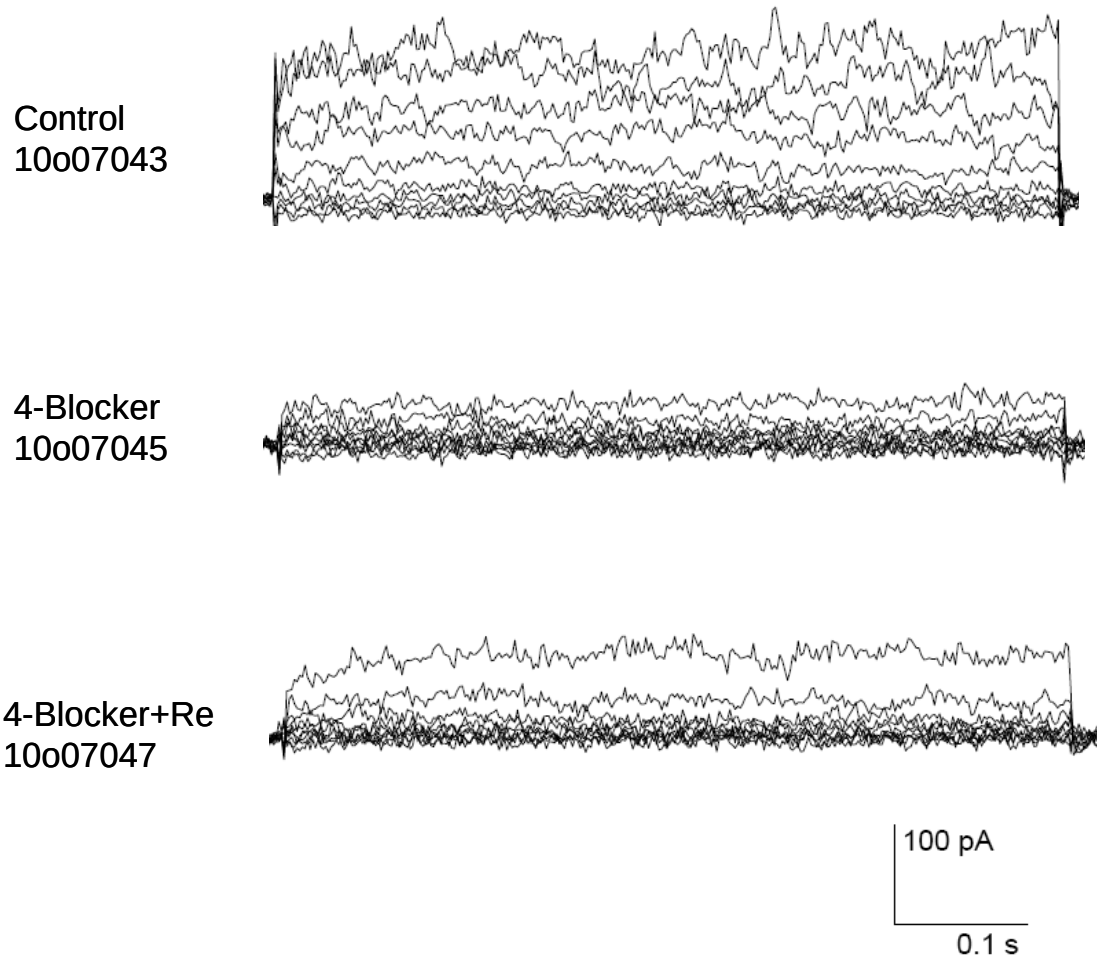

Figure 4.37 Current traces in control, four-blocker and four-blocker plus 1 μM ginsenoside Re, from a representative HCAEC (Cm = 4.67 pF, Rs = 9.5 MΩ, voltage error = 0.79 mV).

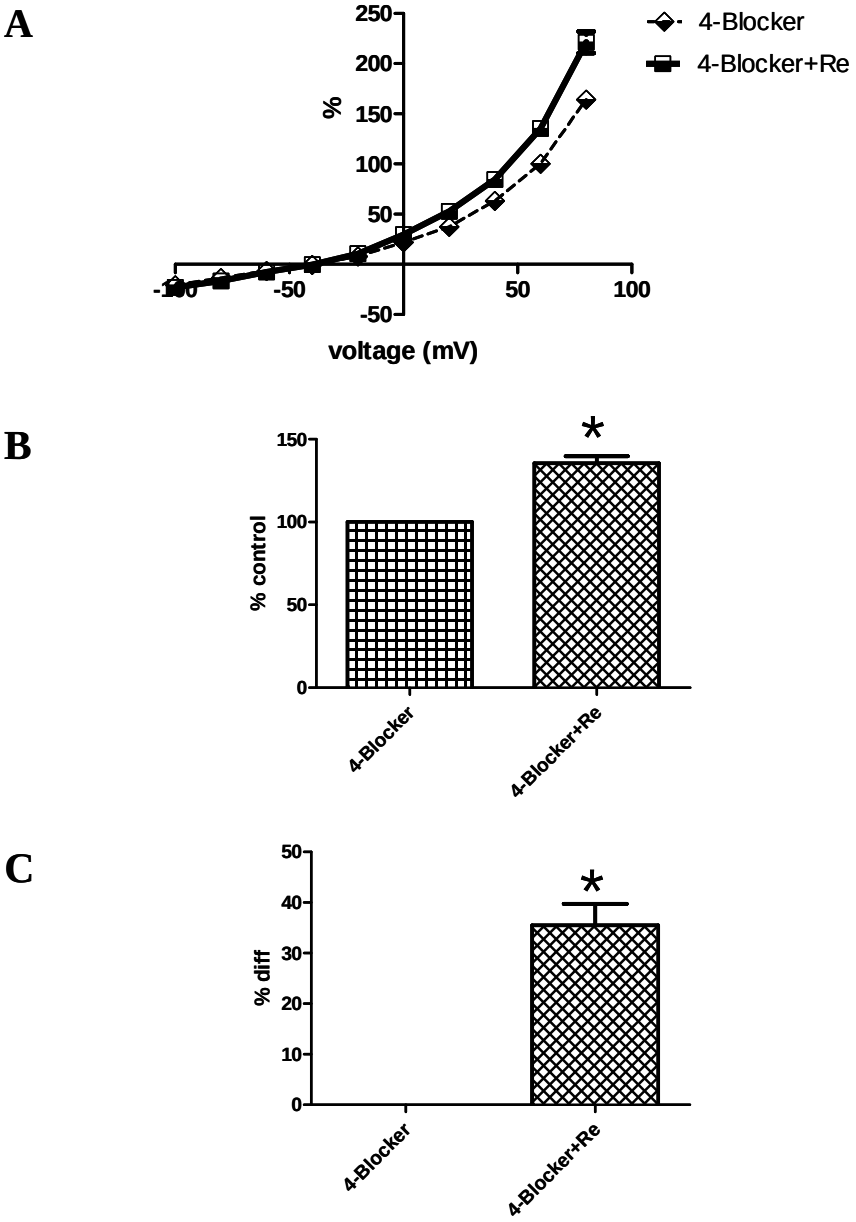

Figure 4.38 Effects of 1 μM ginsenoside Re in the presence of four-blocker solution. Error bars are S.E.M. Asterisks (*) represent significant increases ($P < 0.05$).

A: The average current-voltage curves, plotted from % control data (n = 15).

B: Bar graphs comparing % control currents at +60 mV from all cells. 1 μM Ginsenoside Re caused a significant increase (135.49 ± 4.22 %) in the four-blocker solution (n = 15, $P < 0.0001$, one-sample *t* test).

C: Bar graphs in B, re-plotted in % different.

In the presence of four-blocker solution, the washout currents (on return to four-blocker solution after testing with) could be recorded in four out of fifteen cells. Comparison of current traces in four-blocker, four-blocker plus 1 μM ginsenoside Re, and four-blocker solutions (washout) are shown in figure 4.39, with current voltage curves in figure 4.40. Washout currents were 110.00 ± 6.99 % of control (both in four-blocker solution; n = 4).

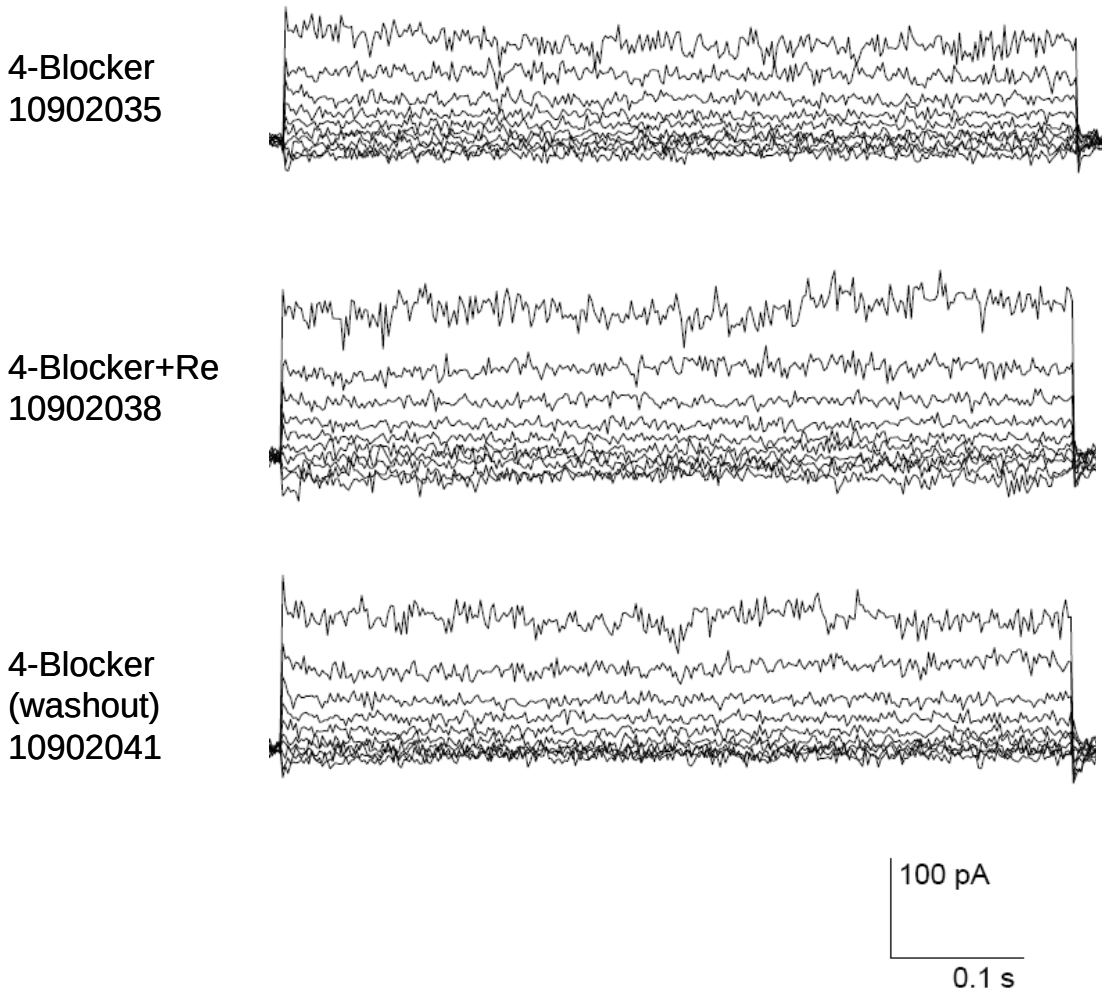

Figure 4.39 Current traces in four-blocker solutions, with and without 1 μM ginsenoside Re, are shown, followed by washout currents (returned to four-blocker solution), from a representative HCAEC (Cm = 9.77 pF, Rs = 6.9 MΩ, voltage error = 1.06 mV).

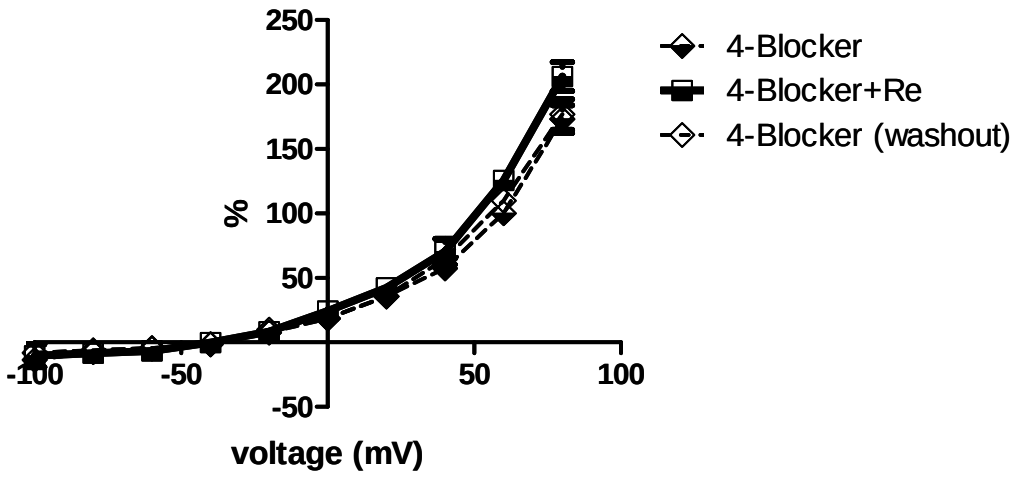

Figure 4.40 The average current-voltage curves in four-blocker solution, with and without 1 μM ginsenoside Re and washout (four-blocker) solution (n = 4).

4.3.2. Effect of apamin on ginsenoside Re-induced currents in the presence of four-blocker solution.

To demonstrate if SKCa was increased by ginsenoside Re, apamin was added in the presence of four-blocker solution and 1 μM ginsenoside Re. The result from a representative cell is shown in figure 4.41. The average current-voltage curves and bar graphs are shown in figure 4.42. In three cells and in the presence of four-blocker solution, 1 μM ginsenoside Re could increase HCAEC currents to 179.00 ± 18.43 %. Addition of 100 nM apamin reduced the ginsenoside Re-induced currents to 39.56 $\pm$ 7.30 % compared to currents before apamin (in four-blocker solution + ginsenoside Re) or to 72.00 ± 19.64% compared to currents in four-blocker solution only. Returning to four-blocker solution plus 1 μM ginsenoside Re (apamin washout) could return the currents to 107.20 $\pm$ 15.87 % of currents before apamin (or 190.00 ± 28.62 % compared to four-blocker only). These data suggested that the currents induced by 1 μM ginsenoside Re may pass through SK_{Ca} channels.

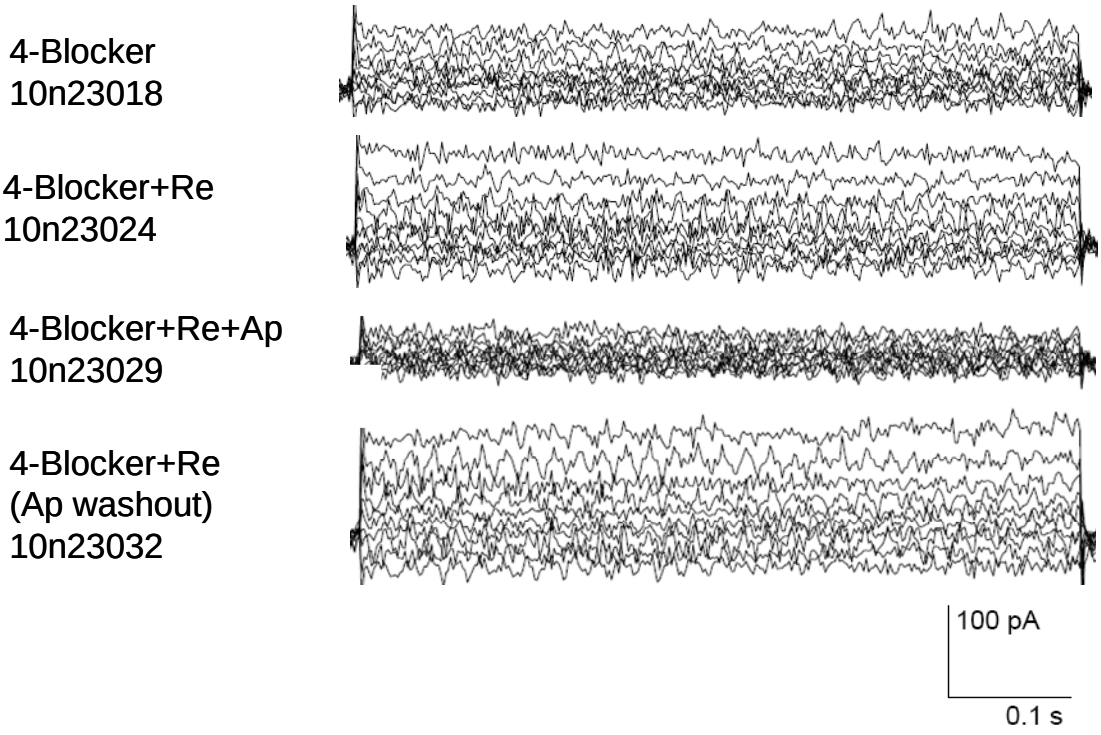

Figure 4.41 An experiment in four-blocker solution, four-blocker, four-blocker + 1 μM ginsenoside Re, four-blocker with both 1 μM ginsenoside Re and 100 nM apamin, and back to four-blocker with 1 μM ginsenoside Re (apamin washout), from a representative HCAEC (Cm = 59.67 pF, Rs = 5.5 MΩ, voltage error 0.68 = mV).

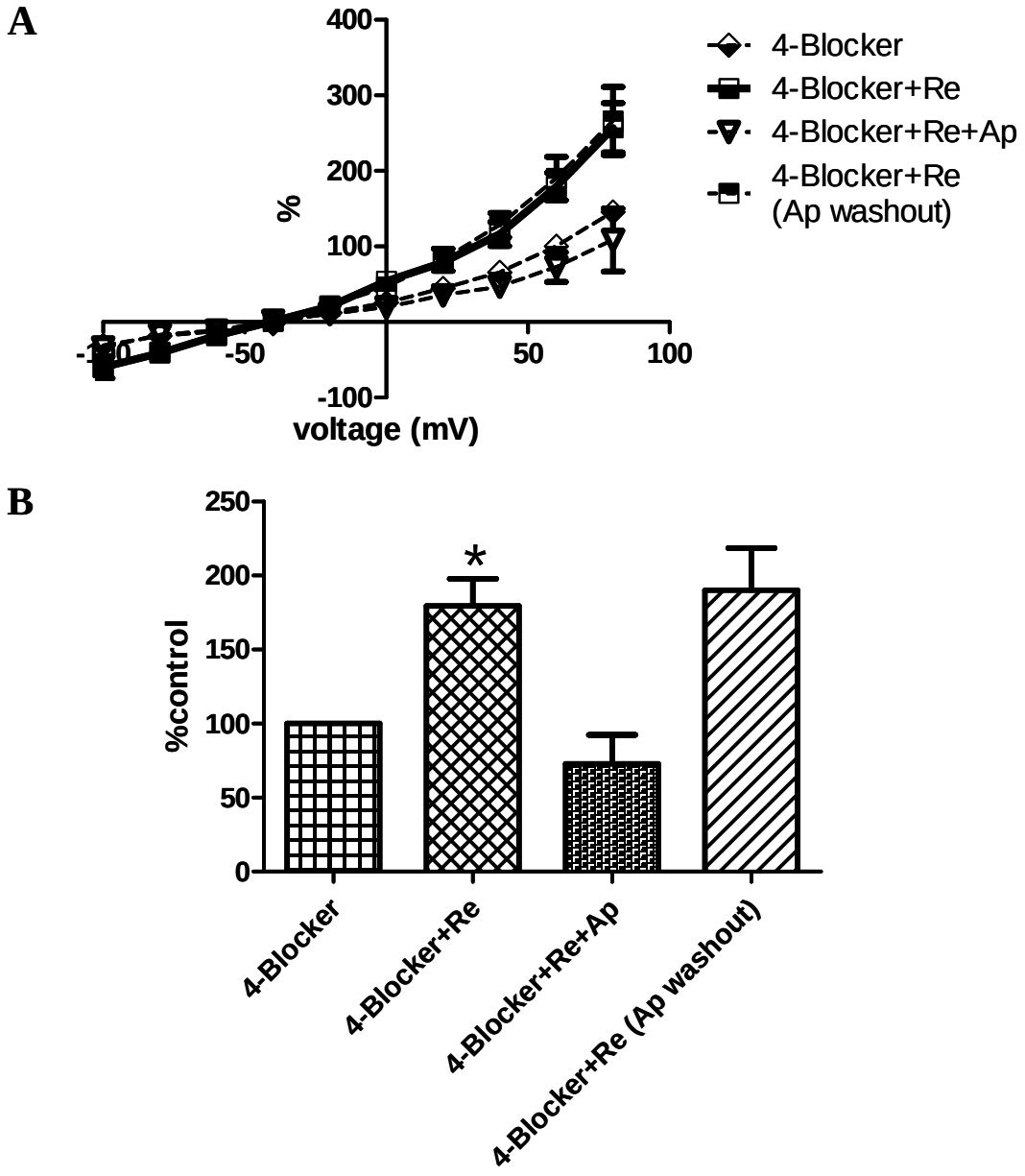

Figure 4.42 Effect of apamin on ginsenoside Re-induced currents. Error bars are S.E.M. .

A: The average current-voltage curves in four-blocker, four-blocker with 1 μM ginsenoside Re, four-blocker + 1 μM ginsenoside Re + 100 nM apamin, and on return to four-blocker + 1 μM ginsenoside Re (apamin washout) solutions data (n = 3).

B: Bar graphs of experiments in A, comparing % control currents at +60 mV from all cells.

4.4 Effect of ginsenoside Re on non-selective cation channels in HCAECs: La^{3+} experiments

4.4.1 Effect of ginsenoside Re when NSC was blocked

La^{3+} is a specific blocker of nonselective cation (NSC) channel, a member of the transient receptor potential (TRP) family. To test the role of NSC channels, experiments were performed in external solution with 10 μM La^{3+}, with and without 1 μM ginsenoside Re. Current traces of a representative cell are shown in figure 4.43, while average current-voltage curves and bar graphs are shown in figure 4.44. 1 μM Ginsenoside Re could significantly increase the outward currents of HCAECs in the presence of La^{3+} (28.93 ± 7.54 % increase, n = 9, P = 0.0050, one-sample t test).

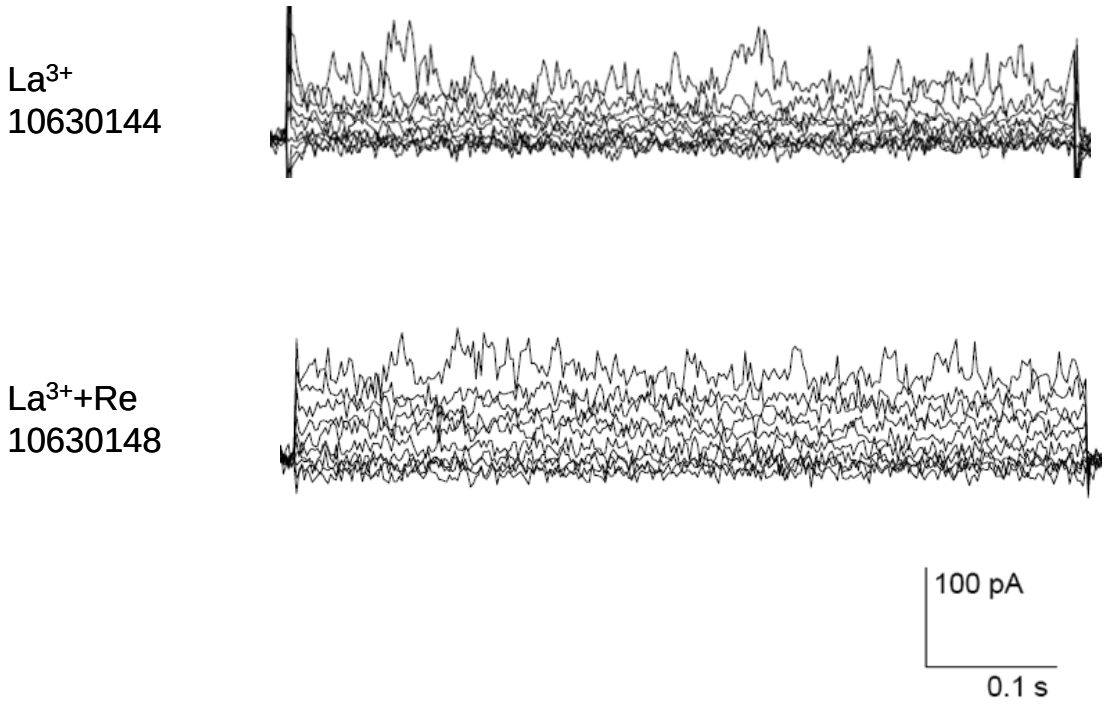

Figure 4.43 Current traces in 10 μM La^{3+}, with and without 1 μM ginsenoside Re, from a representative HCAEC (Cm = 45.12 pF, Rs = 4.2 MΩ, voltage error = 0.36 mV).

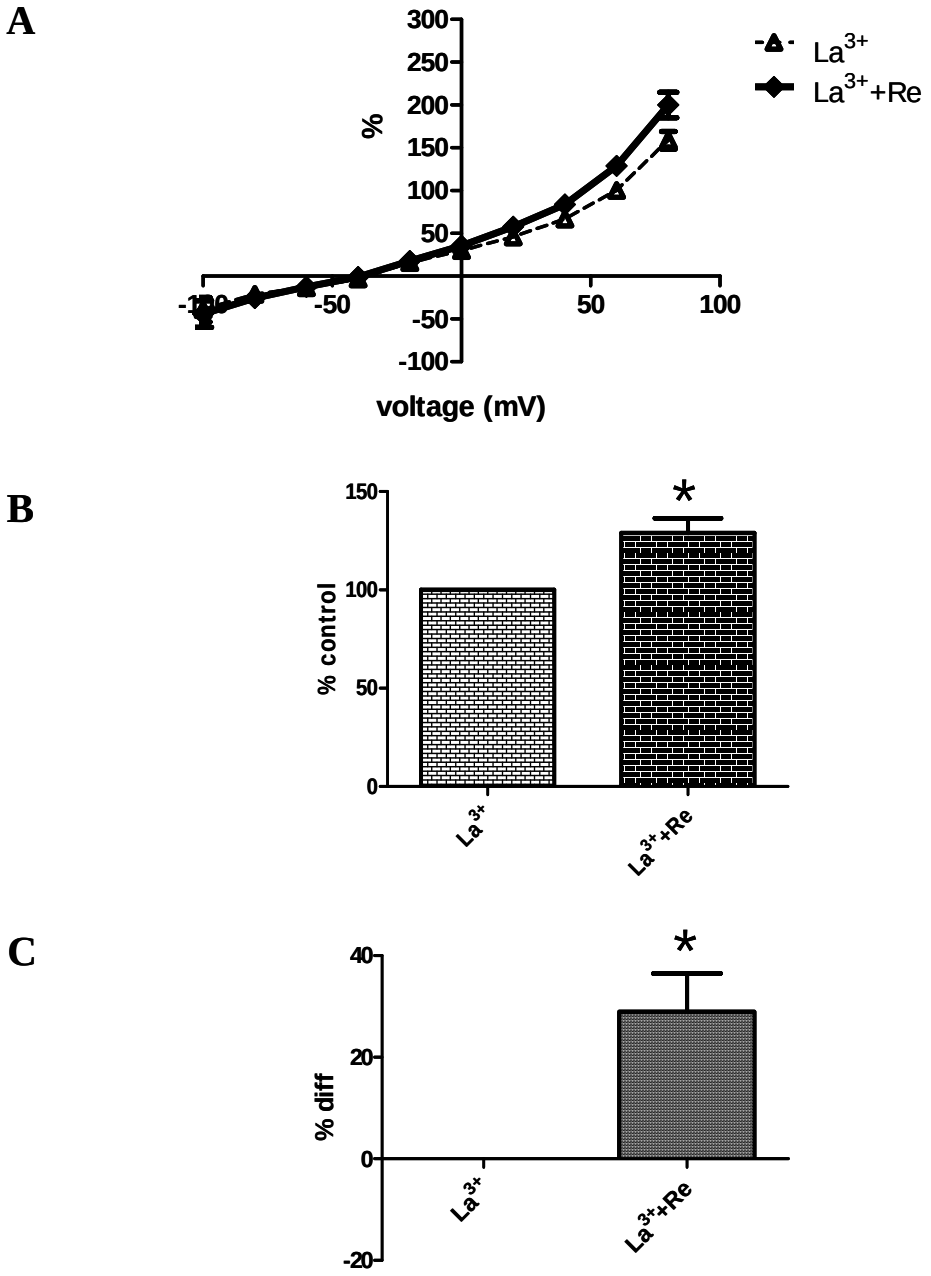

Figure 4.44 Effect of 1 μM ginsenoside Re in the presence of 10 μM La^{3+}. Error bars are S.E.M. Asterisks (*) represent significant increases ($P < 0.05$).

A: The average current-voltage curves, plotted from % control data (n = 9).

B: Bar graphs comparing currents at +60 mV in % control from all cells. 1 μM Ginsenoside Re caused a significant increase (128.93 ± 7.54 %) in the La^{3+} solution (n = 9, $P = 0.0050$, one-sample *t* test).

C: Bar graphs comparing % different at +60 mV from all cells.

In four out of nine cells, currents in external solution only were also recorded before 10 μM La^{3+} was added. An example of such recording is shown in figure 4.45. The corresponding I-V curves are shown in figure 4.46. On average, La^{3+} could block 34.41 ± 4.00 % of control currents (n = 4)

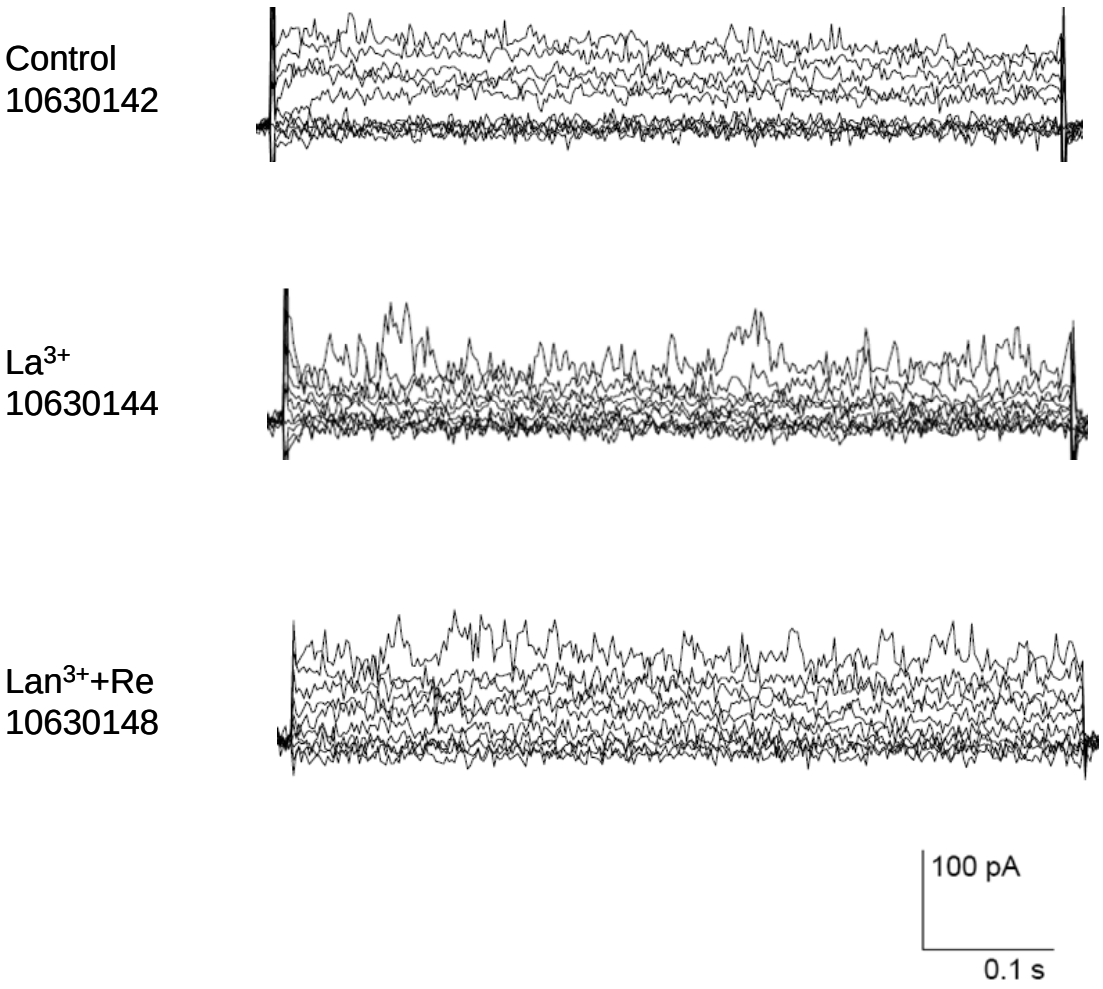

Figure 4.45 Current traces in control, 10 μM La^{3+} and 10 μM La^{3+} with 1 μM ginsenoside Re, from a representative HCAEC (Cm = 45.12 pF, Rs = 4.2 MΩ, voltage error = 0.36 mV).

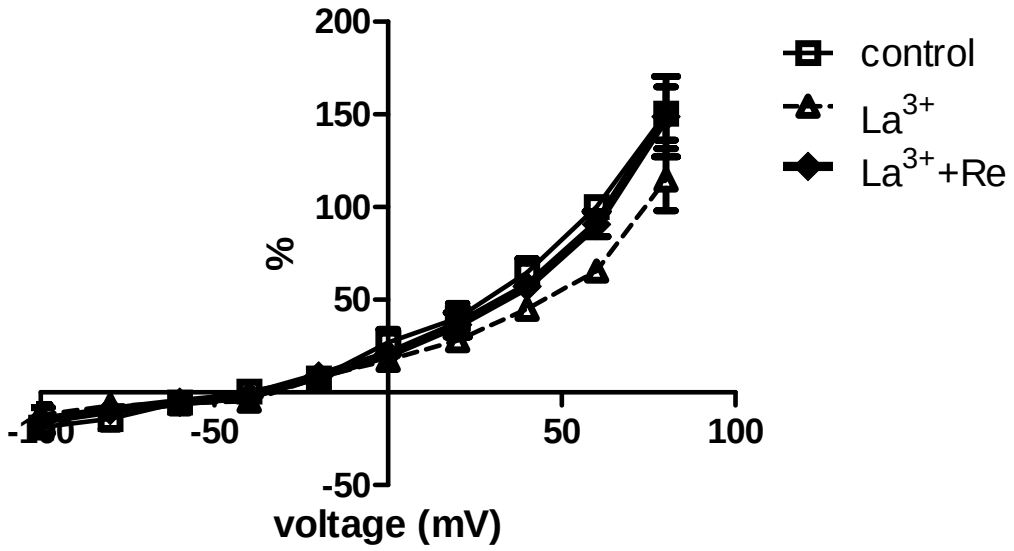

Figure 4.46 Average current-voltage curves from four cells where control currents were recorded before addition of 10 μM La^{3+} and 10 μM La^{3+} + 1 μM ginsenoside Re. Error bars are S.E.M.

4.4.2 Effect of La^{3+} on ginsenoside Re-induced currents

In this experiment, currents were first recorded in 1 μM ginsenoside Re, followed by 1 μM ginsenoside Re with 10 μM La^{3+}. Current traces from a representative cell are shown in figure 4.47. The average current-voltage curves and bar graphs are in figure 4.48. We found that the outward currents at +60 mV were significantly decreased after adding La^{3+}, (remaining currents after La^{3+} 65.43 ± 6.68 % compared with ginsenoside Re alone, or -34.58 ± 6.68 % different, n = 6, P = 0.0035, one-sample t test).

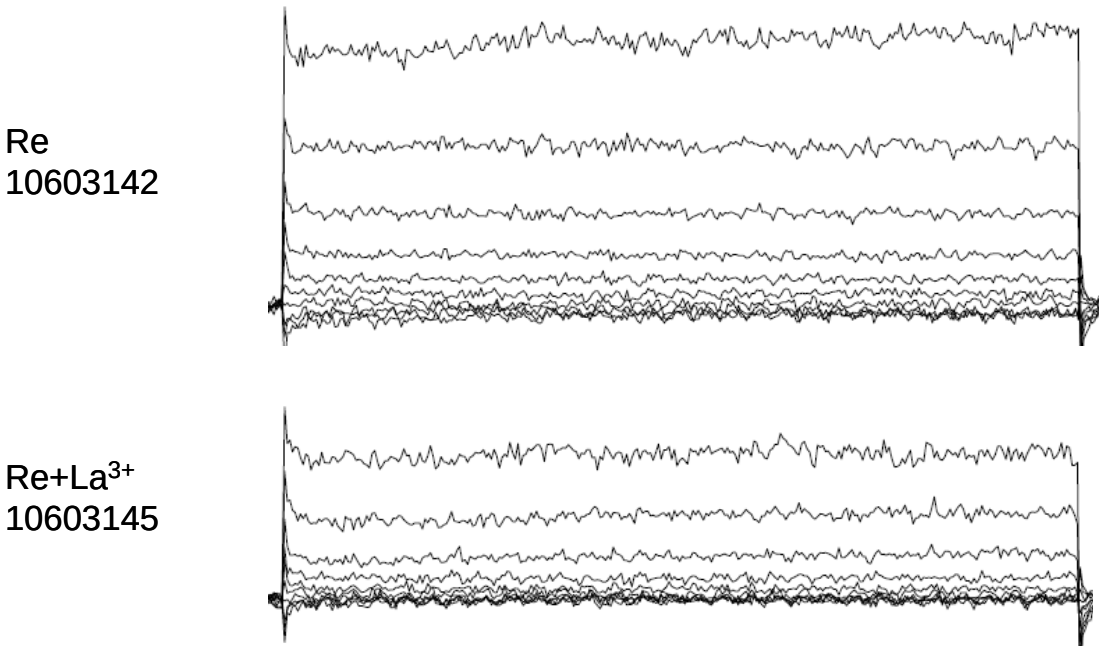

Figure 4.47 Current traces in 1 μM ginsenoside Re, with and without 10 μM La^{3+}, from a representative HCAEC (Cm = 16.75 pF, Rs = 10 MΩ, voltage error = 1.51 mV).

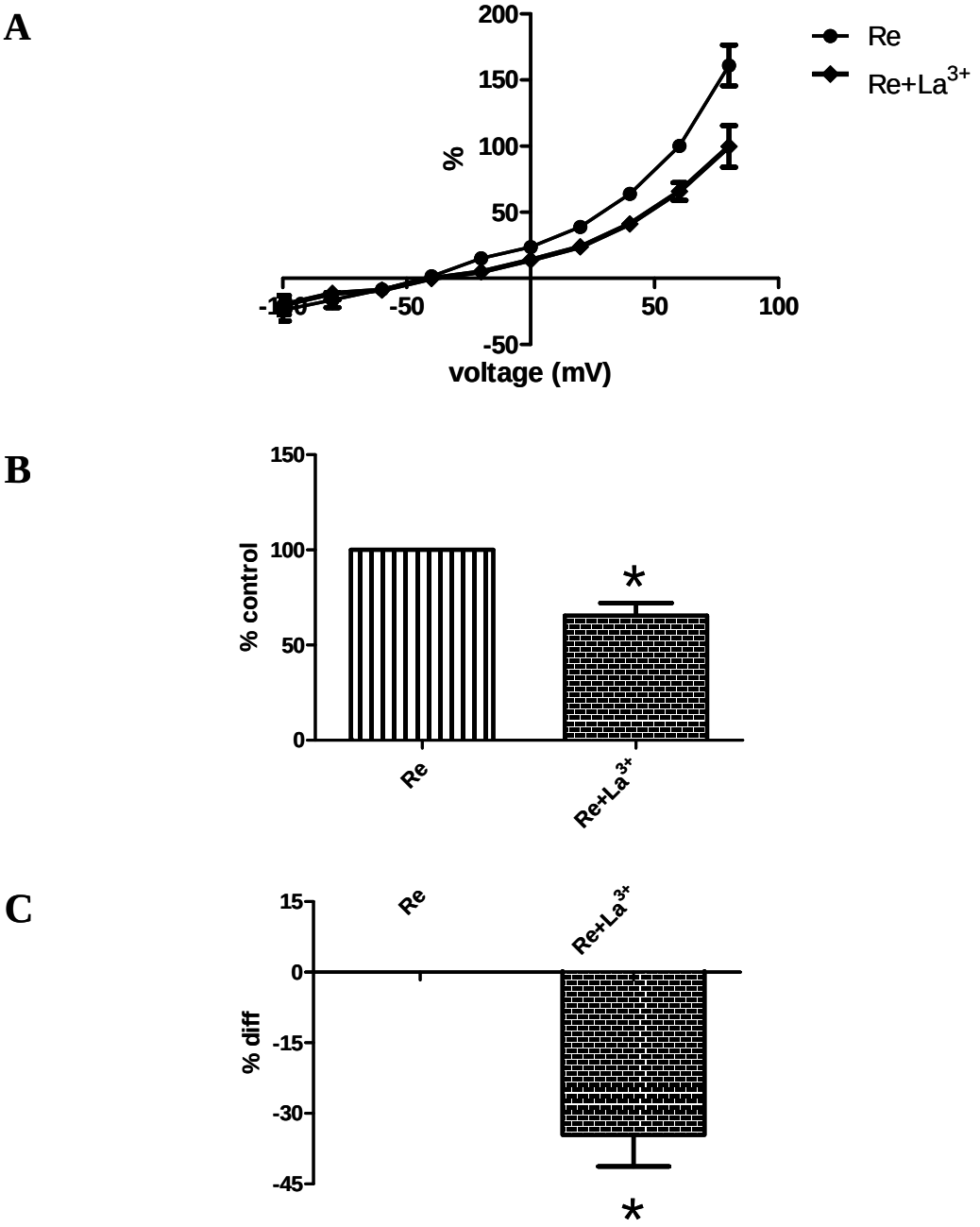

Figure 4.48 Effects of 10 μM La^{3+} in the presence of 1 μM ginsenoside Re. Error bars are S.E.M. Asterisks (*) represent significant changes.

A: The average current-voltage curves, plotted from % control data (n = 6).

B: Bar graphs comparing % control currents at +60 mV from all cells. Significant difference between 1 μM ginsenoside Re and 1 μM ginsenoside Re with La^{3+} was found (100 % vs 65.43 ± 6.68 %, n = 6, $P = 0.0035$, one-sample t test).

C: Bar graphs showing average % different of currents at +60 mV from all cells.

Reversibility of La^{3+} blockade on ginsenoside Re-induced currents could be demonstrated in four out of six cells. Figure 4.49 shows the current traces in 1 μM ginsenoside Re, 1 μM ginsenoside Re + 10 μM La^{3+}, and 1 μM ginsenoside Re (washout) in a representative cell. Corresponding average current-voltage curves are shown in figure 4.50. The washout currents at +60 mV were 84.76 ± 14.76 % of control (both in ginsenoside Re). The difference was not significant (n = 4, P = 0.3777, one-sample t test).

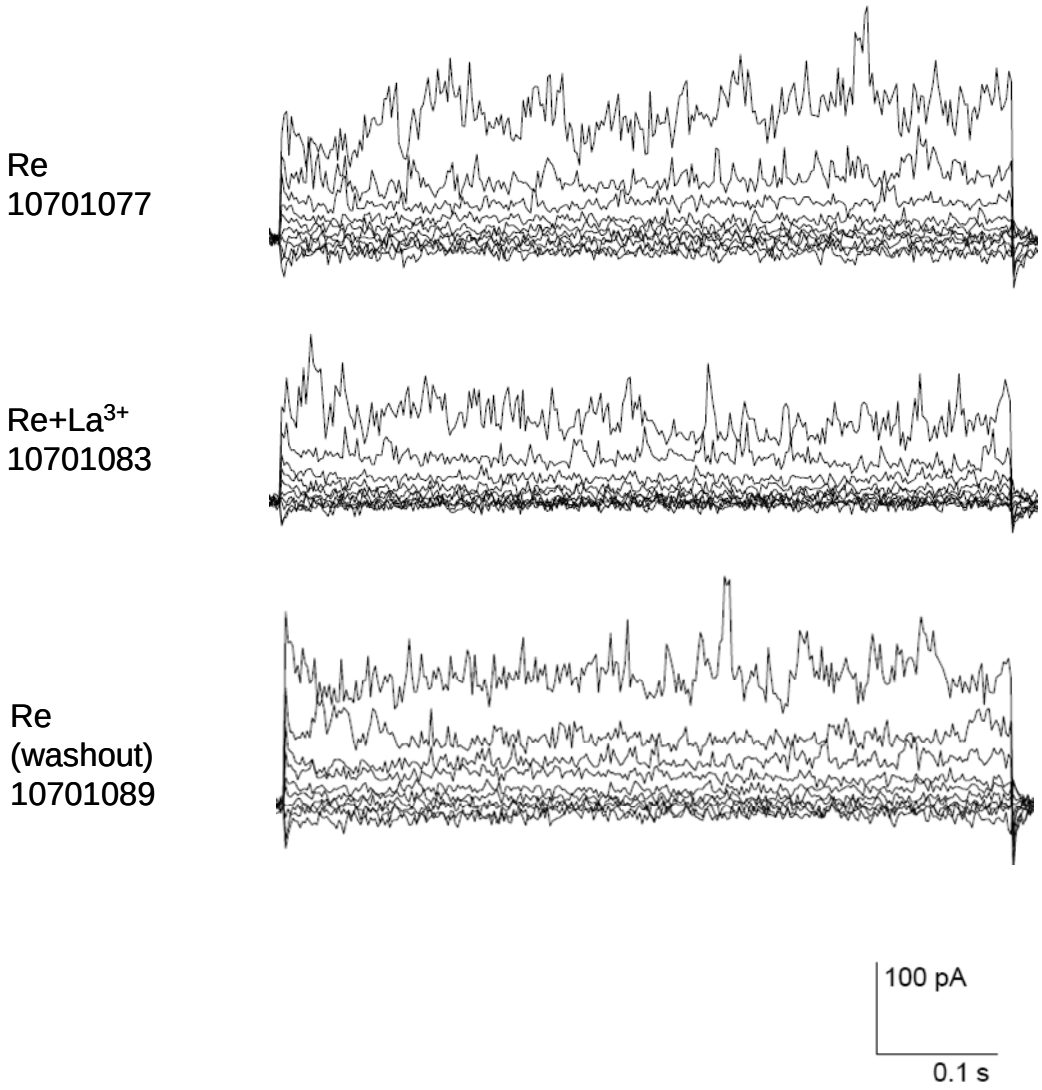

Figure 4.49 Current traces recorded in 1 μM ginsenoside Re ("Re"), 1 μM ginsenoside Re with 10 μM La^{3+} ("Re+La^{3+}") and on return to 1 μM ginsenoside Re ("Re (washout)"), from a representative HCAEC (Cm = 10.74 pF, Rs = 9.6 MΩ, voltage error = 1.42 mV).

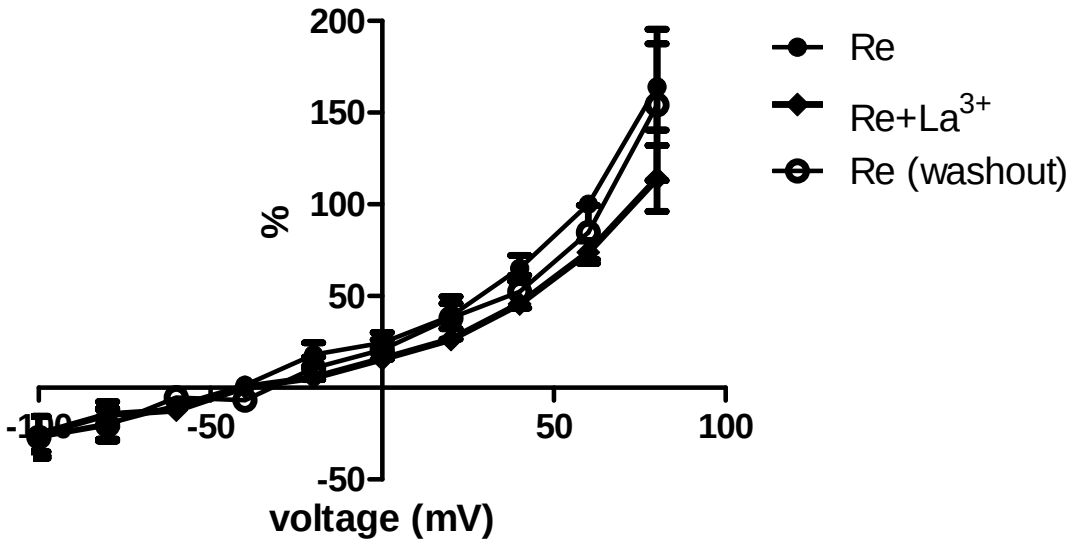

Figure 4.50 The average current-voltage curves, showing the effect of 10 μM La^{3+} on ginsenoside Re-induced currents and washout (on return to 1 μM ginsenoside Re), plotted from % control data (n = 4). Re *vs* Re (washout) = 100 % vs 84.76 $\pm$ 14.76 % (P = 0.3777, one-sample t test).

CHAPTER V
DISCUSSION

This study was the first to investigate the effect of ginsenoside Re on total currents of human coronary artery endothelial cells (HCAECs). We found that ginsenoside Re could dose-dependently increase the outward currents of HCAECs, with an EC50 of 0.409 μM and a maximal increase of 36.20 $\pm$ 5.62 %. The increase of outward currents was still found in the presence of lanthanum (La^{3+}), an NSC channel blocker. On the other hand pre-blocking with apamin, a small-conductance Ca^{2+}-activated K^+ (SK_{Ca}) channel blocker, could prevent the ginsenoside Re-induced current. Moreover, simultaneous application of La^{3+}, clotrimazole (IK_{Ca} channel blocker), TEA (BK_{Ca} channel blocker) and Ba^{2+} (K_{ir} channel blocker) could not prevent the enhancement of outward currents by ginsenoside Re. However, the increment of outward currents by ginsenoside Re in the four-blocker solution was inhibited by apamin. Taken together, these data indicate that ginsenoside Re increased outward currents of HCAECs by enhancing SK_{Ca} channels.

5.1 Effect of DMSO on whole-cell current

Before investigating the action of ginsenoside Re on HCAEC currents, the effect of DMSO, the solvent for all ginsenoside Re concentrations, was first examined. The maximum final concentration of DMSO in external solution was calculated to be 1.8% v/v for 100 μM ginsenoside Re. Our results showed that 1.8% DMSO did not affect the whole-cell currents of HCAECs (figure 4.2, 4.3). We later decided not to test the 100 μM ginsenoside Re concentration, because the maximum response was already attained with concentrations of 1, 3, 10 and 30 μM. In actuality, therefore, the maximum concentration of DMSO was 0.57 %, for 30 μM ginsenoside Re. We did

study the effect of 0.57 % of DMSO on HCAEC currents: no effect of 0.57 % DMSO was found either. However, there were only two cells in this study (figure 5.1, 5.2).

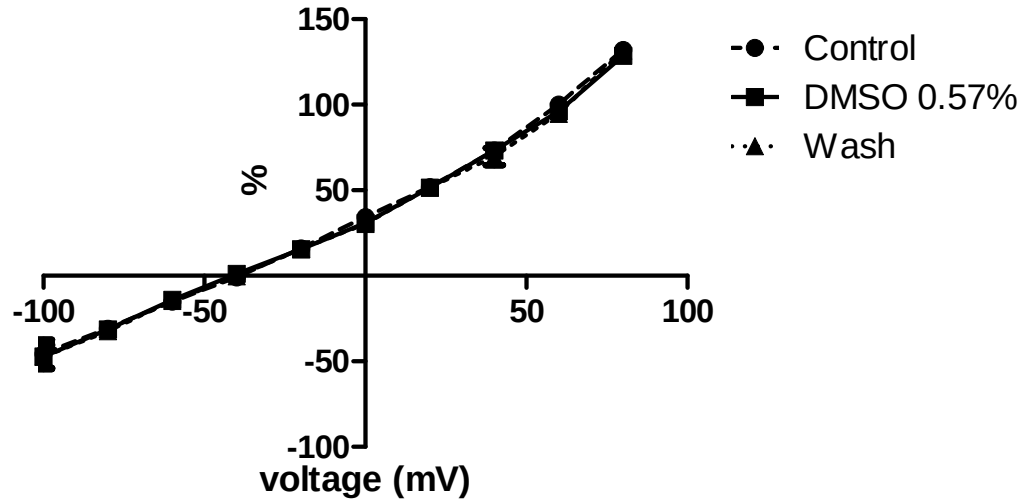

Figure 5.1 The current-voltage curves in control (external solution), 0.57% DMSO and washout (returning to external solution) from two cells. Data were in % control.

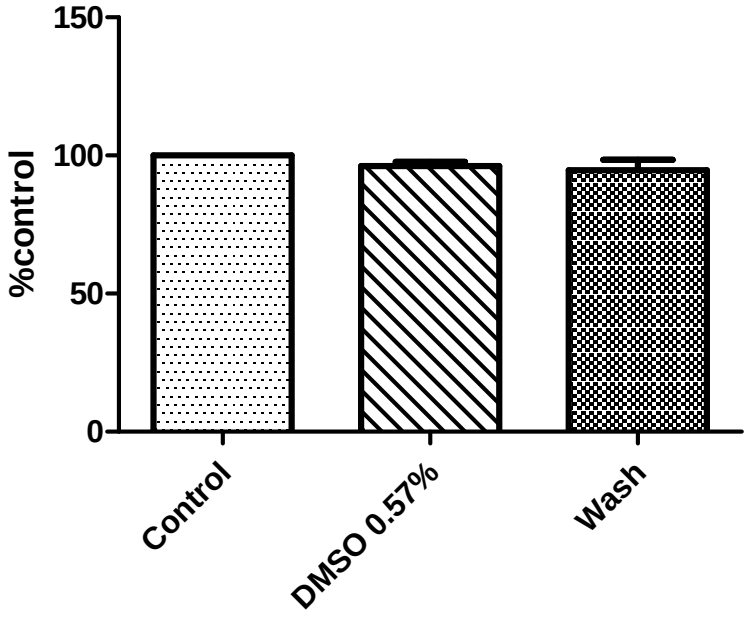

Figure 5.2 Bar graphs comparing currents at +60 mV, in % control, of the experiments in figure 5.1. Currents in 0.57% DMSO were 96.14 $\pm$ 1.58 % of control (n=2).

5.2 The dose-response relationship of ginsenoside Re effect on HCAEC whole-cell currents

Ginsenoside Re at 0.1 µM and 0.3 µM did not affect whole cell currents, while 1 µM increased the outward currents maximally (figure 4.24, 4.25). The explanation for this increase of outward currents from minimum to maximum by only a small increase of ginsenoside Re concentration, from 0.3 to 1 µM, is still unclear. Investigating the in-between concentrations, such as 0.7 µM, may provide a better resolution for the shape of the slope.

From the dose-response curve (figure 4.26), the maximum current increased by ginsenoside Re had a mean value of 36.20 $\pm$ 5.62 % and an EC50 of 408.90 $\pm$ 1.59 nM. This effect was fully reversible, as evident in experiments where the washout currents were successfully recorded (for example, figures 4.18 and 4.19). In embryonic rat thoracic aortic smooth muscle cells, ginsenoside Re could increase potassium currents in a dose-dependent manner, with an EC50 of 4.1µM (12), about ten times of that found in this study. In guinea pig ventricular myocytes, 3 µM ginsenoside Re could increase delayed rectifier K^+ (I_{Ks}) tail currents from +6.1 ± 1.1 pA/pF to +8.3 ± 1.2 pA/pF (10). The EC50 in guinea pig ventricular myocytes was found in other studies to be 1.3 ± 0.1 and 1.4 ± 0.4 µM (5, 37). The discrepancy in EC50 among studies was probably due to the difference in cell type used. Nevertheless, all reports demonstrated similar results, that ginsenoside Re effect was a dose-dependent, reversible enhancement of K^+ currents, in agreement with the present results.

5.3 Endothelial K_{Ca} channels

Many reports have shown that endothelial cells from different sources possess K_{Ca} channels, which cause cell hyperpolarization, $[Ca^{2+}]_i$ increase and NO production (17, 96, 100, 101). The types of K_{Ca} channels associated with the above mechanisms consist of IK_{Ca} and SK_{Ca}, but the evidence for BK_{Ca} channels is variable

(17, 96, 100, 102). Histamine-activated outward currents in human umbilical vein endothelial cells (HUVECs) was abolished by apamin (a SK_{Ca} channel blocker) but was not affected by iberiotoxin (a BK_{Ca} channel blocker) (96). Additionally, in bovine coronary endothelial cells, whole cell currents were not affected by iberiotoxin and NS 1619 (a BK_{Ca} channel activator) (102). Similarly, in mouse aortic endothelial cells, it was found that IK_{Ca} and SK_{Ca} channel blockers significantly reduced the whole cell currents, but BK_{Ca} and K_{ir} channel blockers had no effect (17). In contrast, EA-hy-926, a cell line derived from HUVEC, was shown to express BK_{Ca} channels, which had a conductance of 190 pS and were voltage sensitive, with a reversal potential for -80 mV (103). Some evidence suggested that in vascular tissues, BK_{Ca} channels were predominantly found in vascular smooth muscle cells, while IK_{Ca} and SK_{Ca} channels were associated with endothelial cells (101).

In the latter part of section 4.2.1 (figures 4.29 and 4.30), apamin could reduce the HCAEC whole-cell currents by about 25 % (24.91% ± 11.04%, n = 3), which might approximate the fraction of currents contributed by SK_{Ca} under control conditions in our experiments, although the data were derived from only three cells. Previous results from our lab showed that a lower concentration of apamin, 1 nM, could block 16.63 $\pm$ 4.04 % of HCAEC total currents (n = 5) (104).

5.4 Effect of ginsenoside Re on SK_{Ca} channels

As summarized at the beginning of this chapter, the evidence in the present study strongly suggested that the ginsenoside Re-induced outward currents were contributed by SK_{Ca} channels. When 100 nM apamin was applied first, addition of 1 µM ginsenoside Re could not increase HCAEC currents (figures 4.27, 4.28). On the other hand, adding apamin in the continued presence of ginsenoside Re could decrease the currents by 27 % (26.98 ± 4.76 %; figures 4.31, 4.32). These data were consistent with several reports in different cells, suggesting that HCAECs consisted of SK_{Ca} channels which were important for ginsenoside Re activation (12, 17, 96).

In an attempt to partially isolate the currents going through SK_{Ca} channels, experiments were carried out in the presence of blockers of other K^+ channels and

NSC channel. The four-blocker solution consisted of La^{3+} (NSC channel blocker), clotrimazole (IK_{Ca} channel blocker), TEA (BK_{Ca} channel blocker) and Ba^{2+} (K_{ir} channel blocker). K_{ATP} channels were blocked by addition of 2 mM ATP in the pipette solution. It turned out that the four-blocker could inhibit 58.53% of the whole-cell currents (section 4.3.1; figures 4.35, 4.36). The remaining currents were 41.47%, a larger fraction than that obtained from blocking with apamin (~ 25%; figures 4.29 and 4.30). Thus, we believe that, apart from SK_{Ca} channels, the remaining currents may be attributable to Cl^-. HUVECs were reported to contain Cl_{Ca} currents which was activated by $[Ca^{2+}]_i$ increase and had outward rectification property (85, 105). Activation occurred at positive potential, while the channel was inactivated at negative potential (85). In contrast, Cl_{vol} currents found in HUVECs were inactivated at positive potential (> 50 mV), although they similarly displayed outward rectification behavior (85). It is therefore more likely that the Cl^- currents in this study might be Cl_{Ca} than Cl_{vol} currents. However, the reported $[Ca^{2+}]_i$ for activating Cl_{Ca} was higher than 200 nM (106), a little higher than the estimated free $[Ca^{2+}]_i$ in the pipette solution (115.4 nM). Therefore, it is not clear whether Cl_{Ca} could be activated under our conditions.

In the continued presence of the four-blocker solution, 1 µM ginsenoside Re was able to increase HCAEC outward currents (figures 4.37, 4.38). This result may rule out the involvement of NSC, IK_{Ca}, BK_{Ca}, K_{ATP} and K_{ir} channels as targets of ginsenoside Re. The magnitude of the current increase by 1 µM ginsenoside Re in the four-blocker experiments averaged only 35.49 ± 4.22%, which is lower than expected because in the four-blocker solution there should be a higher fraction of SK_{Ca} channels and thus we expected a greater stimulation than in total HCAEC currents (36.2 %).

In the experiments of section 4.3.2, ginsenoside Re seemed to exhibit the expected larger effect; it could increase the currents in the four-blocker solution by 79 ± 18.43% (before apamin application) and 90.0 ± 28.62% (on recovery from apamin block). Unfortunately, this might reflect the small sample size and the high variability in the HCAEC culture (see Limitations), precluding any meaningful quantitative analysis of current percentage.

That SK_{Ca} channels were responsible for most of the ginsenoside Re-induced current was confirmed by addition of apamin, in the presence of the four-blocker solution and 1 µM ginsenoside Re, which could abolish the ginsenoside Re effect to an even lower amplitude than that obtained originally (i.e. than in four-blocker solution alone; figures 4.41, 4.42); the block likely included SK_{Ca} opening in control and after induction by ginsenoside Re. In addition, the apamin inhibition was reversible (figures 4.41, 4.42). The results strongly indicated that 1 µM ginsenoside Re increased outward currents of HCAECs via SK_{Ca} channels.

5.5 La^{3+} Experiments

Pre-blocking with La^{3+} could not prevent the action of ginsenoside Re: 1 µM Ginsenoside Re could increase the outward currents of HCAECs by 28.93 ± 7.54% (figures 4.43, 4.44). This indicates that ginsenoside Re effect did not involve NSC channels. However, a report suggested that ginsenoside Re might cause Ca^{2+}influx via activation of NSC channels in HUVECs (11). On the other hand, there were also studies indicated that Ca^{2+} entry via NSC channels may not affect the increase in outward currents activated by ginsenoside Re. In HUVECs, it was suggested that internal Ca^{2+} released from endoplasmic reticulum was responsible for activating K_{Ca} channels and NSC channels, whereas external Ca^{2+} entry via NSC channels was responsible for eNOS activation (100). In mice aortic endothelial cells, depletion of $[Ca^{2+}]_i$ led to reduction of SK_{Ca} and IK_{Ca} currents, which could not be adequately substituted by local Ca^{2+} influx (17).

The current enhancement found in this experiment was lower than 36.2 % increase for the effect in total HCAEC currents. Again this was attributed to the small sample size and variation of the HCAECs. Subsequent experiments involving application of La^{3+} to the ginsenoside Re-induced current resulted in significant and reversible current decrease by 34.58 ± 6.68 % (figures 4.47, 4.48). However, in four cells, La^{3+} could inhibit 34.41 ± 4 % of total, unactivated currents (figures 4.45, 4.46). This was contrary to the expectation that NSC channel should contribute less when

another channel was activated by ginsenoside Re. Our laboratory's previously reported number in total basal HCAEC currents was 41.15 $\pm$ 5.72 % (104).

5.6 Mechanism of ginsenoside Re effect on SK_{Ca} channels

The mechanism of ginsenoside Re was not addressed in this project. In cardiomyocytes, ginsenoside Re has been shown to increase I_{Ks} currents, $[Ca^{2+}]_i$, eNOS activation and NO production via a c-Src/PI3-kinase/Akt dependent mechanism which was associated with the non-genomic pathway of sex steroid receptors.[5, 10, 37, 38] Similarly, in vascular smooth muscle cells (VSMCs), ginsenoside Re could non-genomicly activate K_{Ca} currents and eNOS activation in a dose-dependent manner (EC50 = 4.1±0.3 μM) via c-Src/PI3-kinase/Akt pathway of estrogen receptor.[12] In HUVECs, ginsenoside Re dose-dependently increased $[Ca^{2+}]_i$ and NO production with EC50 of 316 nM and 615 nM, respectively (11). The $[Ca^{2+}]_i$ increase resulted from Ca^{2+}influx via NSC channels which has been activated by ginsenoside Re coupling with glucocorticoid receptors (11). Ginsenosides induced vascular relaxation in vascular rings which was associated with K_{Ca} channels activation (but not K_{ATP} activation) and NO production.[1, 15] Moreover, in both VSMCs and endothelial cells, ginsenosides could induce K_{Ca} channels activation and NO production (1, 13). Therefore, evidence from the literature has suggested that ginsenosides activated K_{Ca} channels, causing NO production, vascular smooth muscle hyperpolarization and vascular relaxation (1, 13, 15). The actions of ginsenosides and ginsenoside Re causing K_{Ca} activation and NO production via c-Src/PI3-kinase/Akt pathway of steroid receptors, leading ultimately to vascular relaxation, were similar to those of ginsenoside Rg3 (14, 107, 108), Rg1 (2) and Rg1 (9).

Taken together, the possible pathway for ginsenoside Re's action *in vivo* may be summarized as follows. First, ginsenoside Re may act on HCAECs by interacting with steroid receptors. The interaction activates c-Src/PI3-kinase/Akt mechanisms, leading to increment of $[Ca^{2+}]_i$ via endoplasmic reticular Ca^{2+} release channels. The Ca^{2+} increase enhances the open probability of SK_{Ca} channels, causing

the membrane potential to move closer to the equilibrium potential of K^+, i.e. more negative, according to the Goldman-Hodgkin-Katz equation (78). This leads to cell membrane hyperpolarization, enhancing the Ca^{2+} driving force because of equilibrium of Ca^{2+} was at a positive potential. Since endothelial cells do not possess voltage-gated Ca^{2+} channels, hyperpolarization and enhancement of Ca^{2+} driving force would result in higher Ca^{2+} influx via NSC channels, an important determinant for eNOS activation and the consequent NO production. NO from endothelial cells was sent to smooth muscle cells which caused vasorelaxation.

In our whole-cell patch clamp experiments, however, intracellular proteins had been dialyzed out by internal pipette solution and $[Ca^{2+}]_i$ were held constant by the EGTA buffer. Thus, ginsenoside Re might not have increased Ca^{2+} release from endoplasmic reticulum for SK_{Ca} channel opening. Therefore, our results raise a possibility that ginsenoside Re could directly affect SK_{Ca} channels or a membrane-delimited second messenger system close to SK_{Ca} channels.

5.7 Limitations

It has been suggested that ion channel expression of endothelial cell in culture may vary in different passages (102). We limited the HCAECs used to passages 4-8 to minimize variation (109-112).

The small sample size was another limitation. In our laboratory's experience, endothelial cells are more difficult to form seal and whole-cell access than classical excitable cells, such as neurons and muscles. In addition, cells were excluded according to exclusion criteria (section 3.4.3). We therefore kept the sample size to at least six cells, the smallest number that could be tested by the Kolmogorov-smirnov test for normal distribution. No statistics was applied to smaller sample size (in a subset of data) (111).

5.8 Further investigations

The involvement of Cl^- channels should be further studied. Signalling pathway mediating the ginsenoside effect on HCAEC currents can also be studied using whole-cell patch-clamp technique, or the perforated-patch variant, using a similar approach as in the present study. The involvement of a suspected pathway component can be inferred from measuring currents in the presence of a specific blocker, Candidates include steroid receptors (estrogen, androgen, progesterone and glucocorticoid receptors), c-Src, PI3-kinase, Akt and $[Ca^{2+}]_i$.

Western blot analysis may provide more information on the percentage different channel protein existing in HCAECs. However, the percentage of different currents cannot be inferred directly from the result of this technique, so the method cannot substitute for functional assessment in this regard. Single-channel analysis may be an appropriate approach for studying the effect of ginsenoside Re on a particular channel, but not the percentage contribution of each current.

Finally, association between ginsenoside Re and NO production in HCAECs may be proven with eNOS inhibitors and NO measurement.

CHAPTER VI
CONCLUSION

6.1 Human coronary artery endothelial cells (HCAECs) had an average outward current at +60 mV of 104.70 $\pm$ 3.80 pA (n = 245), an average cell capacitance of 24.17 $\pm$ 1.13 pF (n = 245) and an average normalized currents at +60 mV of 6.84 $\pm$ 0.40 pA/pF (n = 245).

6.2 DMSO at 1.8 % v/v did not affect whole-cell currents of HCAECs. Mean current in 1.8 % DMSO was 91.43 ± 9.39 % of currents in control external solution. No statistical significance was found.

6.3 Ginsenoside Re at 1, 3, 10 and 30 µM significantly increased outward currents in HCAECs by 34.00 ± 8.11 % (n = 10), 31.50 ± 6.24 % (7), 27.67 ± 11.70 % (9), and 47.19 ± 16.13 % (9), respectively (P < 0.05, one-way ANOVA with post hoc Dunnett's multiple comparison test, and also one-sample t test). The EC50 and maximal effect, obtained from fitting the data to the dose-response equation, were 408.90 $\pm$ 1.59 nM and 36.20 $\pm$ 5.62 %, respectively.

6.4 Ginsenoside Re at 1 µM could not increase outward currents in the presence of 100 nM apamin (1.20 ± 6.56 % difference, n = 8, P = 0.8654, one-sample t test). However, apamin could significantly decrease ginsenoside Re-induced outward currents by 26.98 ± 4.76 % (n = 8, P = 0.0008, one-sample t test). Ginsenoside Re may increase outward currents via SK_{Ca} channels.

6.5 Ginsenoside Re at 1 µM significantly increased outward currents in the presence of four-blocker solution, containing 10 µM La^{3+}, 10 µM clotrimazole, 1 mM TEA and 2 mM Ba^{2+}. (35.49 ± 4.22 % different, n = 15, P < 0.0001, one-sample t test). Addition

of 100 nM apamin abolished this effect (n = 3). These data strongly suggested that ginsenoside Re could increase outward currents of HCAECs via SK_{Ca} channels.

6.6 In the presence of 10 µM La^{3+}, 1 µM ginsenoside Re significantly increased outward currents by 28.93 ± 7.54 % (n = 9, *P* = 0.0050, one-sample *t* test). Furthermore, outward currents activated by 1 µM ginsenoside Re were significantly decreased after adding La^{3+} (34.58 ± 6.68 % different, n = 6, *P* = 0.0035, one-sample *t* test). This study suggested that ginsenoside Re did not affect NSC channels.

6.7 These data demonstrated that 1 µM ginsenoside Re increased outward currents of HCAECs via SK_{Ca} channels. Thus ginsenoside Re could have potential therapeutic application in cardiovascular disease.

.

REFERENCES

1. Li Z, Chen X, Niwa Y, Sakamoto S, Nakaya Y. Involvement of Ca^{2+} -activated K^{+} channels in ginsenosides-induced aortic relaxation in rats. J Cardiovasc Pharmacol2001 Jan;37(1):41-7.
2. Yu J, Eto M, Akishita M, Kaneko A, Ouchi Y, Okabe T. Signaling pathway of nitric oxide production induced by ginsenoside Rb1 in human aortic endothelial cells: a possible involvement of androgen receptor. Biochem Biophys Res Commun2007 Feb 16;353(3):764-9.
3. Gillis CN. Panax ginseng pharmacology: a nitric oxide link? Biochem Pharmacol 1997 Jul 1;54(1):1-8.
4. Kitts D, Hu C. Efficacy and safety of ginseng. Public Health Nutr2000 Dec;3(4A): 473-85.
5. Furukawa T, Bai CX, Kaihara A, Ozaki E, Kawano T, Nakaya Y, et al. Ginsenoside Re, a main phytosterol of Panax ginseng, activates cardiac potassium channels via a nongenomic pathway of sex hormones. Mol Pharmacol2006 Dec;70(6):1916-24.
6. E.Court W. GINSENG The Genus *Panax*. the Harwood Academic Publishers imprint, part of The Gordon and Breach Publishing Group2006.
7. Panax ginseng. Monograph. Altern Med Rev2009 Jun;14(2):172-6.
8. Tenney D. Ginseng. Woodland Publishing, Inc Pleasant Grove, UT1996.
9. Leung KW, Cheng YK, Mak NK, Chan KK, Fan TP, Wong RN. Signaling pathway of ginsenoside-Rg1 leading to nitric oxide production in endothelial cells. FEBS Lett2006 May 29;580(13):3211-6.
10. Bai CX, Sunami A, Namiki T, Sawanobori T, Furukawa T. Electrophysiological effects of ginseng and ginsenoside Re in guinea pig ventricular myocytes. Eur J Pharmacol2003 Aug 22;476(1-2):35-44.

11. Leung KW, Leung FP, Huang Y, Mak NK, Wong RN. Non-genomic effects of ginsenoside-Re in endothelial cells via glucocorticoid receptor. FEBS Lett2007 May 29;581(13):2423-8.
12. Nakaya Y, Mawatari K, Takahashi A, Harada N, Hata A, Yasui S. The phytoestrogen ginsensoside Re activates potassium channels of vascular smooth muscle cells through PI3K/Akt and nitric oxide pathways. J Med Invest2007 Aug;54(3-4):381-4.
13. Li Z, Nakaya Y, Niwa Y, Chen X. K(Ca) channel-opening activity of Ginkgo Biloba extracts and ginsenosides in cultured endothelial cells. Clin Exp Pharmacol Physiol2001 May-Jun;28(5-6):441-5.
14. Kim ND, Kang SY, Park JH, Schini-Kerth VB. Ginsenoside Rg3 mediates endothelium-dependent relaxation in response to ginsenosides in rat aorta: role of K^+ channels. Eur J Pharmacol1999 Feb 12;367(1):41-9.
15. Chen X, Salwinski S, Lee TJ. Extracts of Ginkgo biloba and ginsenosides exert cerebral vasorelaxation via a nitric oxide pathway. Clin Exp Pharmacol Physiol1997 Dec;24(12):958-9.
16. Baranowska M, Kozlowska H, Korbut A, Malinowska B. [Potassium channels in blood vessels: their role in health and disease]. Postepy Hig Med Dosw (Online)2007;61:596-605.
17. Ledoux J, Bonev AD, Nelson MT. Ca^{2+}-activated K^+ channels in murine endothelial cells: block by intracellular calcium and magnesium. J Gen Physiol2008 Feb;131(2):125-35.
18. Nilius B, Droogmans G. Ion channels and their functional role in vascular endothelium. Physiol Rev2001 Oct;81(4):1415-59.
19. Busse R, Mulsch A. Calcium-dependent nitric oxide synthesis in endothelial cytosol is mediated by calmodulin. FEBS Lett1990 Jun 4;265(1-2):133-6.
20. Yue PY, Mak NK, Cheng YK, Leung KW, Ng TB, Fan DT, et al. Pharmacogenomics and the Yin/Yang actions of ginseng: anti-tumor, angiomodulating and steroid-like activities of ginsenosides. Chin Med2007;2:6.

21. Persson IA, Dong L, Persson K. Effect of Panax ginseng extract (G115) on angiotensin-converting enzyme (ACE) activity and nitric oxide (NO) production. J Ethnopharmacol2006 May 24;105(3):321-5.

22. Samukawa K, Yamashita H, Matsuda H, Kubo M. [Simultaneous analysis of ginsenosides of various ginseng radix by HPLC]. Yakugaku Zasshi1995 Mar;115(3):241-9.

23. Lee BH, Jeong SM, Ha TS, Park CS, Lee JH, Kim JH, et al. Ginsenosides regulate ligand-gated ion channels from the outside. Mol Cells2004 Aug 31;18(1):115-21.

24. Sun J, Hu S, Song X. Adjuvant effects of protopanaxadiol and protopanaxatriol saponins from ginseng roots on the immune responses to ovalbumin in mice. Vaccine2007 Jan 22;25(6):1114-20.

25. Zhu S, Zou K, Cai S, Meselhy MR, Komatsu K. Simultaneous determination of triterpene saponins in ginseng drugs by high-performance liquid chromatography. Chem Pharm Bull (Tokyo)2004 Aug;52(8):995-8.

26. Joo KM, Lee JH, Jeon HY, Park CW, Hong DK, Jeong HJ, et al. Pharmacokinetic study of ginsenoside Re with pure ginsenoside Re and ginseng berry extracts in mouse using ultra performance liquid chromatography/mass spectrometric method. J Pharm Biomed Anal2010 Jan 5;51(1):278-83.

27. Xia C, Wang G, Sun J, Hao H, Xiong Y, Gu S, et al. Simultaneous determination of ginsenoside Rg1, Re, Rd, Rb1 and ophiopogonin D in rat plasma by liquid chromatography/electrospray ionization mass spectrometric method and its application to pharmacokinetic study of 'SHENMAI' injection. J Chromatogr B Analyt Technol Biomed Life Sci2008 Feb 1;862(1-2):72-8.

28. Liu YM, Yang L, Zeng X, Deng YH, Feng Y, Liang WX. [Pharmacokinetics of ginsenosides Rg1 and Re in Shenmai injection]. Yao Xue Xue Bao2005 Apr;40(4):365-8.

29. Leung KW, Wong AS. Pharmacology of ginsenosides: a literature review. Chin Med2010;5:20.

30. Yang L, Xu S, Liu C, Su Z. In vivo metabolism study of ginsenoside Re in rat using high-performance liquid chromatography coupled with tandem mass spectrometry. Anal Bioanal Chem2009 Nov;395(5):1441-51.

31. Bae EA, Shin JE, Kim DH. Metabolism of ginsenoside Re by human intestinal microflora and its estrogenic effect. Biol Pharm Bull2005 Oct;28(10):1903-8.

32. Tawab MA, Bahr U, Karas M, Wurglics M, Schubert-Zsilavecz M. Degradation of ginsenosides in humans after oral administration. Drug Metab Dispos2003 Aug;31(8):1065-71.

33. Chi H, Ji GE. Transformation of ginsenosides Rb1 and Re from Panax ginseng by food microorganisms. Biotechnol Lett2005 Jun;27(11):765-71.

34. Ji ZN, Dong TT, Ye WC, Choi RC, Lo CK, Tsim KW. Ginsenoside Re attenuate beta-amyloid and serum-free induced neurotoxicity in PC12 cells. J Ethnopharmacol 2006 Aug 11;107(1):48-52.

35. Lopez MV, Cuadrado MP, Ruiz-Poveda OM, Del Fresno AM, Accame ME. Neuroprotective effect of individual ginsenosides on astrocytes primary culture. Biochim Biophys Acta2007 Sep;1770(9):1308-16.

36. Zhou XM, Cao YL, Dou DQ. Protective effect of ginsenoside-Re against cerebral ischemia/reperfusion damage in rats. Biol Pharm Bull2006 Dec;29(12):2502-5.

37. Bai CX, Takahashi K, Masumiya H, Sawanobori T, Furukawa T. Nitric oxide-dependent modulation of the delayed rectifier K^+ current and the L-type Ca^{2+} current by ginsenoside Re, an ingredient of Panax ginseng, in guinea-pig cardiomyocytes. Br J Pharmacol2004 Jun;142(3):567-75.

38. Wang YG, Zima AV, Ji X, Pabbidi R, Blatter LA, Lipsius SL. Ginsenoside Re suppresses electromechanical alternans in cat and human cardiomyocytes. Am J Physiol Heart Circ Physiol2008 Aug;295(2):H851-9.

39. Xie JT, Shao ZH, Vanden Hoek TL, Chang WT, Li J, Mehendale S, et al. Antioxidant effects of ginsenoside Re in cardiomyocytes. Eur J Pharmacol2006 Feb 27;532(3):201-7.

40. Scott GI, Colligan PB, Ren BH, Ren J. Ginsenosides Rb1 and Re decrease cardiac contraction in adult rat ventricular myocytes: role of nitric oxide. Br J Pharmacol2001 Nov;134(6):1159-65.

41. Mehendale S, Aung H, Wang A, Yin JJ, Wang CZ, Xie JT, et al. American ginseng berry extract and ginsenoside Re attenuate cisplatin-induced kaolin intake in rats. Cancer Chemother Pharmacol2005 Jul;56(1):63-9.

42. Cho WC, Chung WS, Lee SK, Leung AW, Cheng CH, Yue KK. Ginsenoside Re of Panax ginseng possesses significant antioxidant and antihyperlipidemic efficacies in streptozotocin-induced diabetic rats. Eur J Pharmacol2006 Nov 21;550(1-3):173-9.

43. Son YM, Kwak CW, Lee YJ, Yang DC, Park BC, Lee WK, et al. Ginsenoside Re enhances survival of human CD4+ T cells through regulation of autophagy. Int Immunopharmacol May;10(5):626-31.

44. Endemann DH, Schiffrin EL. Endothelial dysfunction. J Am Soc Nephrol2004 Aug;15(8):1983-92.

45. Caramori PR, Zago AJ. Endothelial dysfunction and coronary artery disease. Arq Bras Cardiol2000 Aug;75(2):163-82.

46. Vanhoutte PM. Endothelial dysfunction and atherosclerosis. Eur Heart J1997 Nov;18 Suppl E:E19-29.

47. Popov D, Costache G, Georgescu A, Enache M. Beneficial effects of L-arginine supplementation in experimental hyperlipemia-hyperglycemia in the hamster. Cell Tissue Res2002 Apr;308(1):109-20.

48. Boger RH, Bode-Boger SM. The clinical pharmacology of L-arginine. Annu Rev Pharmacol Toxicol2001;41:79-99.

49. Davignon J, Ganz P. Role of endothelial dysfunction in atherosclerosis. Circulation2004 Jun 15;109(23 Suppl 1):III27-32.

50. Shimokawa H. Primary endothelial dysfunction: atherosclerosis. J Mol Cell Cardiol1999 Jan;31(1):23-37.

51. Ross R. Atherosclerosis--an inflammatory disease. N Engl J Med1999 Jan 14;340(2):115-26.

52. Hackam DG, Anand SS. Emerging risk factors for atherosclerotic vascular disease: a critical review of the evidence. JAMA2003 Aug 20;290(7):932-40.

53. Raines EW, Ross R. Biology of atherosclerotic plaque formation: possible role of growth factors in lesion development and the potential impact of soy. J Nutr1995 Mar;125(3 Suppl):624S-30S.

54. Bennett-Richards K, Kattenhorn M, Donald A, Oakley G, Varghese Z, Rees L, et al. Does oral folic acid lower total homocysteine levels and improve endothelial function in children with chronic renal failure? Circulation2002 Apr 16;105(15):1810-5.

55. Wang BY, Singer AH, Tsao PS, Drexler H, Kosek J, Cooke JP. Dietary arginine prevents atherogenesis in the coronary artery of the hypercholesterolemic rabbit. J Am Coll Cardiol1994 Feb;23(2):452-8.

56. Saleh AI, Abdel Maksoud SM, El-Maraghy SA, Gad MZ. Protective Effect of L-Arginine in Experimentally Induced Myocardial Ischemia: Comparison With Aspirin. J Cardiovasc Pharmacol Ther2010 Oct 11.

57. Orozco-Gutierrez JJ, Castillo-Martinez L, Orea-Tejeda A, Vazquez-Diaz O, Valdespino-Trejo A, Narvaez-David R, et al. Effect of L-arginine or L-citrulline oral supplementation on blood pressure and right ventricular function in heart failure patients with preserved ejection fraction. Cardiol J2010;17(6):612-8.

58. Drexler H, Zeiher AM, Meinzer K, Just H. Correction of endothelial dysfunction in coronary microcirculation of hypercholesterolaemic patients by L-arginine. Lancet1991 Dec 21-28;338(8782-8783):1546-50.

59. Trocha M, Szuba A, Merwid-Lad A, Sozanski T. Effect of selected drugs on plasma asymmetric dimethylarginine (ADMA) levels. Pharmazie2010 Aug;65(8):562-71.

60. Cross JM, Donald AE, Nuttall SL, Deanfield JE, Woolfson RG, Macallister RJ. Vitamin C improves resistance but not conduit artery endothelial function in patients with chronic renal failure. Kidney Int2003 Apr;63(4):1433-42.

61. Levine GN, Frei B, Koulouris SN, Gerhard MD, Keaney JF, Jr., Vita JA. Ascorbic acid reverses endothelial vasomotor dysfunction in patients with coronary artery disease. Circulation1996 Mar 15;93(6):1107-13.

62. Engler MM, Engler MB, Malloy MJ, Chiu EY, Schloetter MC, Paul SM, et al. Antioxidant vitamins C and E improve endothelial function in children with hyperlipidemia: Endothelial Assessment of Risk from Lipids in Youth (EARLY) Trial. Circulation2003 Sep 2;108(9):1059-63.

63. Tiefenbacher CP, Friedrich S, Bleeke T, Vahl C, Chen X, Niroomand F. ACE inhibitors and statins acutely improve endothelial dysfunction of human coronary arterioles. Am J Physiol Heart Circ Physiol2004 Apr;286(4):H1425-32.

64. Mehta JL, Li DY, Chen HJ, Joseph J, Romeo F. Inhibition of LOX-1 by statins may relate to upregulation of eNOS. Biochem Biophys Res Commun2001 Dec 14;289(4):857-61.

65. Qipshidze N, Metreveli N, Lominadze D, Tyagi SC. Folic acid improves acetylcholine-induced vasoconstriction of coronary vessels isolated from hyperhomocysteinemic mice: An implication to coronary vasospasm. J Cell Physiol2010 Dec 30.

66. Moat SJ, Madhavan A, Taylor SY, Payne N, Allen RH, Stabler SP, et al. High- but not low-dose folic acid improves endothelial function in coronary artery disease. Eur J Clin Invest2006 Dec;36(12):850-9.

67. Szmitko PE, Fedak PW, Weisel RD, Stewart DJ, Kutryk MJ, Verma S. Endothelial progenitor cells: new hope for a broken heart. Circulation2003 Jun 24;107(24):3093-100.

68. Aicher A, Heeschen C, Mildner-Rihm C, Urbich C, Ihling C, Technau-Ihling K, et al. Essential role of endothelial nitric oxide synthase for mobilization of stem and progenitor cells. Nat Med2003 Nov;9(11):1370-6.

69. van Oostrom O, de Kleijn DP, Fledderus JO, Pescatori M, Stubbs A, Tuinenburg A, et al. Folic acid supplementation normalizes the endothelial progenitor cell transcriptome of patients with type 1 diabetes: a case-control pilot study. Cardiovasc Diabetol2009;8:47.

70. Mobius-Winkler S, Hollriegel R, Schuler G, Adams V. Endothelial progenitor cells: implications for cardiovascular disease. Cytometry A2009 Jan;75(1):25-37.

71. Yip H, Chan WY, Leung PC, Kwan HY, Liu C, Huang Y, et al. Expression of TRPC homologs in endothelial cells and smooth muscle layers of human arteries. Histochem Cell Biol2004 Dec;122(6):553-61.

72. Smedlund K, Tano JY, Vazquez G. The constitutive function of native TRPC3 channels modulates vascular cell adhesion molecule-1 expression in

coronary endothelial cells through nuclear factor kappaB signaling. Circ Res2010 May 14;106(9):1479-88.

73. Yoshida H, Feig JE, Morrissey A, Ghiu IA, Artman M, Coetzee WA. K ATP channels of primary human coronary artery endothelial cells consist of a heteromultimeric complex of Kir6.1, Kir6.2, and SUR2B subunits. J Mol Cell Cardiol2004 Oct;37(4):857-69.
74. Zunkler BJ, Henning B, Grafe M, Bass R, Hildebrandt AG, Fleck E. Electrophysiological properties of human coronary endothelial cells. Basic Res Cardiol1995 Nov-Dec;90(6):435-42.
75. Liu GX, Vepa S, Artman M, Coetzee WA. Modulation of human cardiovascular outward rectifying chloride channel by intra- and extracellular ATP. Am J Physiol Heart Circ Physiol2007 Dec;293(6):H3471-9.
76. Aguilar-Bryan L, Clement JPt, Gonzalez G, Kunjilwar K, Babenko A, Bryan J. Toward understanding the assembly and structure of K_{ATP} channels. Physiol Rev1998 Jan;78(1):227-45.
77. Nilius B, Viana F, Droogmans G. Ion channels in vascular endothelium. Annu Rev Physiol1997;59:145-70.
78. HILLE B. Ion channels of excitable membranes. . 3rd ed. Sunderland, MA: Sinauer Associates; 2001.
79. Dick GM, Tune JD. Role of potassium channels in coronary vasodilation. Exp Biol Med (Maywood)2010 Jan;235(1):10-22.
80. Ledoux J, Werner ME, Brayden JE, Nelson MT. Calcium-activated potassium channels and the regulation of vascular tone. Physiology (Bethesda)2006 Feb;21:69-78.
81. Watanabe H, Murakami M, Ohba T, Takahashi Y, Ito H. TRP channel and cardiovascular disease. Pharmacol Ther2008 Jun;118(3):337-51.
82. Clapham DE, Runnels LW, Strubing C. The TRP ion channel family. Nat Rev Neurosci2001 Jun;2(6):387-96.
83. Vazquez G, Wedel BJ, Aziz O, Trebak M, Putney JW, Jr. The mammalian TRPC cation channels. Biochim Biophys Acta2004 Dec 6;1742(1-3):21-36.
84. Minke B, Cook B. TRP channel proteins and signal transduction. Physiol Rev2002 Apr;82(2):429-72.

85. Zhong N, Fang QZ, Zhang Y, Zhou ZN. Volume- and calcium-activated chloride channels in human umbilical vein endothelial cells. Acta Pharmacol Sin2000 Mar;21(3):215-20.

86. Fuller CM, Ji HL, Tousson A, Elble RC, Pauli BU, Benos DJ. Ca(2+)-activated Cl(-) channels: a newly emerging anion transport family. Pflugers Arch2001;443 Suppl 1:S107-10.

87. Feletou M. Calcium-activated potassium channels and endothelial dysfunction: therapeutic options? Br J Pharmacol2009 Feb;156(4):545-62.

88. Grgic I, Kaistha BP, Hoyer J, Kohler R. Endothelial Ca^{2+}-activated K^{+} channels in normal and impaired EDHF-dilator responses--relevance to cardiovascular pathologies and drug discovery. Br J Pharmacol2009 Jun;157(4):509-26.

89. Kohler R, Ruth P. Endothelial dysfunction and blood pressure alterations in K^{+}-channel transgenic mice. Pflugers Arch2010 May;459(6):969-76.

90. Molleman A. Patch clamping: an introductory guide to patch clamp electrophysiology. England: John Wiley & Sons, Ltd; 2003.

91. Sherman-Gold R. The axon guide for electrophysiology and biophysics laboratory techniques. USA: Axon instruments, Inc; 1993.

92. Karmazinova M, Lacinova L. Measurement of cellular excitability by whole cell patch clamp technique. Physiol Res2010;59 Suppl 1:S1-7.

93. Walz W. Patch-clamp analysis: advance techniques. 2nd ed. Totowa, New Jersey: Humana Press Inc; 2007.

94. Zhao Y, Inayat S, Dikin D A, Singer J H, Ruoff R S, B TJ. Patch clamp technique: review of the current state of the art and potential contributions from nanoengineering. J Nanoengineering and Nanosystems2009;222 part N.

95. Treiber K, Singer A, Henke B, Muller WE. Hyperforin activates nonselective cation channels (NSCCs). Br J Pharmacol2005 May;145(1):75-83.

96. Muraki K, Imaizumi Y, Ohya S, Sato K, Takii T, Onozaki K, et al. Apamin-sensitive Ca^{2+}-dependent K^{+} current and hyperpolarization in human endothelial cells. Biochem Biophys Res Commun1997 Jul 18;236(2):340-3.

97. Loganathan A. Basolateral potassium (IK_{Ca}) channel inhibition prevents increased colonic permeability induced by chemical hypoxia. Am J Physiol Gastrointest Liver Physiol2011;300(1):G146-53.

98. Murata T. Identification of a site involved in the block by extracellular Mg^{2+} and Ba^{2+} as well as permeation of K^{+} in the Kir2.1 K^{+} channel. Journal of Physiology 2002;544.3:pp.665-77.

99. Fertig N. Whole Cell Patch Clamp Recording Performed in a Planae Glass Chip. Biophysical Journal2002;82:3056-62.

100. Sheng JZ, Braun AP. Small- and intermediate-conductance Ca^{2+}-activated K^{+} channels directly control agonist-evoked nitric oxide synthesis in human vascular endothelial cells. Am J Physiol Cell Physiol2007 Jul;293(1):C458-67.

101. Kohler R. Single-nucleotide polymorphisms in vascular Ca^{2+}-activated K^{+}-channel genes and cardiovascular disease. Pflugers Arch2010 Jul;460(2):343-51.

102. Gauthier KM, Liu C, Popovic A, Albarwani S, Rusch NJ. Freshly isolated bovine coronary endothelial cells do not express the BK Ca channel gene. J Physiol2002 Dec 15;545(Pt 3):829-36.

103. Haburcak M, Wei L, Viana F, Prenen J, Droogmans G, Nilius B. Calcium-activated potassium channels in cultured human endothelial cells are not directly modulated by nitric oxide. Cell Calcium1997 Apr;21(4):291-300.

104. Ruamyod K, Watanapa WB, C. S. Characterization of ion channels in human coronary artery endothelial cells. Abstracts of the 39th Annual Conference of The Physiological Society of Thailand2010;May 5-8:120.

105. Fang QZ, Zhong N, Zhang Y, Zhou ZN. Tetrandrine inhibits Ca^{2+}-activated chloride channel in cultured human umbilical vein endothelial cells. Acta Pharmacol Sin2004 Mar;25(3):327-33.

106. Hartzell C, Putzier I, Arreola J. Calcium-activated chloride channels. Annu Rev Physiol2005;67:719-58.

107. Hien TT, Kim ND, Pokharel YR, Oh SJ, Lee MY, Kang KW. Ginsenoside Rg3 increases nitric oxide production via increases in phosphorylation and expression of endothelial nitric oxide synthase: Essential roles of estrogen

receptor-dependent PI3-kinase and AMP-activated protein kinase. Toxicol Appl Pharmacol2010 May 27.

108. Kim ND, Kim EM, Kang KW, Cho MK, Choi SY, Kim SG. Ginsenoside Rg3 inhibits phenylephrine-induced vascular contraction through induction of nitric oxide synthase. Br J Pharmacol2003 Oct;140(4):661-70.

109. Smedlund K, Vazquez G. Involvement of native TRPC3 proteins in ATP-dependent expression of VCAM-1 and monocyte adherence in coronary artery endothelial cells. Arterioscler Thromb Vasc Biol2008 Nov;28(11):2049-55.

110. Mendoza SA, Fang J, Gutterman DD, Wilcox DA, Bubolz AH, Li R, et al. TRPV4-mediated endothelial Ca2+ influx and vasodilation in response to shear stress. Am J Physiol Heart Circ Physiol2009 Feb;298(2):H466-76.

111. Kuhlmann CR, Wu Y, Li F, Munz BM, Tillmanns H, Waldecker B, et al. bFGF activates endothelial Ca^{2+}-activated K^{+} channels involving G-proteins and tyrosine kinases. Vascul Pharmacol2004 Jul;41(6):181-6.

112. Kefaloyianni E, Coetzee WA. Transcriptional Remodeling of Ion Channel Subunits by Flow Adaptation in Human Coronary Artery Endothelial Cells. J Vasc Res2011 Mar 9;48(4):357-67.

BIOGRAPHY

NAME	Miss. Suporn Sukrittanon
DATE OF BIRTH	17 Apr 1985
PLACE OF BIRTH	Bangkok, Thailand
INSTITUTIONS ATTENDED	Srinakharinwirot University, 2007 Bachelor of Science (Physical therapy) Mahidol University, 2011 Master of Science (Physiology)
SCHOLARSHIP	Siriraj graduate thesis scholarship, 2009 The 60th Year Supreme Reign of His Majesty King Bhumibol Adulyadej, 2008-2009 Cerebos Awards, 2009
HOME ADDRESS	4/1378 Sahakorn village, soi. Serithai 57, Serithai Road, Klong-kum, Bueng-kum, Bangkok, Thailand 10240